INL/RPT-22-67132
Revision 0

Uncertainty Quantification of Calculated Temperatures for AGR-5/6/7 Experiment

May 2022

Binh T. Pham and Grant L. Hawkes

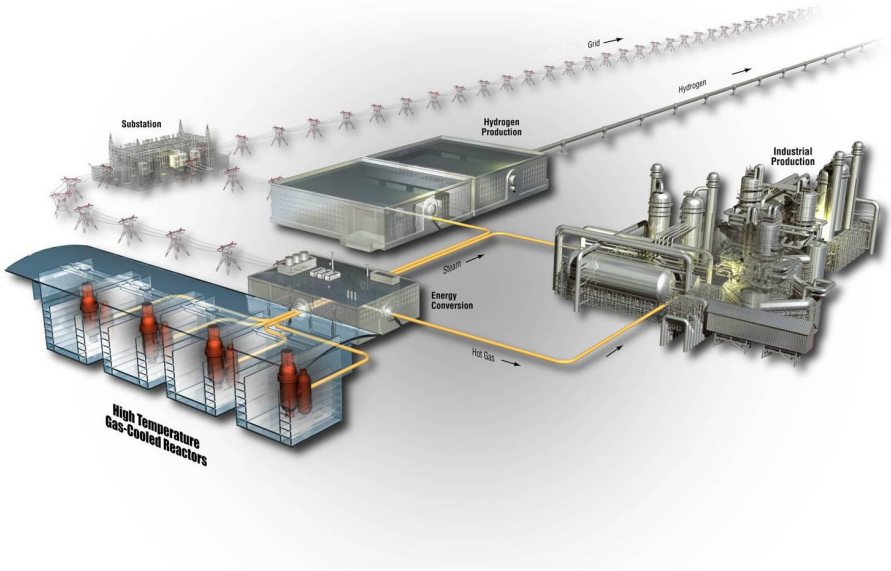

Idaho National Laboratory

INL is a U.S. Department of Energy National Laboratory
operated by Battelle Energy Alliance, LLC

INL/RPT-22-67132
Revision 0

Uncertainty Quantification of Calculated Temperatures for AGR-5/6/7 Experiment

Binh T. Pham and Grant L. Hawkes

May 2022

Idaho National Laboratory
INL ART Program
Idaho Falls, Idaho 83415

http://www.ART.INL.gov

Prepared for the
U.S. Department of Energy
Office of Nuclear Energy
Under DOE Idaho Operations Office
Contract DE-AC07-05ID14517

Page intentionally left blank

INL ART Program

Uncertainty Quantification of Calculated Temperatures for AGR-5/6/7 Experiment

INL/RPT-22-67132

May 2022

Technical Reviewer: (Confirmation of mathematical accuracy, correctness of data, and appropriateness of assumptions.)

Mitchell A. Plummer — May 10, 2022
Mitchell A. Plummer — Date
NDMAS Technical Lead

Approved by:

Paul Demkowicz — May 11, 2022
Paul A. Demkowicz — Date
AGR Program Technical Director

Travis Mitchell — 5/11/2022
Travis R. Mitchell — Date
INL ART Program Manager

Michelle Sharp — 5/10/2022
Michelle T. Sharp — Date
INL Quality Assurance

Page intentionally left blank

ACKNOWLEDGEMENTS

This work is supported by the Department of Energy Advanced Reactor Technologies Program at Idaho National Laboratory under U.S. Department of Energy contract DEAC0705ID14517.

ABSTRACT

This report documents the quantification of uncertainty of the calculated temperature data for the Advanced Gas Reactor (AGR)-5/6/7 fuel irradiation experiment conducted in the Advanced Test Reactor at Idaho National Laboratory in support of the Advanced Reactor Technologies' research and development program. Recognizing that uncertainties are inherent in physics and thermal simulations of the AGR-5/6/7 capsules, the results of the numerical simulations are used in combination with statistical analysis methods to improve the qualification of measured data. The calculated fuel temperatures for AGR tests are also used for validation of the fission product transport and fuel performance simulation models. These crucial roles of the calculated fuel temperatures in ensuring achievement of the AGR experimental program objectives require accurate determination of model temperature uncertainties. This report covers temperature uncertainty results for each of the five AGR-5/6/7 capsules.

To quantify the uncertainty of calculated temperatures determined using the ABAQUS finite element heat transfer code, this study identifies and analyzes model parameters of potential importance to the calculated temperatures of fuel compacts and thermocouples. The selection of input parameters for uncertainty quantification is based on ranking their influences on temperature predictions. Thus, the selected input parameters include those with high sensitivity and those with the largest uncertainty. The propagation of model parameter uncertainty and sensitivity is then used to quantify the overall uncertainty of calculated temperatures. Measurement uncertainty, analysis of modeling assumptions, and expert judgment are used as the basis to quantify the uncertainty range for selected input parameters. The input uncertainties are dynamic, accounting for the effect of unplanned events and changes in the thermal properties of capsule components over extended exposure to high temperatures and fast neutron irradiation.

The sensitivity analysis performed in this work went beyond the traditional local sensitivity. Using experimental design, analysis of pairwise interactions of model parameters was performed to establish the sufficiency of the time-dependent first-order (linear) expansion terms in constructing the temperature response surface. To achieve completeness, uncertainty propagation made use of the pairwise noise correlations of model parameters. Furthermore, using an interpolation scheme over the input parameter domain, the analysis obtained time-dependent sensitivities over the test campaign duration. This enables the computation of uncertainty for the calculated fuel temperatures and the calculated graphite temperatures at thermocouple locations throughout the entire irradiation period.

SUMMARY

S-1 Introduction

This report documents the quantification of uncertainty in the calculated temperatures for the five capsules of the Advanced Gas Reactor (AGR)-5/6/7 fuel irradiation experiment. The irradiation, conducted in the northeast flux trap location of the Advanced Test Reactor (ATR) at Idaho National Laboratory (INL), supported the Advanced Reactor Technologies (ART) research and development (R&D) program. While impossible to obtain via direct measurements in the tests, essential fuel irradiation conditions (e.g., temperature, fast neutron fluence, and burnup) were calculated using core physics (JMOCUP) and thermal modeling (ABAQUS) codes. Calculated fuel temperatures serve crucial roles in quality assessments of tristructural isotropic (TRISO) fuel irradiated in AGR experiments and require accurate determination of the model temperature uncertainties. One such role is the validation of the fission product transport and fuel performance simulation models.

S-2 Approach

In general, uncertainty in simulation model predictions arises from two main sources: input uncertainty and model uncertainty. This assumes that the numerical errors can be eliminated using adequate spatial resolution in the computing code. Consequently, the overall uncertainty of simulation model predictions in terms of variance can be expressed as:

$$\sigma_T^2 = \sigma_M^2 + \sigma_P^2 \tag{S-1}$$

where

σ_T = overall uncertainty of calculated temperature in terms of standard deviation
σ_M = model form uncertainty
σ_p = parameter uncertainty in terms of standard deviation.

Model Form Uncertainty

Early analysis of thermocouple (TC) data indicated that the TCs performed reliably, especially during the first irradiation cycle. Therefore, the thermal models for all capsules were jointly calibrated by varying several inputs within their uncertainty bounds (e.g., the emissivity of surfaces of the graphite holder and stainless-steel capsule shell and graphite thermal expansion coefficient) to best match calculated temperatures at TC locations with actual TC measurements during the first irradiation cycle. The TC residuals are the differences between measured and calculated temperatures for operational TCs. Continued monitoring and analysis of residuals beyond the calibration period show a pattern of non-zero horizontal lines of TC residuals as a function of effective full power days (EFPDs) of irradiation for TCs in most of the capsules. This suggests the existence of model bias.

However, the model form uncertainty in terms of the relative standard deviation for all capsules cannot be estimated based solely on TC residuals because they were caused by both model bias and input uncertainties. In the absence of the model bias compensation for AGR-5/6/7, the model bias is unknown and thus not included in the overall calculated temperature uncertainty.

Parameter Uncertainty

The parameter uncertainty of a calculated temperature is caused by uncertainties of inputs to the simulation model. To quantify the parameter uncertainty of AGR-5/6/7 calculated temperatures, the ABAQUS code's potentially important finite element-based thermal model input parameters were identified. Identification is conducted in two steps: (1) using expert judgment, determine the parameters with the largest uncertainties and estimate these uncertainties, and (2) using sensitivity analysis, determine the parameters to which the modeling is most sensitive. A set of parameters was selected for calculated temperature uncertainty quantification, including those with high sensitivity and/or those with large uncertainty. The parameter uncertainties and sensitivity coefficients were combined and propagated to quantify the temperature parameter uncertainty using Equation (S-2), because the calculated temperature can be assumed to be the weighted summation of input parameters. This assumption was confirmed during sensitivity analysis.

$$\sigma_P^2 = \sum_i^n a_i^2 \sigma_i^2 + \sum_i^n \sum_{j \neq i}^n \rho_{ij} a_i \sigma_i \, a_j \sigma_j \quad \text{(S-2)}$$

where

σ_P = Temperature uncertainty in terms of standard deviation due to parameter uncertainties
a_i = the sensitivity coefficient for parameter *i*
σ_i = the uncertainty of parameter *i*
ρ_{ij} = the correlation coefficient between parameter *i* and *j*

The seven model parameters identified as the most influential on uncertainty are gas gap size, fuel compact heat rate, graphite heat rate, neon fraction, fuel thermal conductivity, graphite thermal conductivity, and graphite emissivity. Unlike previous AGR irradiation experiments, AGR-5/6/7 capsules had three different designs, as shown in the cross-section views of the AGR-5/6/7 capsules in Figure S-1. These designs led to one temperature control gas gap between the graphite holder and capsule shell for Capsules 1, 2, 4, and 5, but two gas gaps for the middle Capsule 3, with an additional inner gap between outer and inner graphite holders.

Gas gaps were modeled as linearly changing with fast neutron fluence (Hawkes 2021). The as-built dimensions for the gas gaps were adjusted to the hot gas gap dimensions, which are slightly smaller than the room temperature gas gap dimensions. However, an error in capsule fabrication led to a radial clearance of 0.005 in. between the graphite holder nubs and capsule shell (i.e., nub-to-shell clearance), which could allow the holder to shift inside the capsule shell more than intended. This, in turn, will lead to higher gap width uncertainty and thus higher calculated temperature uncertainty.

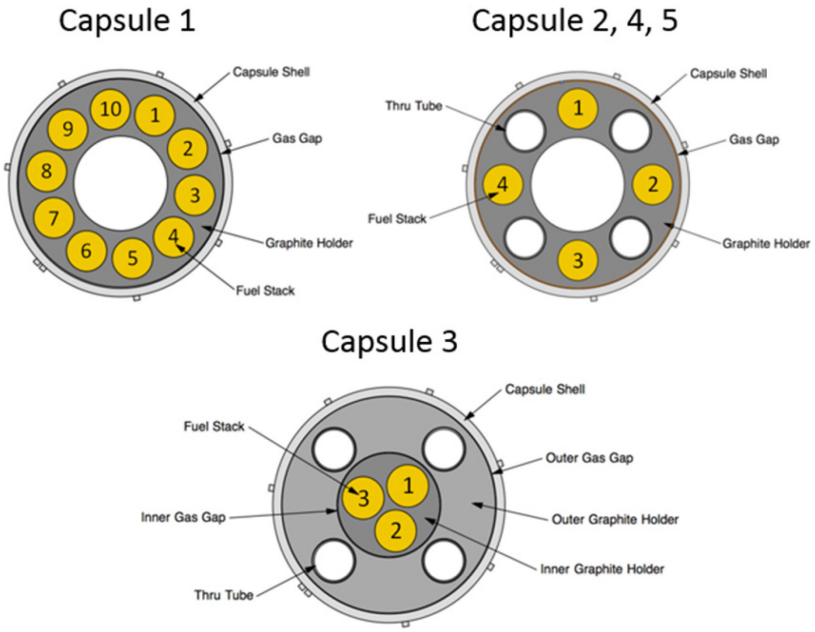

Figure S-1. Cross-section view of AGR-5/6/7 capsules.

S-3 Uncertainty of Input Parameters

The uncertainties in the input parameters of interest in the thermal model for the AGR-5/6/7 capsules were presented in Table S-1 along with the basis for the estimates. The input uncertainties in the gas gap width and neon fraction are dynamic, accounting for the effect of changes in the thermal properties of capsule components over extended exposure to high temperatures and fast neutron irradiation (e.g., gas gap width change assumptions add uncertainty to the gas gap).

Table S-1. Uncertainties of identified significant inputs to the thermal model of the AGR-5/6/7 capsule.

Parameter	One standard deviation	Rationale
Gas gap Inner gap in Capsule 3	24–40%	0.0254 mm, due to diameter measurement uncertainty 0.006 mm, due to 20% uncertainty in the graphite thermal expansion coefficient Graphite material shrinkage: increase gas gap size uncertainties from the start to the end of irradiation 0.127 mm radial clearance between the holder nubs and capsule shell (nub-to-shell clearance)
Neon fraction	Function of neon fraction	The uncertainty is based on a 1 sccm flow rate tolerance and estimated from the neon fraction prediction equation.
Fuel compact heat rate	5%	The same as for AGR-3/4 (Pham et al. 2016)
Graphite holders heat rate	3%	
Graphite conductivity	15%	
Fuel conductivity	20%	
Graphite emissivity	10%	According to the thermal modeler

S-4 Input Parameter Sensitivity

A parameter sensitivity analysis of the thermal model was performed to determine the sensitivity coefficients of the most influential variables. A sensitivity coefficient describes how the model calculated temperature would be influenced by changes in an input parameter. The overall uncertainty of the model output increases as the absolute sensitivity coefficient of an input parameter increases.

The sensitivity analysis performed here went beyond the traditional local sensitivity. Using experimental design, analysis of pairwise interactions of model parameters was also performed to establish the sufficiency of the first-order (linear) expansion terms in the uncertainty propagation formula of Equation (S-2). For each capsule, the sensitivity analysis was performed for 3 days throughout irradiation, and an interpolation scheme over the input parameter domain was then used to obtain time-dependent sensitivity. This enables uncertainty quantification for the instantaneous temperatures of fuel compacts and TCs over the whole irradiation period. The parameter sensitivity coefficients for all temperatures of interest in Capsule 3 for 1 day are presented in Figure S-2. Even though input sensitivities vary from capsule to capsule and from day to day during the irradiation, the pattern of input sensitivities is similar across capsules and time steps. The following conclusions can be drawn:

- For the heat rates, gas gap, and neon fraction (top panel in Figure S-2), the sensitivity coefficients of fuel heat rate (red bars) are highest for volume-averaged, peak fuel, and TC temperatures, followed by the neon fraction (blue bars) and then the gap width (purple bars). Of these inputs, the graphite heat rate (green bars) is least sensitive to the calculated temperatures.
- The sensitivity coefficients of the fuel compact thermal conductivity and graphite thermal conductivity (bottom panel in Figure S-2) are negative and less than 0.15 in absolute value for all temperatures of interest. The sensitivity coefficients of fuel thermal conductivity (orange bars) are near zero for TC temperatures, leading to a negligible impact on the uncertainty in these temperatures, but graphite conductivity sensitivities (light green) are non--zero for most temperatures of interest.
- The graphite emissivity in Capsule 3 (pink bars) is significant for fuel temperatures and TCs located in the inner holder (i.e., TC5, TC6, and TC8) because of the large drop in temperatures between the surfaces of the inner and outer holders. For the other four capsules (not shown in Figure S-2), the graphite emissivity is much less sensitive to all temperatures of interest.

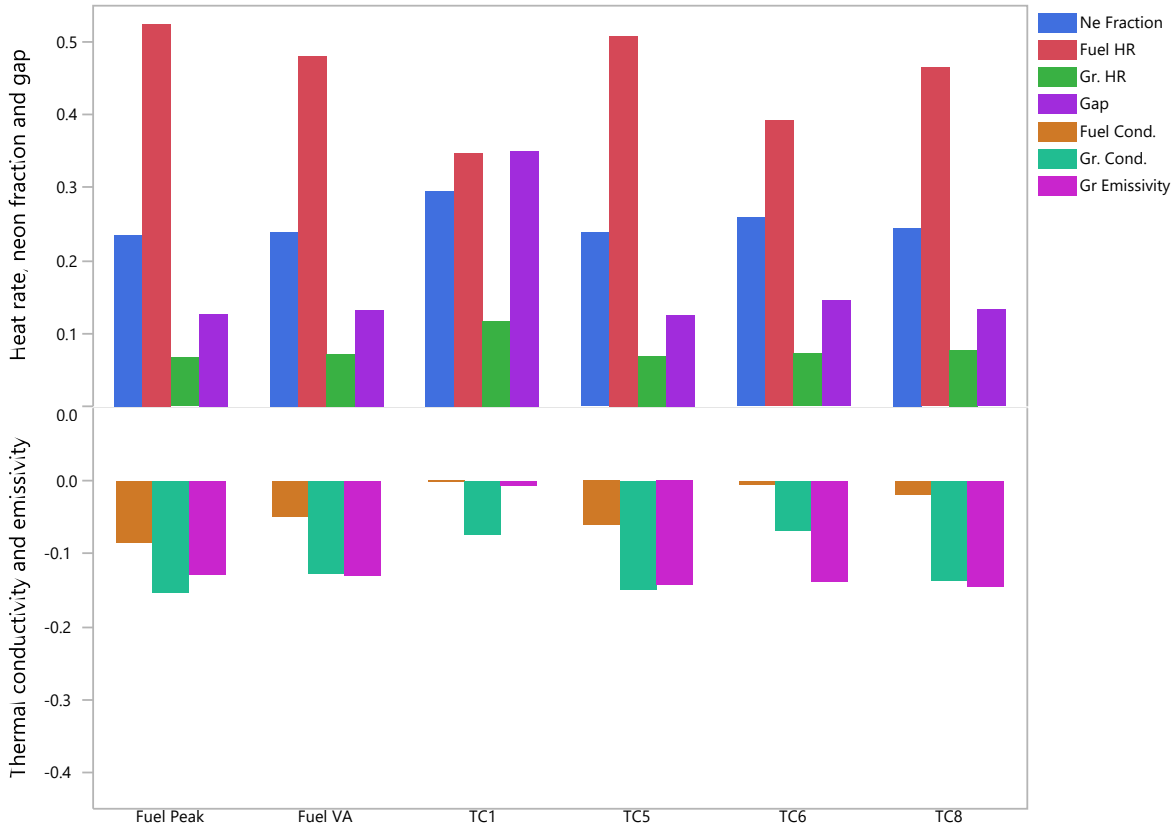

Figure S-2. Parameter sensitivity coefficients for fuel and TC temperatures in Capsule 3.

S-5 Combining Parameter Sensitivity and Uncertainty

The parameter uncertainty of a calculated temperature in terms of variance is obtained by propagating the model parameter uncertainty as the summation of the parameter variances, weighted by the squares of their sensitivity coefficients (Equation [S-2]). Thus, the effect of a parameter on the model prediction variation is the product of input uncertainty and its sensitivity coefficient. As an example, Figure S-3 shows the Capsule 5 daily input uncertainty, input sensitivity for peak fuel temperature, and resulting peak fuel temperature weighted variance as a function of EFPDs. The sensitivity plots are largely similar for all capsules but can be quite different for different temperatures (Figure S-2). The following impacts of each input uncertainty on the uncertainties of the calculated temperature can be seen:

- The gas gap has the highest relative input uncertainty (up to 22% at the start of irradiation, as shown by the cyan line in Panel 1 of Figure S-3 for Capsule 5). The gap sensitivities are also significant (~0.3 is shown in Panel 2 of Figure S-3). As a result, gas gap uncertainty is the most significant factor contributing to the uncertainty of the fuel temperature predictions (cyan line in Panel 3 in Figure S-3).
- The remaining six inputs (fuel and graphite heat rate, neon fraction, fuel and graphite thermal conductivities, and graphite emissivity) have an insignificant impact on the uncertainty in all temperatures of interest, due to low sensitivity and/or small input uncertainty (bottom panel in Figure S-3).

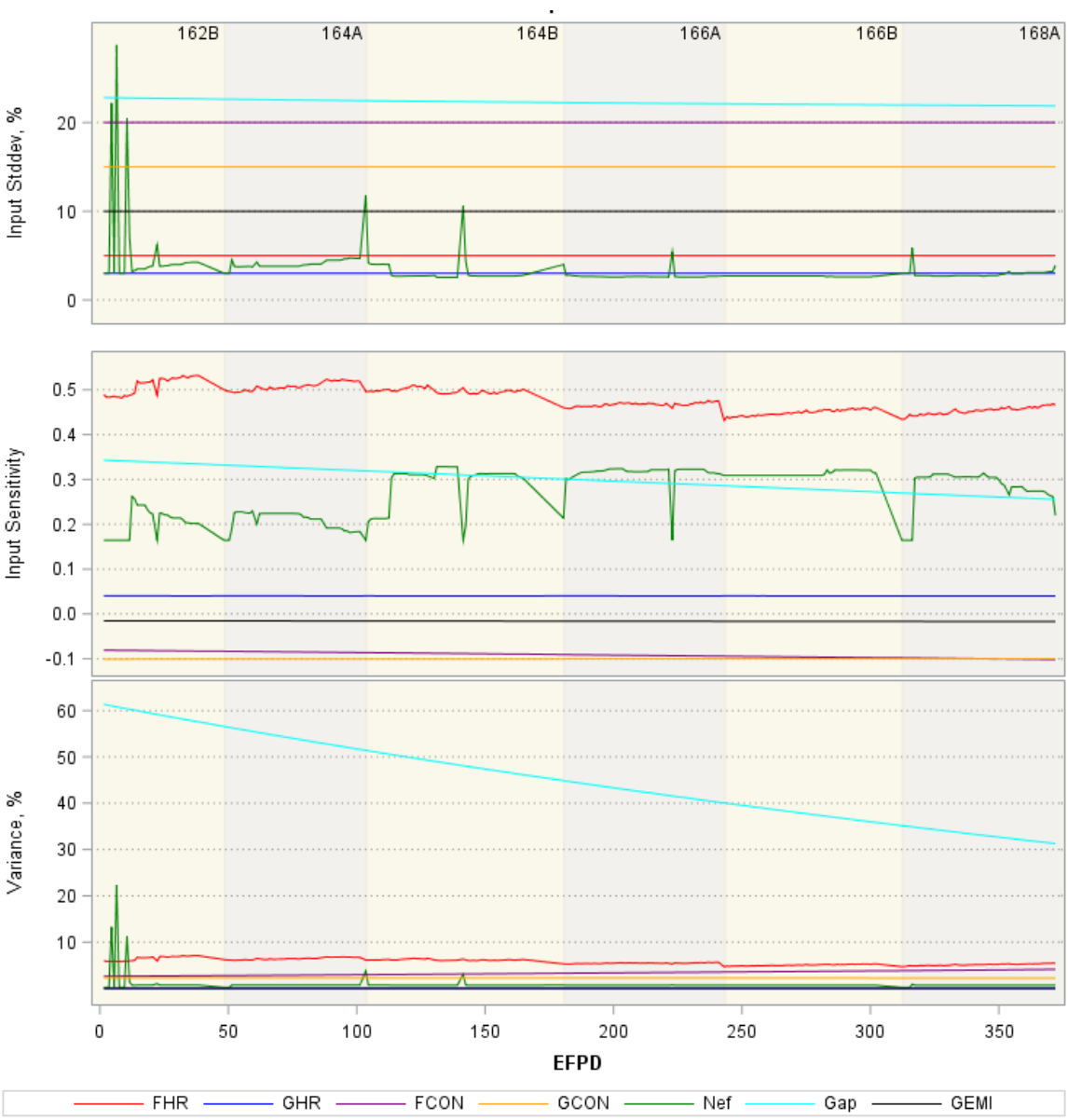

Figure S-3. Capsule 5 daily input uncertainty, and input sensitivity and weighted variance for peak fuel temperature during six regular cycles.

S-6 Overall Input Uncertainty

The overall uncertainty in all calculated temperatures of interest ranged from 7 to 14% (excluding a few peak uncertainties, as high as 15.8% in Capsule 2, due to a few high uncertainties in the neon fraction when the fraction was near zero). The uncertainties vary depending on irradiation time (thermal conditions), capsule, and the temperature parameter being calculated. The daily uncertainties in terms of the relative (%) and absolute (°C) standard deviations for instantaneous volume average (VA) and peak fuel, and of the TC temperatures in the five capsules, as a function of EFPDs, are presented in Figure S-3 and Figure S-5, respectively. Since the calculated uncertainties for several TCs are so close, only selected TC uncertainties are shown in these figures. Figure S-5 through Figure S-8 show daily calculated temperatures, together with one standard deviation for all temperatures of interest in the five capsules. For all capsules, the relative uncertainties decrease from the start to the end of irradiation, due to a decrease in the gap width uncertainty. This is caused by an increase in gap width over time, due to the graphite shrinkage with increasing neutron fluence.

Table S-2 summarizes the uncertainty for instantaneous temperatures of fuel compacts, averaged over the entire irradiation. The main factor leading to differences in temperature uncertainty across capsules is gas gap width uncertainty. Resulting highlights, based on Figure S-4 for relative uncertainty and Figure S-5 for absolute uncertainty, are:

- Capsule 1 uncertainties are in the range of 6.4–12.6% for fuel temperatures and 6.4–13.5% for TC temperatures.
- Capsule 2 uncertainties are similar for both fuel and TC temperatures, ranging from 6.3 to 15.8%.
- Capsule 3 has the lowest fuel temperature uncertainty (3.5–8.3%) because of lower gap width uncertainties. These are due to the relatively larger gaps and lower gap width sensitivity because fuel compacts are in the inner holder, away from the outer gap. However, the uncertainties for several TCs located in the outer holder (TC1 through TC4) are higher (up to 14%) due to higher gap sensitivity.
- Capsules 4 and 5 have higher uncertainty (up to ~10% for fuel temperatures at the start of irradiation) than Capsule 3, due to higher gas gap width uncertainties and sensitivity. Uncertainties for TC temperatures are higher (up to 11.1%) than fuel temperature because of higher gap width sensitivity.
- For AGR-1 and AGR-2, assuming negligible model bias, the relative uncertainty ranged from 3 to 4% for VA and 3 to 5% for peak fuel temperature. In addition, AGR-1 Capsule 6 had a 10% bias in the fuel heat rate, causing the overall uncertainty to increase to 5.8% for instantaneous, and 5.0% for time averaged, fuel temperature at the end of irradiation. Input temperature uncertainties for the AGR3/4 capsules were also similar (up to 5%). Compared to these experiments, the calculated temperature uncertainties for the five AGR-5/6/7 capsules are higher (up to 15.8% in Capsule 2) than those seen in the AGR-1, AGR-2, and AGR-3/4 capsules because of significantly higher gap width uncertainty due to the nub-to-shell clearance.

Table S-2. Uncertainty range for instantaneous temperature averaged over the entire irradiation.

	TCs	Peak Fuel	Volume-Averaged Fuel	Peak Fuel	Volume-Averaged Fuel
	Relative Standard Deviation % [°C/°C]			Standard Deviation °C	
Capsule	Instantaneous Temperature (min – max)				
5	6.8 – 9.5	6.9 – 9.9	6.9 – 9.8	46 – 76	38 – 65
4	6.5 – 11.1	6.5 – 11.1	6.6 – 10.8	49 – 95	43 – 82
3	3.5 – 14.0	3.5 – 8.3	3.6 – 8.3	42 – 89	39 – 78
2	6.5 – 15.8	6.3 – 15.7	6.5 – 15.8	46 – 122	41 – 107
1 (Excluding 168A)	6.4 – 13.5	6.4 – 12.6	7.2 – 14.4	77 – 143	67 – 130

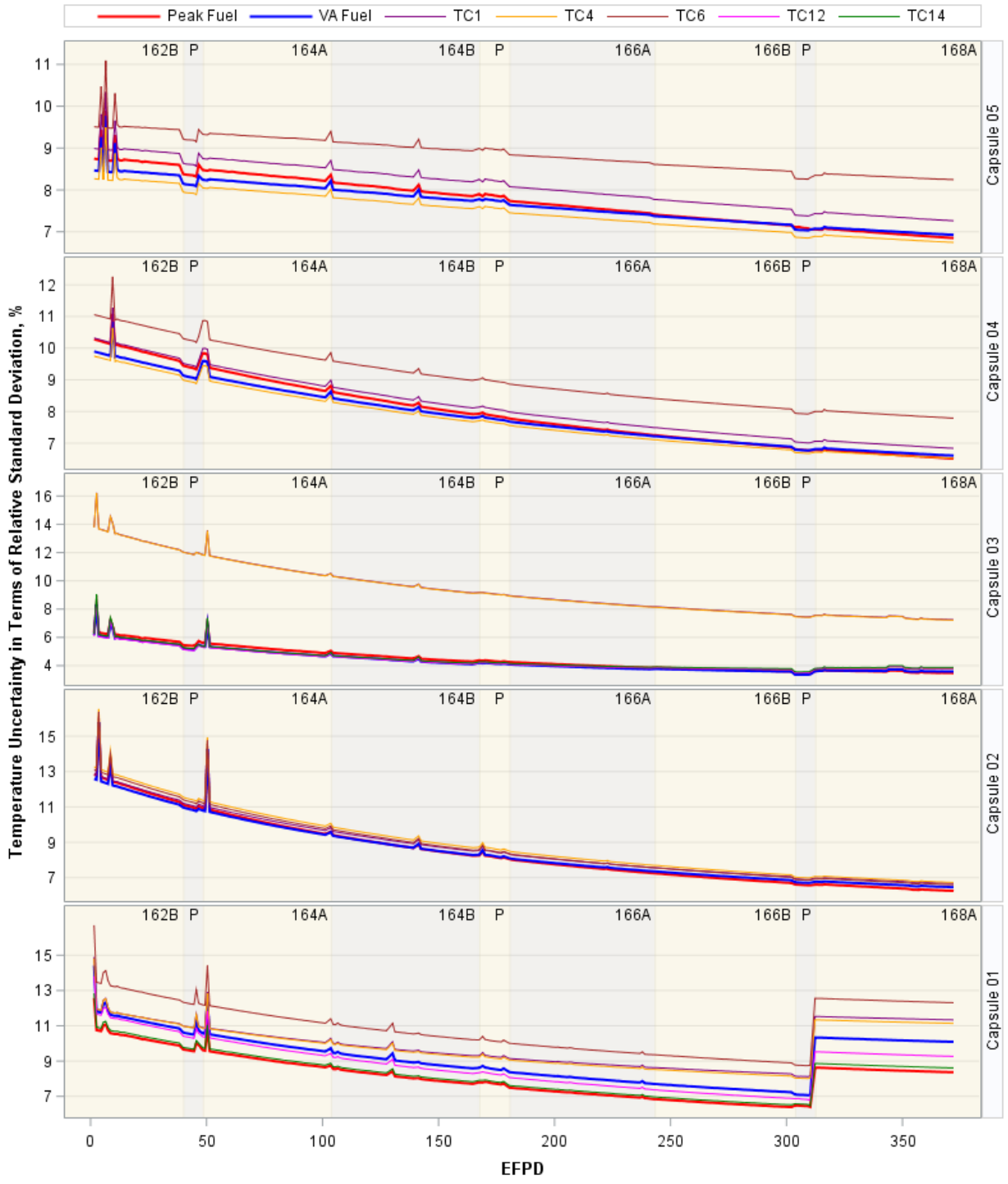

Figure S-4. Daily uncertainty in terms of relative standard deviation for temperatures of interest ("P" – short PALM cycles 163A, 165A, and 167A).

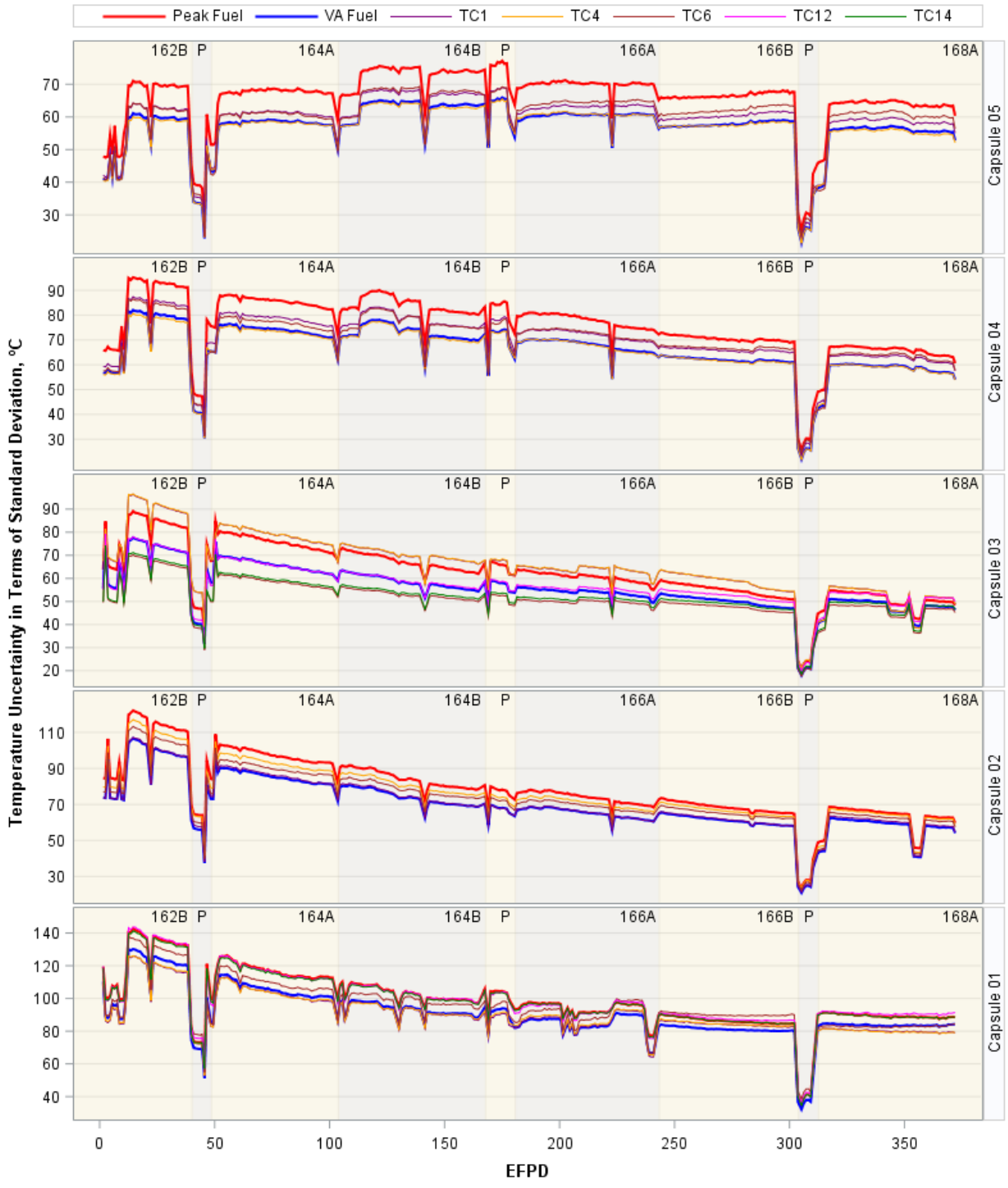

Figure S-5. Daily uncertainty in terms of standard deviation for temperatures of interest ("P" – short PALM cycles 163A, 165A, and 167A).

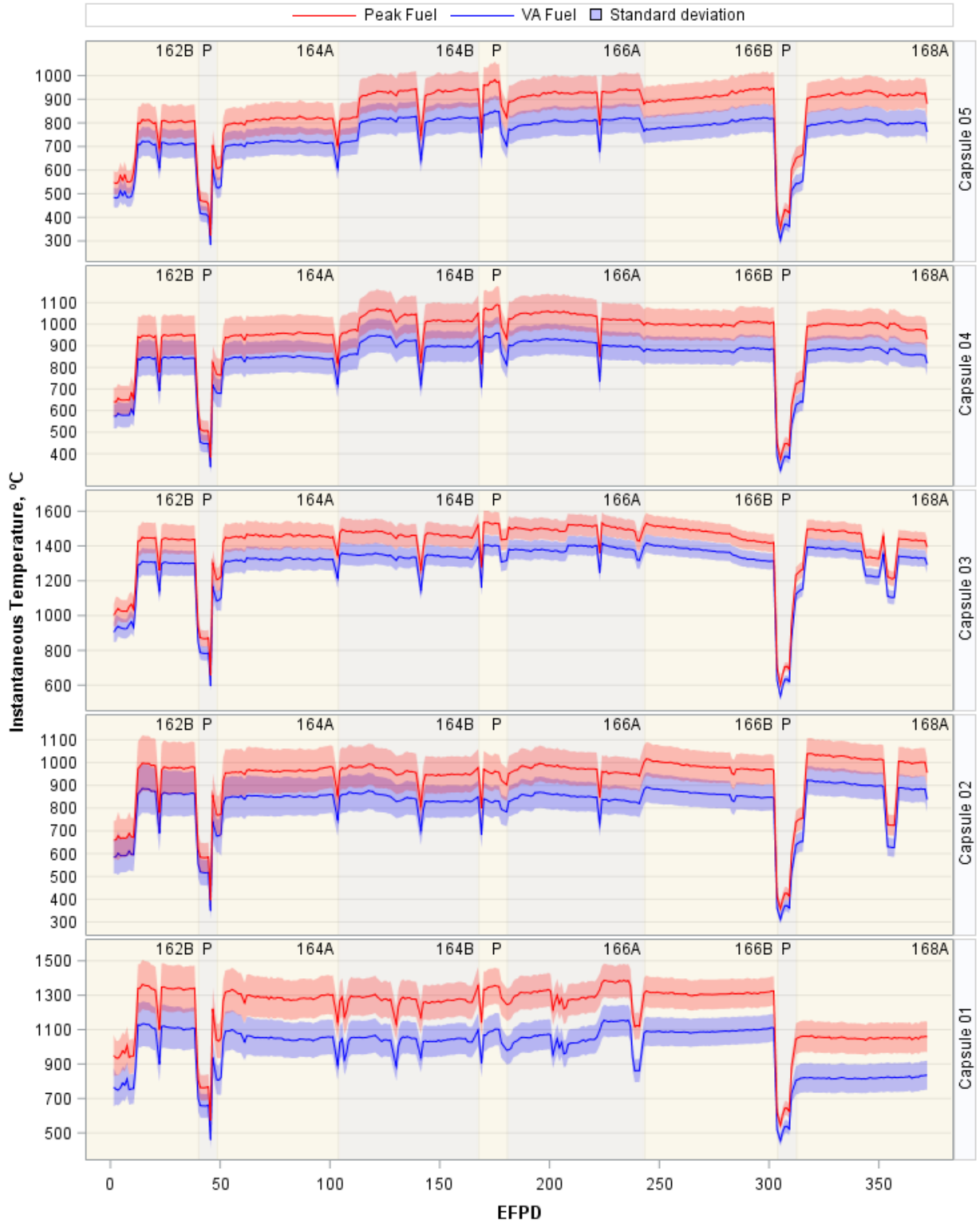

Figure S-6. Instantaneous volume average- fuel and peak fuel temperatures with uncertainty bars ("P" – short PALM cycles 163A, 165A, and 167A).

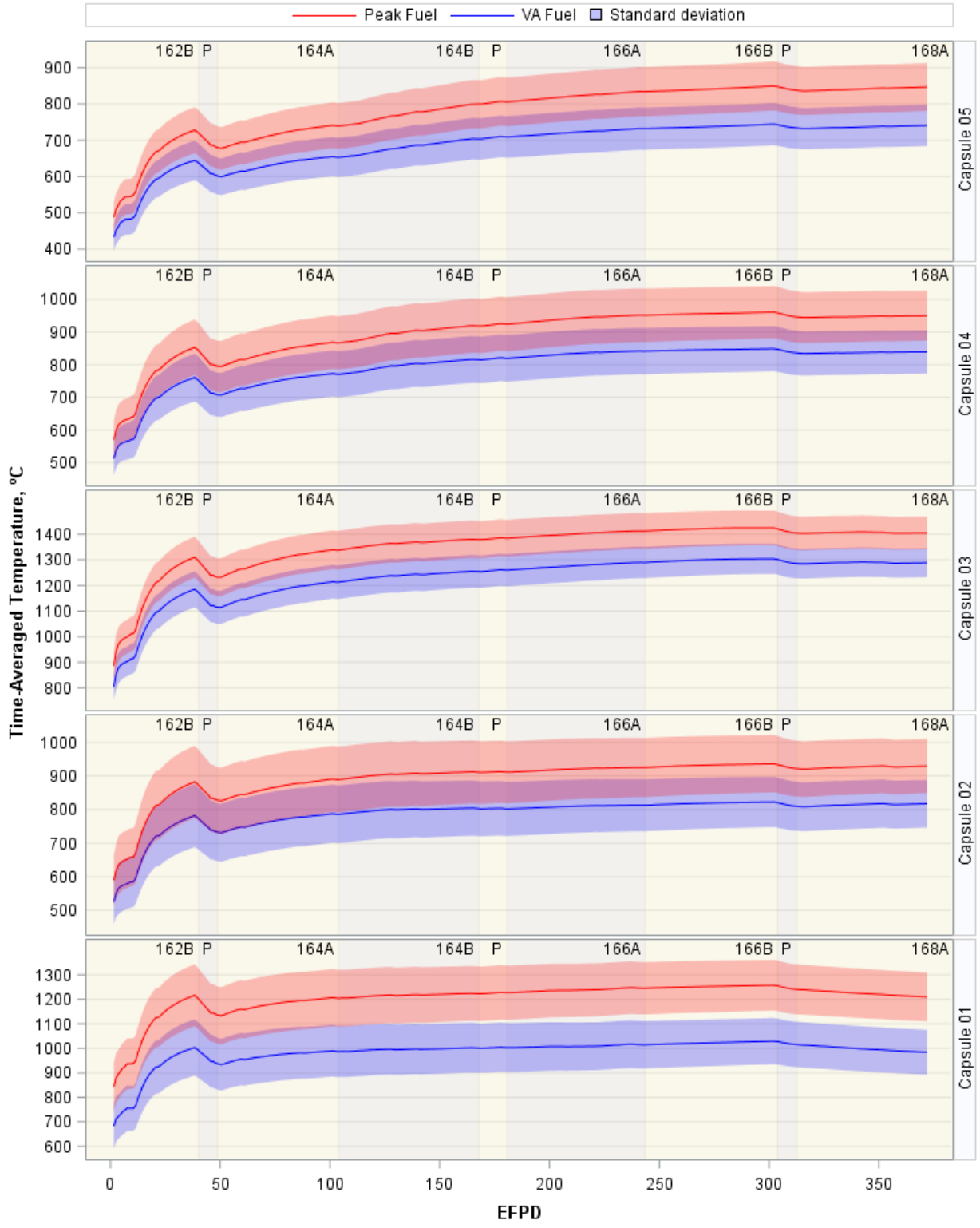

Figure S-7. Time--averaged volume -average fuel and peak fuel temperatures with uncertainty bars ("P" – short PALM cycles 163A, 165A, and 167A).

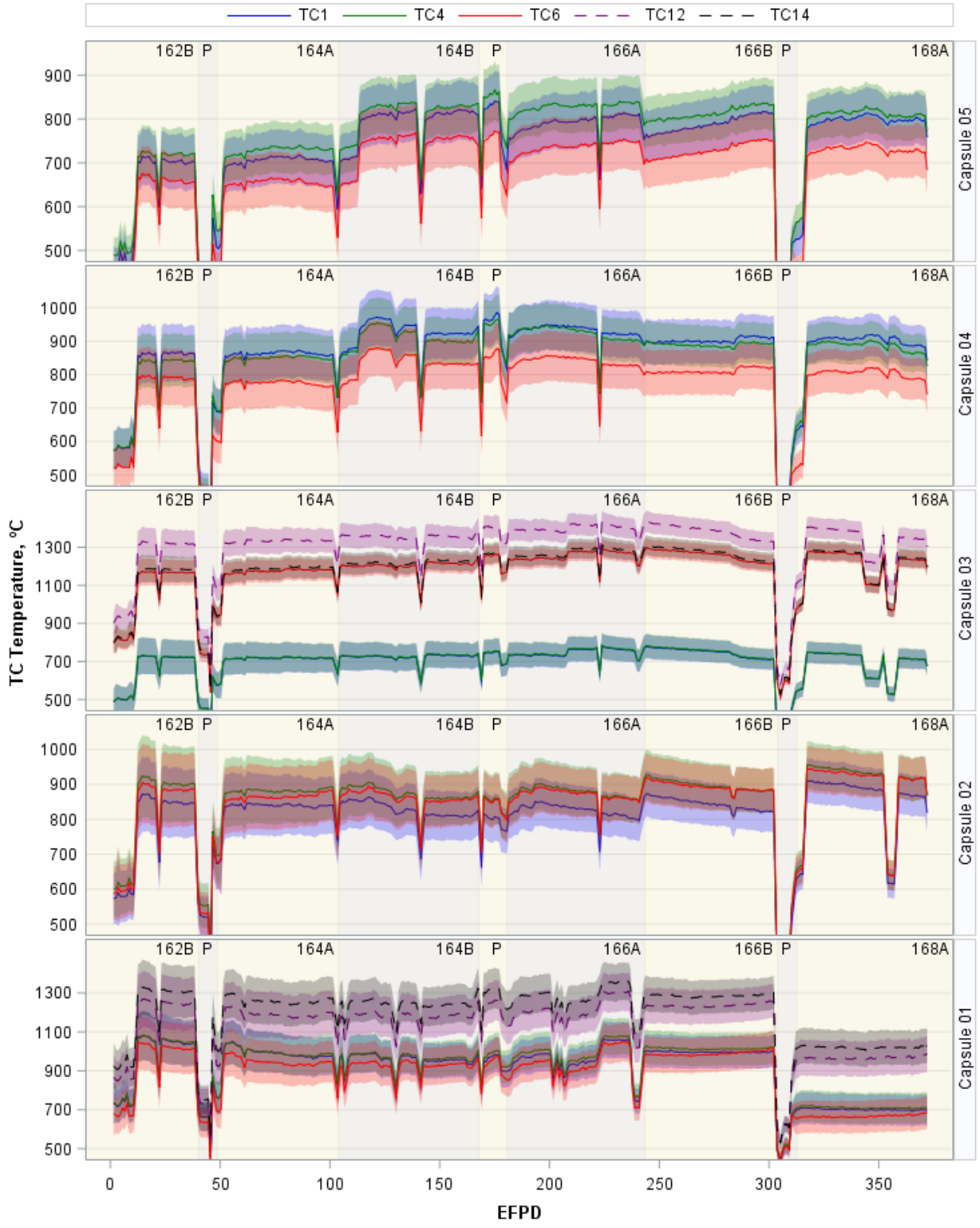

Figure S-8. Instantaneous TC temperatures with uncertainty bars ("P" – short PALM cycles 163A, 165A, and 167A).

S-7 Report Structure

The report is organized into four sections and a conclusion.

- Section 1 introduces the AGR Fuel Development and Qualification Program
- Section 2 summarizes the AGR-5/6/7 measured data, test configuration, and test procedure,
- Section 3 describes the AGR-5/6/7 thermal simulation.
- Section 4 describes the estimation of uncertainties and sensitivities for the thermal model input parameters. This includes parameter uncertainties based on expert judgment, sensitivity analysis of input parameters, and the estimation of correlation coefficients for pairs of input parameters. This section also describes the propagation of uncertainties and sensitivities for estimating the overall uncertainty for the daily VA and peak fuel temperatures, the daily average temperatures at TC locations, and the time-averaged VA and time-averaged peak fuel temperatures.
- Section 5 presents the results of the uncertainty analysis for each of the five AGR-5/6/7 capsules and discusses the parameters driving the uncertainty.
- The Conclusion summarizes the important findings of the uncertainty quantification and identifies possible areas of improvement.

CONTENTS

FIGURES

TABLES

ACRONYMS

AGC	Advanced Graphite Creep
AGR	Advanced Gas Reactor
ART	Advanced Reactor Technologies
ATR	Advanced Test Reactor
ECAR	engineering calculations and analysis report
EFPD	effective full power day
EOI	end of irradiation
FC	fuel thermal conductivity
FHR	fuel heat rate
FT	fuel temperature
GC	graphite thermal conductivity
GHR	graphite holder heat rate
GE	graphite emissivity
GG	gas gap
INL	Idaho National Laboratory
N/A	not applicable
NDMAS	Nuclear Data Management and Analysis System
NeF	neon fraction
NEFT	northeast flux trap
RMS	root mean square
SOI	start of irradiation
TA	time averaged
TC	thermocouple
TE	thermal expansion
TRISO	tristructural isotropic
VA	volume averaged

Uncertainty Quantification of Calculated Temperatures for AGR-5/6/7 Experiment

1. INTRODUCTION

A series of Advanced Gas Reactor (AGR) irradiation experiments were conducted within the Advanced Reactor Technologies (ART) Fuel Development and Qualification Program. The main objectives of the fuel experimental campaigns are to provide the necessary data on fuel performance to support fuel process development, qualify a fuel design and fabrication process for normal operation and potential accident conditions, and support the development and validation of fuel performance and fission product transport models and codes (Mitchell 2020). The AGR-5/6/7 experiment, the last in this series, was inserted in the northeast flux trap (NEFT) position in the Advanced Test Reactor (ATR) core at Idaho National Laboratory (INL) in December 2017. The irradiation began on February 16, 2018, and was completed July 22, 2020, resulting in irradiation of the tristructural isotropic (TRISO) fuel for 360.9 effective full power days (EFPDs) over roughly two and a half years. The AGR-5/6/7 experiment data, including the irradiation data and calculated results, were qualified in the data qualification report (Pham 2021) and summarized in the as-run report (Pham et al. 2021).

To support AGR TRISO fuel performance assessment and provide data for the validation of fuel performance and fission product transport models and codes, a daily as-run thermal analysis was performed for each of the five AGR-5/6/7 capsules for the entire irradiation, as discussed in Hawkes (2021). The ABAQUS code's finite-element-based thermal model predicts the daily average volume-averaged (VA) fuel temperature (FT) and peak FT in each capsule. Fast fluence and fission heat rate data for all components (e.g., fuel compacts, graphite holders, and the stainless-steel capsule shell) are input to the ABAQUS model. They are the results from full-core MCNP models and Oak Ridge Isotope Generation (ORIGEN2) radionuclide generation models coupled using the MCNP ORIGEN Coupled Utility Program, JMOCUP, which also performs depletion calculations (Sterbentz 2020).

Graphite temperatures from thermocouples (TCs) in each capsule during the first cycle were used to calibrate the thermal analysis codes. However, given the possible TC failure under the harsh irradiation and thermal conditions in the AGR-5/6/7 capsules, the thermal analysis results also aid in the TC data qualification process by affording increased confidence in identifying measuring instruments failures due to physical mechanisms that may have shifted the system thermal response (Pham and Einerson 2011).

The thermal model involves complex physical mechanisms (e.g., graphite holder and fuel compact shrinkage) and properties (e.g., conductivity and density). The thermal model predictions are affected by uncertainty in the input parameters and by incomplete knowledge of the underlying physics, leading to modeling assumptions. Therefore, along with the deterministic predictions from a set of input thermal conditions, information on prediction uncertainty is instrumental for the ART program's decision-making process. Well-defined and reduced uncertainty in model predictions helps increase the quality of and confidence in AGR technical findings (Pham et al. 2013, 2014). To quantify the uncertainty in calculated temperatures, potentially important ABAQUS thermal model input parameters are first identified, and then a large suite of simulations is conducted to examine the model sensitivity to those parameters. The identification process consists of two stages: (1) using expert judgment to estimate parameter uncertainties and identify those parameters with the largest uncertainties, and (2) using sensitivity analysis to determine parameters to which the modeling is most sensitive. A set of parameters is selected for quantifying the uncertainty of the calculated temperatures, including those to which the model is highly sensitive and those with large uncertainty. The parameter uncertainties and sensitivity coefficients are combined and propagated to quantify the parameter uncertainty of the temperature outputs. That uncertainty is then compared to an estimate of model error based on the TC measurements obtained during the first few cycles of irradiation, when the TC values are most reliable and most abundant.

2. ADVANCED GAS REACTOR-5/6/7 EXPERIMENT

AGR-5/6/7 was the last of a series of AGR experiments sponsored by ART and conducted in the ATR at INL. The primary experimental objectives were to verify the performance of the reference-design fuel for high-temperature gas reactor (HTGR) normal operating conditions (AGR-5/6) and to explore fuel performance at temperatures substantially beyond those typical of normal operation (AGR-7) in order to establish the temperature margin for acceptable performance (Mitchell 2020). The AGR-5/6/7 test train was inserted into the NEFT location of the ATR core (Figure 1) in December 2017.

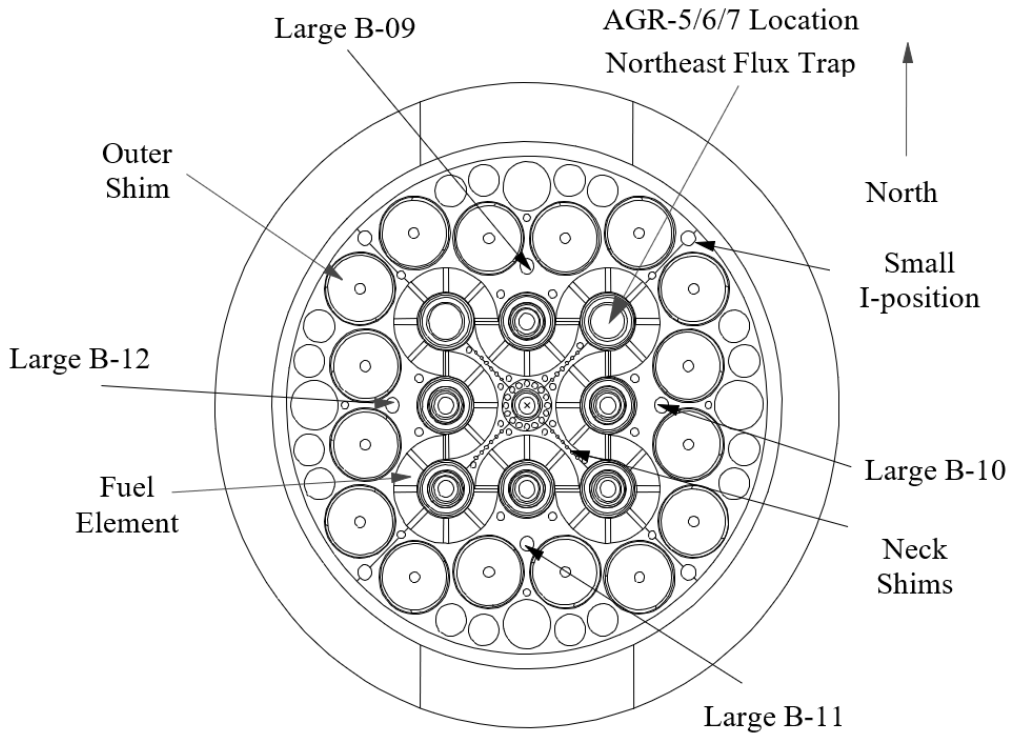

Figure 1. AGR-5/6/7 northeast flux trap location in the Advanced Test Reactor core cross section.

The AGR-5/6/7 test train was comprised of five independently controlled and monitored capsules stacked on top of each other to form a test train using the full 1.22 -m active core height (Figure 2). A stainless-steel leadout tube holds the experiment in position and contains and protects the gas lines and TC wiring extending from the test train to the reactor penetration. Capsules 1, 2, 4, and 5 constitute AGR-5/6, while the margin test AGR-7 is associated with Capsule 3. The experiment was instrumented with 54 TCs that terminated in graphite holders, but 48 had failed by the end of irradiation (Pham et al. 2021). Figure 3 shows the daily average temperatures of all functioning TCs as a function of EFPDs.

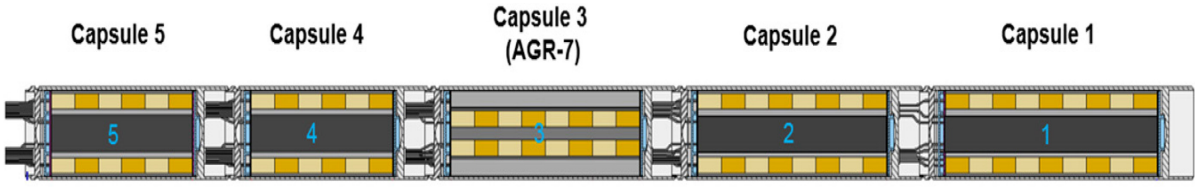

Figure 2. Schematic view of the AGR-5/6/7 test train, rotated 90° from actual orientation (Capsule 5 is at the top of the test train).

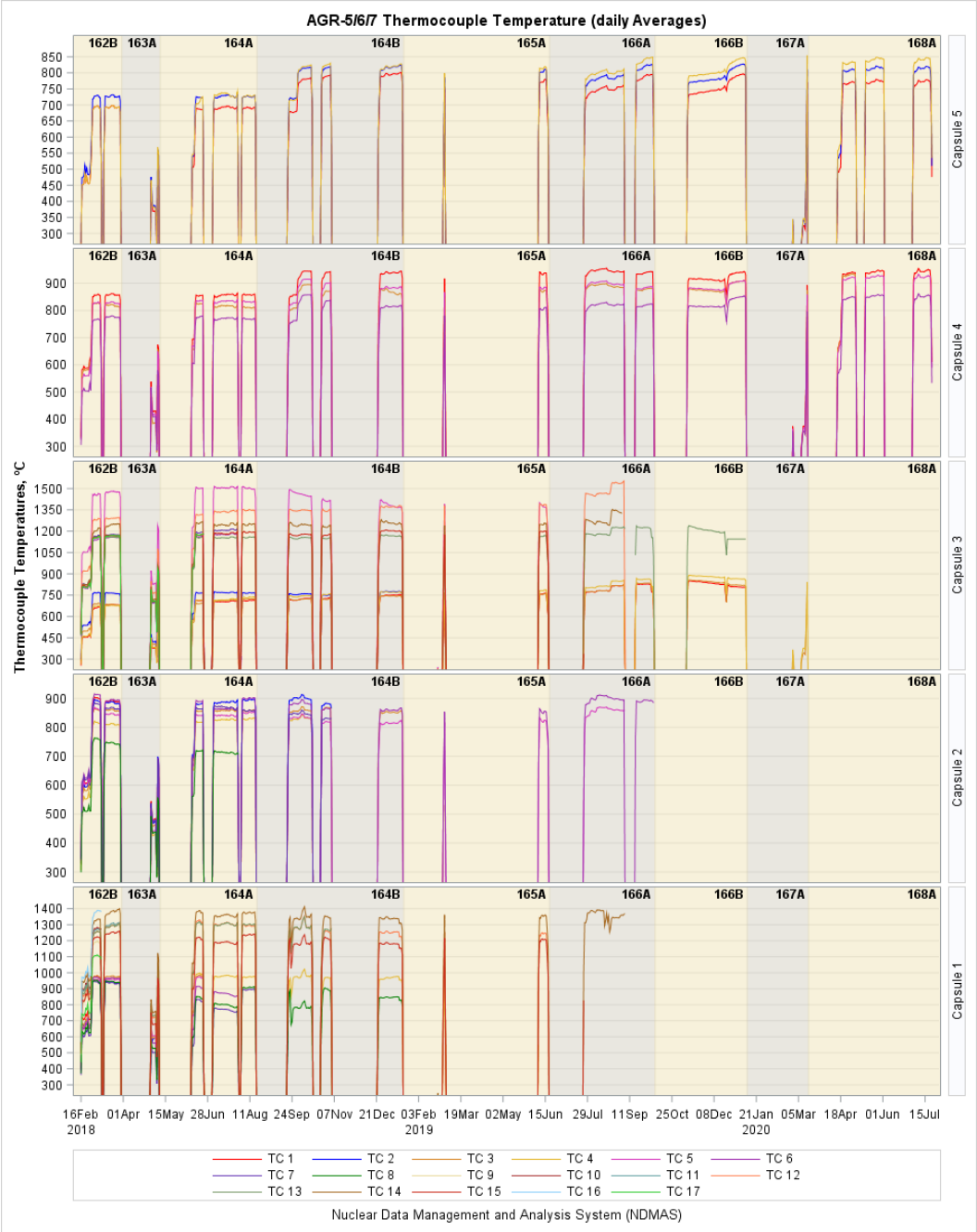

Figure 3. AGR-5/6/7 daily average measured TC temperatures.

3. THERMAL MODEL FOR AGR-5/6/7 CAPSULES

3.1 Capsule Configuration

Each capsule contains various numbers of fuel compacts—nominally 25.3 mm in length and 12.3 mm in diameter—housed in several stacks within a graphite holder (Figure 4). Capsule 1 has 10 fuel stacks; capsules 2, 4, and 5 have four stacks located in the hollow cylinder graphite holder; and capsule 3 has three stacks arranged in an inner graphite holder to raise the temperature. Thru tubes are in capsules 2–5 to hold the TC wires and gas lines. The ATR coolant water flows downward on the outside of the capsules at approximately 40 ft/s and enters the experiment at 125°F.

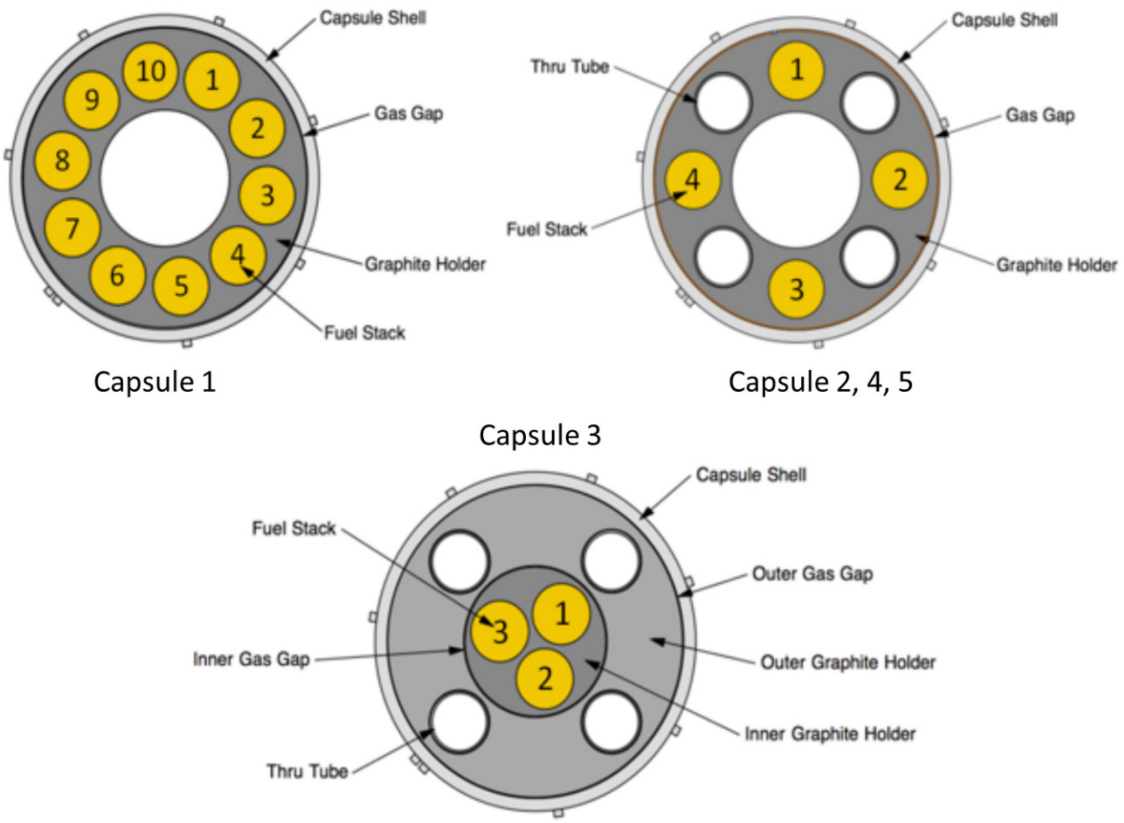

Figure 4. Cross sections of the AGR-5/6/7 capsules, showing the compact stacks and thru tubes.

For temperature control, each capsule had an independent gas line to route a helium/neon gas mixture with a variable composition. This helium/-neon gas mixture flowing through the temperature-control gas gaps between the graphite holder and stainless-steel shell is regulated to maintain target readings of the designated control TC. Periodically, the control TC temperature is redefined so that the target fuel stays within a control band. In addition, the fuel temperature control was achieved by adjusting the northeast lobe power and changing the neutron filter on the outside of the experiment for each cycle as the AGR--5/6/7 fuel depleted. A summary of capsule properties is shown in Table 1. The axially variable temperature-control gas gaps were designed to shape the temperature profile of the compacts. However, the thermal models assumed only two gap widths (top half and bottom half) for each capsule, except Capsule 3, which had three different gap widths for the control gas gap.

Table 1. Summary of properties of AGR-5/6/7 capsules.

	N# of Compacts (levels/stacks)	Number of TCs (installed/failed)	Target Temperature Range (°C)	Avg. Capsule Shell Radii, mm	Avg. Holder Radii, mm
Capsule 5	24 (6/4)	6/3	<900	32.366	32.106
Capsule 4	24 (6/4)	6/3	900 – 1050	32.373	32.146
Capsule 3	24 (8/3)	17/17	1350 – 1500	32.365	32.189
Capsule 2	32 (8/4)	8/8	900 – 1050	32.373	32.188
Capsule 1	90 (9/10)	17/17	900 - 1350	32.368	32.189

3.2 Thermal Model

One ABAQUS-based (version 6.14.2) three-dimensional finite element thermal model was created for each of the five AGR-5/6/7 capsules to predict the daily average temperatures of fuel compacts and TC locations throughout the entire irradiation period in which the ATR core is at power. The ABAQUS thermal model uses a finite element mesh composed of approximately 1,200,000 hexahedral finite-element bricks to estimate temperature profiles for the entire capsule train, as shown in Figure 5. Validation of ABAQUS version 6.14.2 was performed by using 10 thermal models to validate the different aspects of ABAQUS's heat transfer abilities. The maximum difference between the ABAQUS-calculated values and the exact theoretical values is just under 2.25% (Hawkes 2021).

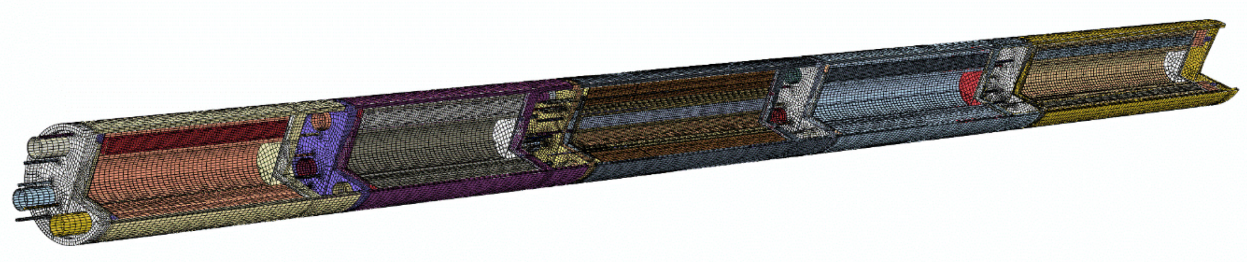

Figure 5. Cutaway view of finite element mesh of the entire capsule train (Hawkes 2021).

Heat transfer through the gas gaps occurs mainly via conduction (about 80 to 85%) and radiation (about 15 to 20%); the advection is negligible (<0.01%), due to the very low gas flow rate (typically ~50 cm^3/min). Graphite shrinkage due to the fast neutron fluence and graphite thermal expansion is incorporated into the gas gap model over irradiation time. Thus, gas gap change is a function of fast neutron fluence and thermal expansion. Only conductive heat transfer through the helium-neon gas mixture (used for temperature control), along with surface-to-surface radiation heat transfer, was used in the thermal calculations. The negligible advection heat transfer was omitted.

The governing equation of steady-state conductive heat transfer is expressed as (Hawkes et al. 2015):

$$0 = \frac{\partial}{\partial x}\left(k(T)\frac{\partial T}{\partial x}\right) + \frac{\partial}{\partial y}\left(k(T)\frac{\partial T}{\partial y}\right) + \frac{\partial}{\partial z}\left(k(T)\frac{\partial T}{\partial z}\right) + \dot{q} \quad (1)$$

where

T is temperature
x, y, and z are the directions
$k(T)$ is the thermal conductivity, which varies with temperature and neutron fluence
q is the heat source.

The governing equation for radiation heat transfer across a gas gap is:

$$q_{net} = \frac{\sigma\left(T_1^4 - T_2^4\right)}{\frac{(1-\varepsilon_1)}{\varepsilon_1 A_1} + \frac{1}{A_1 F_{12}} + \frac{(1-\varepsilon_2)}{\varepsilon_2 A_2}} \quad (2)$$

where

q_{net} is the net heat flux
σ is the Stephan Boltzmann constant
T_1 and T_2 are the surface temperatures
ε_1 and ε_2 are the emissivities of Surfaces 1 and 2, respectively
A_1 and A_2 are the areas of Surfaces 1 and 2, respectively
F_{12} is the view factor from Surface 1 to 2.

The main time -series inputs to the model are daily-component-specific (fuel compacts, graphite holders, and other components) heat rates and fast neutron fluences calculated from the as-run depletion analysis (Sterbentz 2020), as well as the daily gas composition of the helium/neon mixture (neon fraction). The fast neutron fluence is needed for calculating the components' thermal conductivity and estimating the gas gap sizes over the course of the irradiation.

Figure 6 presents, in a cutaway view, an example of the temperature distribution in Capsule 1 compacts (Hawkes 2021). The fuel temperatures in Capsule 1 varied over a wide range [683 to1325°C] because of non-uniform heating across its tall stacks of fuel (nine compacts each). The calculated daily average fuel compact maximum, average, and minimum temperatures as a function of irradiation day (Figure 7) indicated that fuel temperatures were stable throughout irradiation for all capsules, except for a few short periods when the test trains were forced to run on pure helium (i.e., PALM Cycles 163A and 167A, or Cycle 168A for Capsule 1 when its gas line was isolated).

While no direct measurements of FTs are available, the temperatures from the TCs in the graphite holders in the AGR-5/6/7 capsules were used to validate computer codes throughout the irradiation period by minimizing the differences between the calculated and the measured TC temperatures. The model-calculated daily temperature for each TC, along with the TC readings during the first cycle (162B), were used for this model calibration, adjusting input parameters (e.g., Neolube thickness) within their expected ranges to achieve the best match between the measured and the calculated TC temperatures. Figure 8 shows a history plot of the TC residual temperatures (measured minus calculated) for all EFPDs for all cycles. A modest match between the calculated and the measured TC temperatures during the first cycle was achieved, and similar results are seen in Cycles 163A–168A.

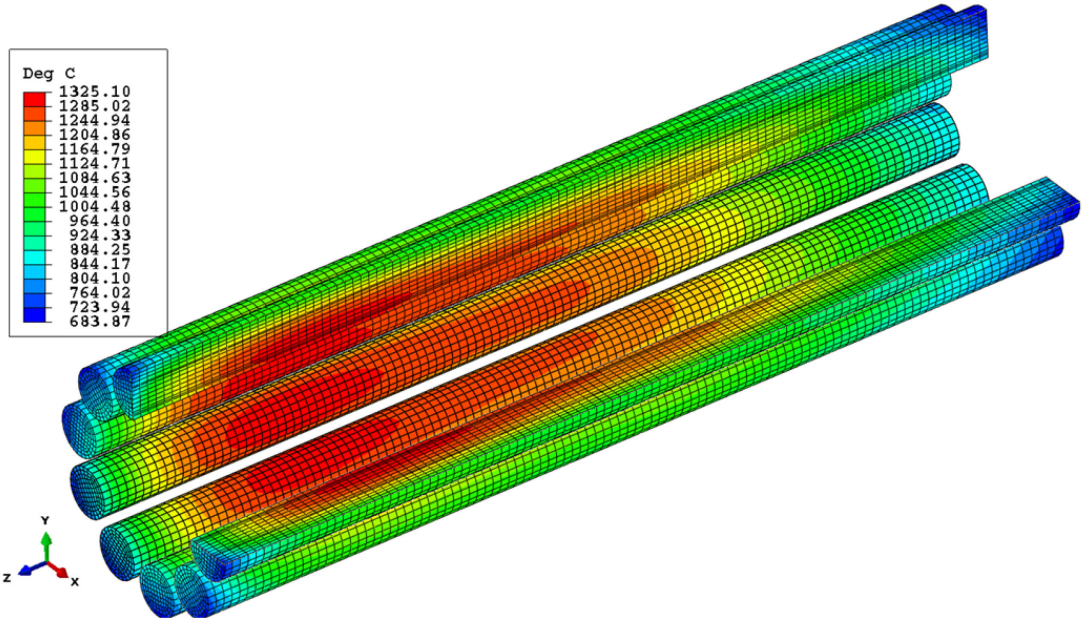

Figure 6. Temperature contour plot cutaway view of Capsule 1 fuel during Cycle 162B, day 20.

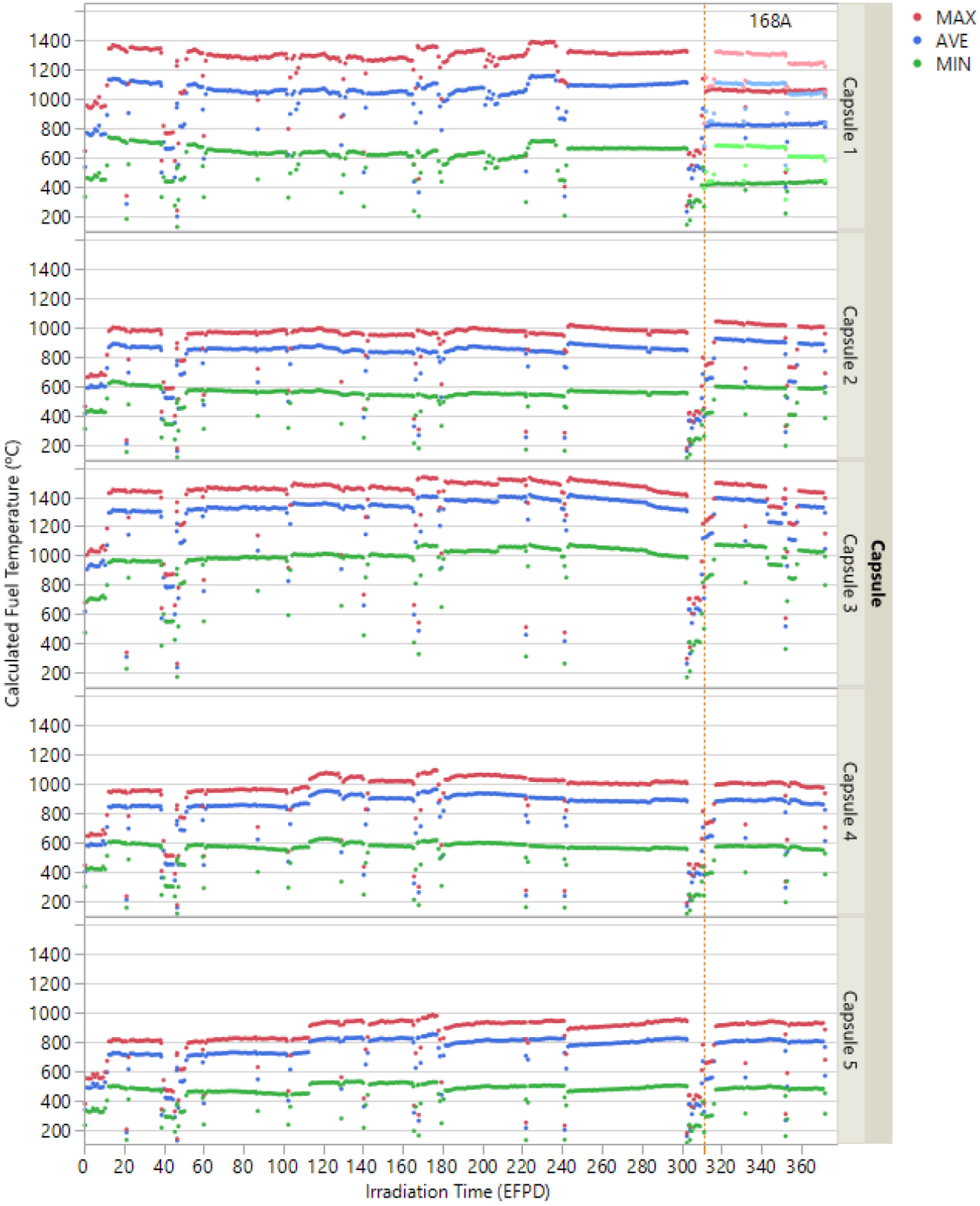

Figure 7. Daily minimum, maximum, and VA fuel temperatures (the light-colored dots for Capsule 1 are for the assumed leadout neon fraction [instead of zero]).

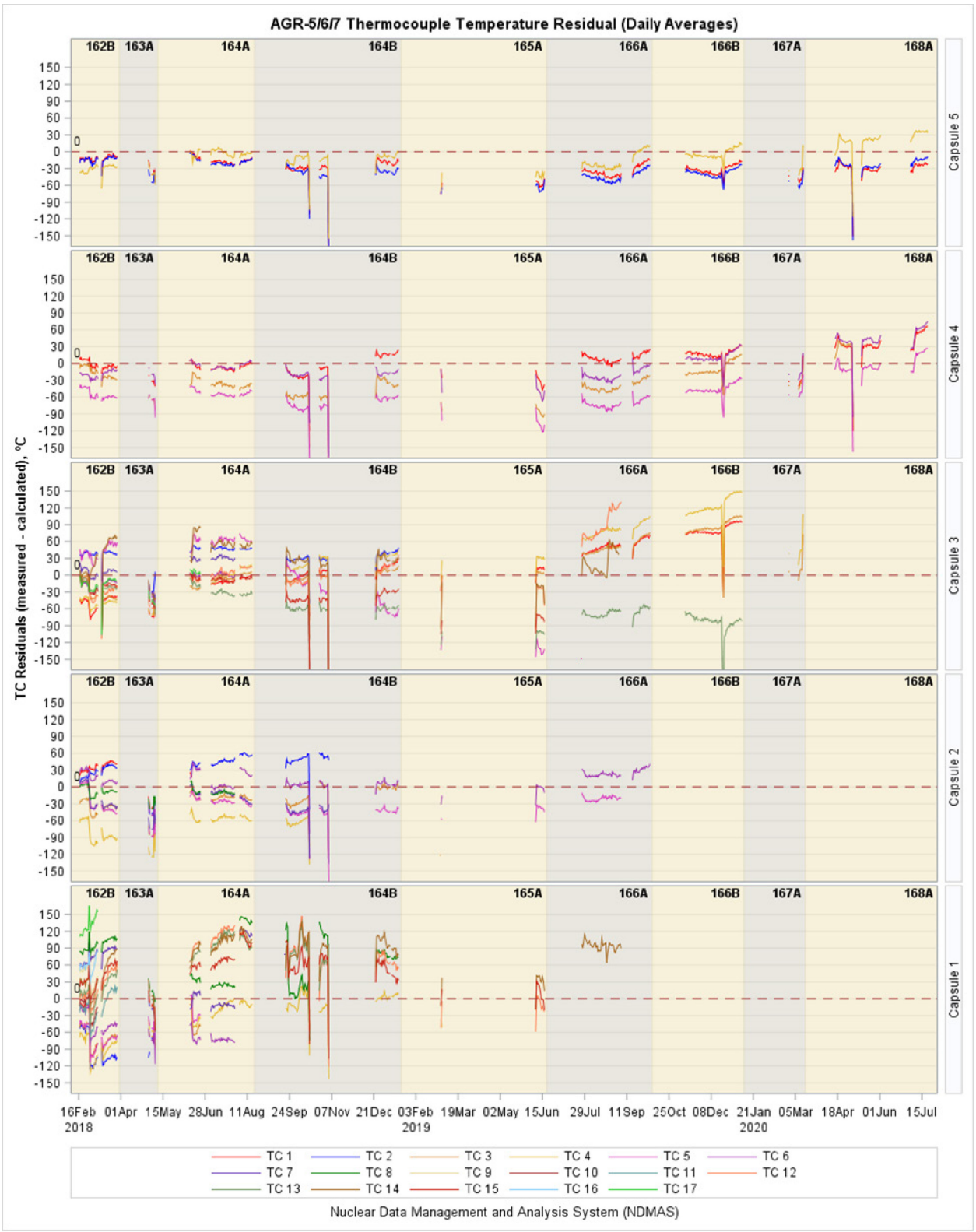

Figure 8. Difference between the measured and the calculated thermocouple temperatures for each capsule.

For calculated temperatures, uncertainties arise due to uncertainties in thermal properties and phenomena such as heat—and neutron—induced changes in the capsule gas gaps. The following is a list of uncertainty factors and model assumptions known to contribute to the uncertainty in calculated temperature (Hawkes 2021):

1. Unknown offset of the holder, due to the 0.127 mm (0.005 in.) clearance between the outside of the nubs and the capsule shell according to the drawing.
2. All dimensions are based on nominal drawing values, except that the average compact diameter for each fuel stack and the appropriate graphite holder hole were used to calculate the compact-holder gas gap.
3. Gas gaps were modeled as changing linearly with time in response to the IG-430 graphite dimensional change with fast neutron fluence.
4. A thickness for the Neolube (a thin layer of the graphite lubricant coated on the capsule shell surface) was assumed for each capsule during the calibration process. This reduced the gap between the graphite holder and capsule wall by 0.0381 mm in Capsules 1–4, and by 0.0457 mm in Capsule 5.
5. The thermal expansion of the graphite holder (varying with fast neutron fluence and temperature) was calculated using the graphite holder annulus mean radial temperature collected at every 2.54 mm of elevation on southeast side of annulus.
6. Compact and various component heat rates were taken from (Sterbentz 2020).
7. Graphite and compact thermal conductivity vary with fluence and temperature, as taken from legacy experiment correlations and scaled for AGR-5/6/7 material density.
8. The gas mixture (helium/neon) thermal conductivity is taken from a report from Brown University (Kestin et al. 1984).
9. Heat transfer through gas occurs via conduction and radiation only, advection is insignificant.
10. Radiation heat transfer occurs across all gas gaps. An emissivity of 0.3 was assumed for the stainless steel, an emissivity of 0.90 for the graphite and grafoil, and an emissivity of 0.52 for the zirconium and zirconia components.
11. The contents of the through tubes are not specifically modeled. A heat flux representing the heat generated from these TCs and gas lines is implemented for each through tube for each capsule.
12. Perfect thermal contact between compacts is assumed.

Several of these uncertainty sources can be estimated and considered as uncertainties of inputs to the thermal model, then used to determine the parameter uncertainty of the calculated temperatures. Impacts from some uncertainty sources (i.e., items 11 and 12, above) are largely unknown, and those effects may contribute to any model bias.

4. UNCERTAINTY QUANTIFICATION OF MODEL-CALCULATED TEMPERATURE

4.1 Technical Approach

In general, the overall uncertainty in the prediction of a simulation model arises from two main sources: input uncertainty and model uncertainty. This is assuming that the numerical errors can be considered negligible when using sufficient resolution of the finite element mesh in the computing code. Thus, the total uncertainty, σ_T, of the simulation predictions in terms of variance can be expressed as the sum squares of model form uncertainty and parameter uncertainty:

$$\sigma_T^2 = \sigma_M^2 + \sigma_P^2 \quad (3)$$

where

σ_T = overall uncertainty of calculated temperature in terms of standard deviation
σ_M = model form uncertainty
σ_P = parameter uncertainty in terms of standard deviation.

The model form uncertainty term includes the effects of choices made in the modeling process that are not easily evaluated, such as the definition of the geometry, equations used to define parameter dependencies, and the computational methods incorporated in the simulation software. These choices are made based on the understanding that they should not impose significant errors in the solution, but the magnitude of these uncertainties is difficult to assess without developing and calibrating additional models, so this term is not estimated in this analysis.

1. Uncertainties associated with the model include a host of inputs to the model and to functions included in the model. These include material properties, heating rates calculated from separate neutron transport simulations, and radiative energy transport parameters. The uncertainties of these inputs can be estimated and propagated to quantify the overall uncertainty for the calculated temperature.
2. The calculation of parameter uncertainty involves a process aimed at assessing the magnitude of the input uncertainties, the sensitivity of the model to them, and calculation of their combined effects. This process may be summarized as follows:
   - Identify model inputs and quantify parameter uncertainties, based on input from modelers and subject matter experts.
   - Calculate a sensitivity coefficient for each input as the ratio between the relative change in the calculated temperature (in %) and the 10% change in the corresponding input. Relative changes in temperature express differences in Celsius, for which the reference value (0°) is reasonably close to the room temperature initial condition of the thermal model.
   - Using one time step calculation, rank the inputs based on the parameter's influence on the output temperatures as a product of input sensitivity and input uncertainty, and select the set of most influential inputs.
   - Estimate the daily uncertainty, sensitivity, and correlation coefficient of selected inputs for the entire AGR-5/6/7 irradiation period.
   - Quantify the daily overall calculated temperature uncertainty for the following temperatures: TC temperatures, instantaneous VA and peak FT, time-averaged (TA) VA and TA peak FT, as follows:

- Calculate the overall temperature uncertainty by combining the effects of all input uncertainties and sensitivities. At each time step, express the results in terms of relative and absolute standard deviation.
- Calculate the uncertainties of corresponding TA fuel temperatures, using the sum of squares of uncertainties for instantaneous temperatures.

4.2 Thermal Model Uncertainty Based on TC Residuals

Calculation of model uncertainty based on its response to variations in inputs is a forward calculation of uncertainty in that it is a prediction of how the model should compare to actual values based on knowledge of the input uncertainties. In the absence of error in the form of the model, input uncertainties, and of inaccuracy in the TC measurements, the TC residuals (measured minus calculated TCs) should equal zero. The distribution of the TC residuals is thus an independent measure of the uncertainty of the thermal model to the extent that TC locations adequately sample the temperature distribution of the volume of interest, over the period of interest (i.e., numerous TCs are located throughout the graphite holders, in all capsules, for the duration of the experiment).

In Capsules 1, 2, and 3, eight to ten TCs located throughout each graphite holder experienced a wide range of temperatures, and were operational through the end of Cycle 164A (Figure 9, 10, and the top plot in 11). Thus, the root mean square (RMS) values of TC residuals listed in Table 2 may be a reasonable measure of the calculated temperature uncertainty for these capsules. In contrast, Capsules 4 and 5 had only a few operational TCs and measured a relatively narrow range of temperatures. Therefore, those TC residuals might not reflect the overall temperature uncertainty in those capsules (11).

Because TCs started to fail during Cycle 164A, only TC residuals during the first two regular cycles (i.e., 162B and 164A) are used to calculate summary statistics for TC residuals for each capsule (Table 2). The fact that TC residuals are approximately equally distributed around zero, resulting in small average values for TC residuals, reflects model calibration efforts aimed at minimizing the differences in the TC values. Capsule 1 TC residuals varied the widest, both across TCs and over time, perhaps reflecting a higher uncertainty of calculated temperatures for this capsule. On the other hand, Capsules 2 and 3 had the lower average TC residuals and low RMS error, which are a good indication of lower calculated temperature uncertainty for this capsule. Capsules 4 and 5 have relatively high average TC residuals but a low RMS value, as a result of having the fewest operational TCs.

Table 2. Capsule average and root mean square of TC residuals, based on Cycle 162B and 164A data.

Capsule	Number of operational TCs	Average TC, °C	Average TC residuals, °C	Root mean square of TC residuals, °C	Relative root mean square of TC residuals(a) [D °C/°C]
5	3	683	-15	18	2.7%
4	4	811	-24	32	4.0%
3	9	1065	3	34	3.2%
2	8	815	-10	36	4.5%
1	10	1031	29	77	7.5%

a. Values are normalized to the capsule average TC values from full power days (EFPD = 1) during the specified period. Capsule RMS values are not weighted by the number of operational TCs per day, due to increasing number of TC failures over time.

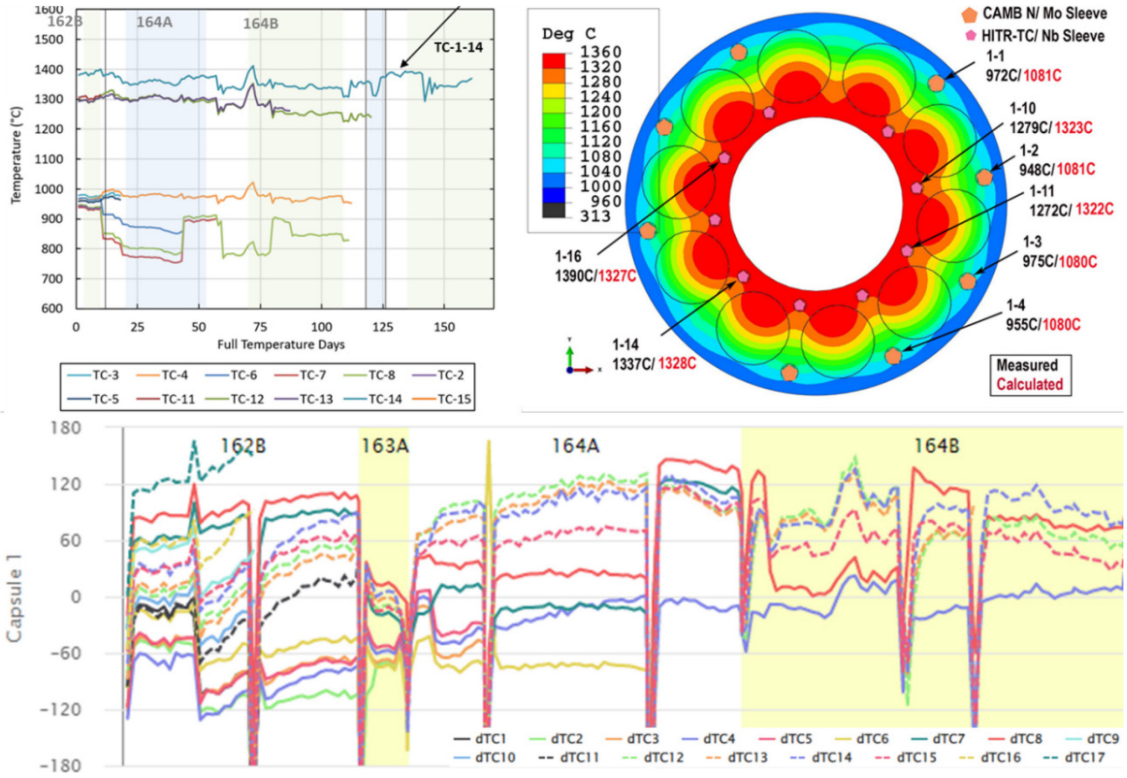

Figure 9. Capsule 1: (top-left) TC readings, (top-right) TC locations on the graphite holder cross section, and (bottom) TC residuals (measured minus calculated) during earlier cycles.

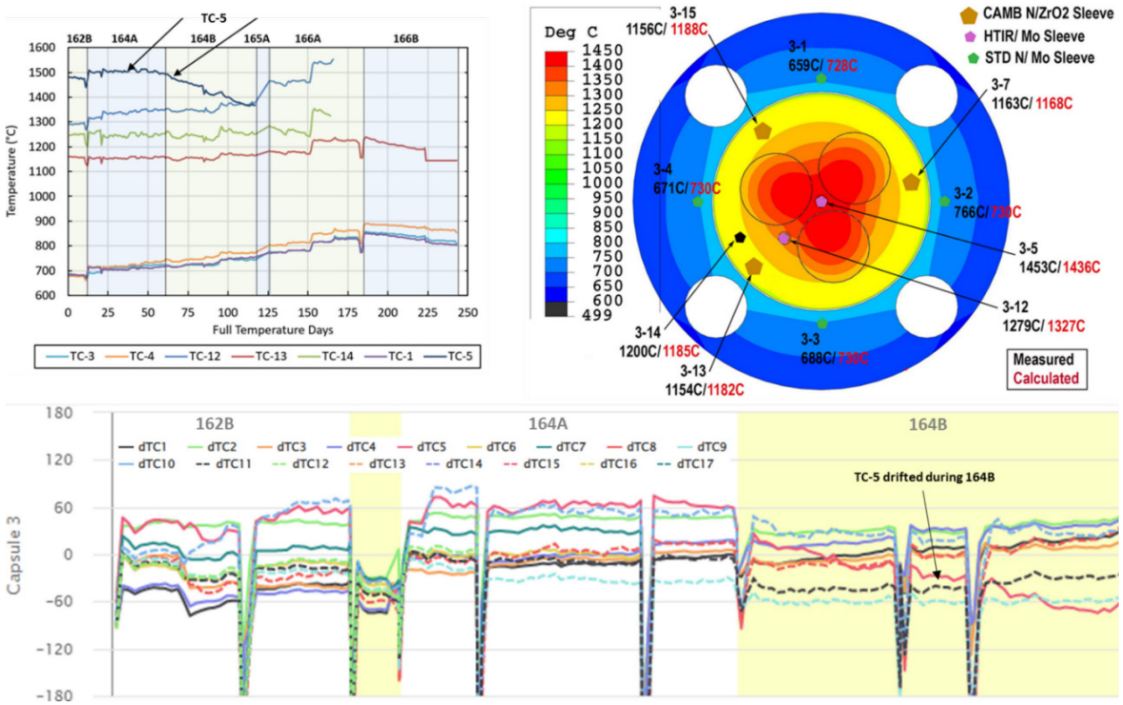

Figure 10. Capsule 3: (top-left) TC readings, (top-right) TC locations on the graphite holder cross section, and (bottom) TC residuals (measured minus calculated) during earlier cycles.

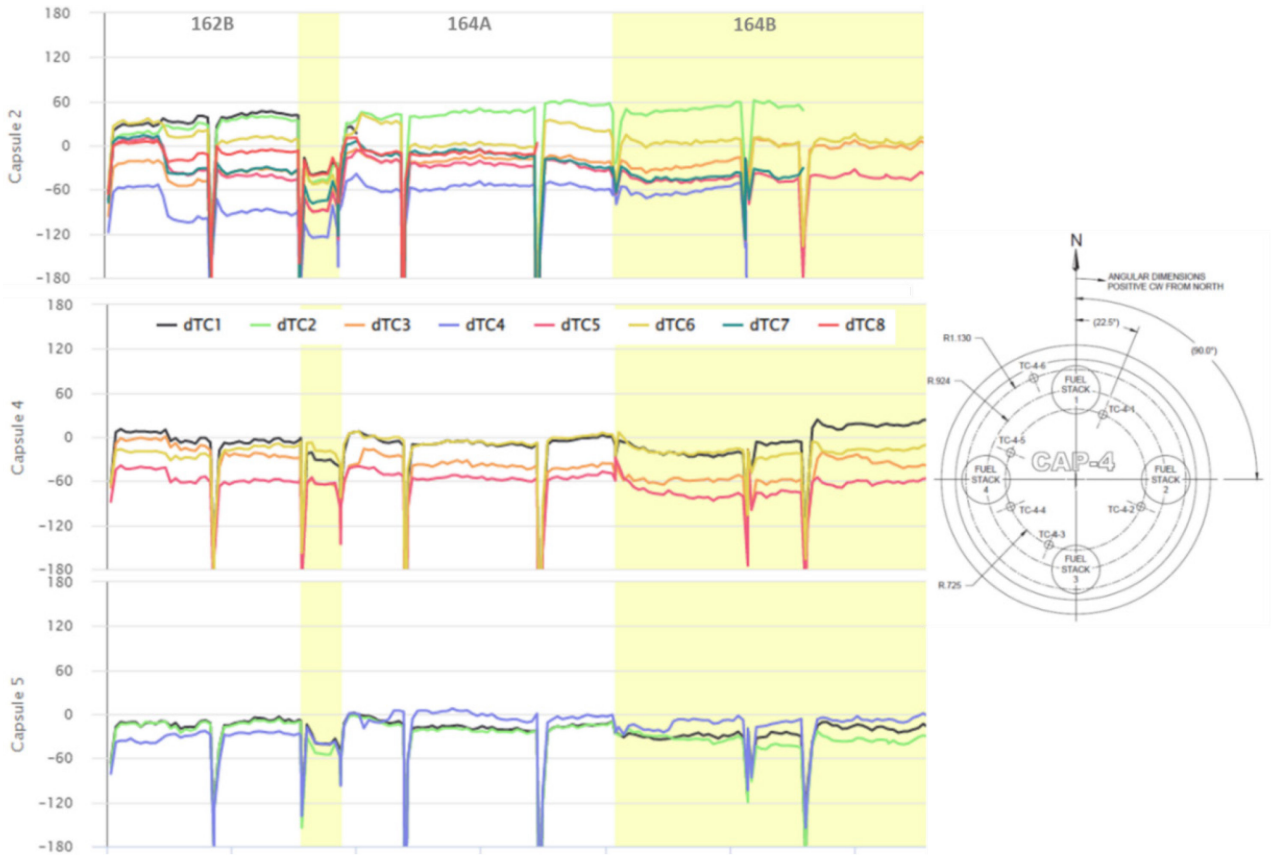

Figure 11. Right image: TC location in Capsule 4 (similar for Capsules 2 and 5); Left plots: TC residuals (measured minus calculated) for Capsules 2, 4, and 5 during earlier cycles.

4.3 Quantify Parameter Uncertainty

Model parameter uncertainty refers to incomplete knowledge of the correct values of model inputs, which exists independently from any particular model but will impact the uncertainty of the model prediction. To quantify the parameter uncertainty of AGR-5/6/7 calculated temperatures, the ABAQUS model input parameters of potential importance are identified. This identification comprises two parts: (1) using expert judgment, estimate the model parameter uncertainties and determine the parameters with the largest uncertainties; and (2) using sensitivity analysis, determine parameters to which the modeling is most sensitive to and refine the estimates of these sensitivities.

Input uncertainties and sensitivity coefficients are combined and propagated to quantify overall parameter uncertainty via the following equation:

$$\sigma_P^2 = \sum_i^n a_i^2 \sigma_i^2 + \sum_i^n \sum_{j \neq i}^n \rho_{ij} a_i \sigma_i \, a_j \sigma_j \qquad (4)$$

where

a_i = the sensitivity coefficient for parameter i (p_i) $[(\Delta T/T_{i0})/(\Delta p/p_{i0})]$

σ_i = the uncertainty of input parameter i

ρ_{ij} = the correlation coefficient for input parameters i and j.

The implicit assumption that the overall uncertainty is a linear combination of the products of the parameter sensitivities and parameter uncertainties is tested, prior to application, in the process of estimating these sensitivities (Section 4.3.3). In addition, while the individual sensitivities are approximated as linear effects, the sensitivity analysis supports that assumption for the ranges to which it is applied.

4.3.1 Influential Input Selection

The selection of input parameters for uncertainty quantification of the AGR-5/6/7 calculated temperatures is based on the ranking of their influences on variation of temperature predictions. The influence ranking is highest for parameters with high uncertainty and/or sensitivity. The range of uncertainties for identified inputs to the thermal model is determined in a manner similar to that employed in the previous experiments. The following factors are considered: machining tolerances for capsule geometry, measurement uncertainty of mass flow controllers, model uncertainty of depletion analysis results, and legacy experience for fuel compact (and graphite) conductivity and emissivity.

The first order of sensitivity evaluation for the temperature calculations was performed by the modeler for the AGR-5/6/7 experiment on an individual capsule. A series of cases was compared to a base case by varying different input parameters to the ABAQUS finite element thermal model for each capsule at Time Step 20 of ATR Cycle 162B. The tornado plots in Figure 12 and in Figure 13 show the most sensitive input parameters on peak fuel temperature, and VA fuel temperature in Capsule 1, arranged from largest to smallest. Figure 14 and Figure 15 show parameter sensitivities for TC1 (located near the capsule wall and exposed to lower temperature) and TC14 (located near the capsule center and exposed to high temperature). Since Capsule 3 had a different design than the remaining four capsules, its sensitivity plots for peak and VA temperatures are presented in Figure 16 and Figure 17 for comparison.

Heat rate in the fuel is the most sensitive parameter for all temperatures in all capsules, followed by control gas composition (e.g., neon fraction) and gas gap widths. The next three influential parameters are heat rate in the graphite, graphite thermal conductivity, and fuel thermal conductivity. The impacts of these parameters are varied at different temperatures. In contrast, the emissivity of the stainless-steel capsule wall had a negligible impact on temperatures in all capsules, but graphite emissivity had a significant impact on the temperatures in Capsule 3, due to the large temperature difference across the gap between the inner and outer graphite holders in Capsule 3 (16 and 17).

After combining input parameter uncertainties with sensitivities, the most influential input parameters on AGR-5/6/7 calculated temperatures are the gas gap sizes, neon fraction, heat rate in the fuel compacts, heat rate in the graphite holder(s), graphite thermal conductivity, fuel compact thermal conductivity, and graphite conductivity (Table 3). The gas gap was selected due to high uncertainties, which significantly impact the calculated temperature uncertainty. Neon fraction, fuel compact heat rates, and graphite heat rates were chosen because of their high sensitivity. Graphite conductivity and fuel compact conductivity, having much lower sensitivity, were chosen because of their considerably higher input uncertainty. Graphite emissivity was included because of its high sensitivity for temperature in Capsule 3.

Table 3. Uncertainties of significant inputs to the Advanced Gas Reactor 5/6/7 thermal models.

Parameter	Uncertainty	Rationale
Outer gas gap Inner gas gap (only in Capsule 3)	24% – 40%	Gas gap size uncertainty sources are: o Dimensional fabrication tolerance of 0.0254 -mm o 20% uncertainty of thermal expansion coefficient results o 0.127 mm clearance between the holder nubs and capsule shell o Graphite material shrinkage uncertainty.
Neon fraction	±3 – ±5%	Uncertainty is based on the 1-sccm flow rate tolerance and was estimated via the neon fraction prediction equation (Subsection 4.3.2.2).
Fuel compacts' heat rate	±5%	Based on the AGR-1 comparison by J. Harp with additional input from J. Sterbentz (Subsection 4.3.2.3).
Graphite rings' heat rate	±3%	
Graphite conductivity	±15%	Additional conductivity data for the test graphite allow for a lower uncertainty for graphite than for fuel.
Fuel compact conductivity	±20%	Uncertainty is based on work done on surrogate compacts by C. Folsom at Utah State University.
Graphite emissivity	±10%	The emissivity 0.9 used fells within the expected range [0.8 – 1.0].

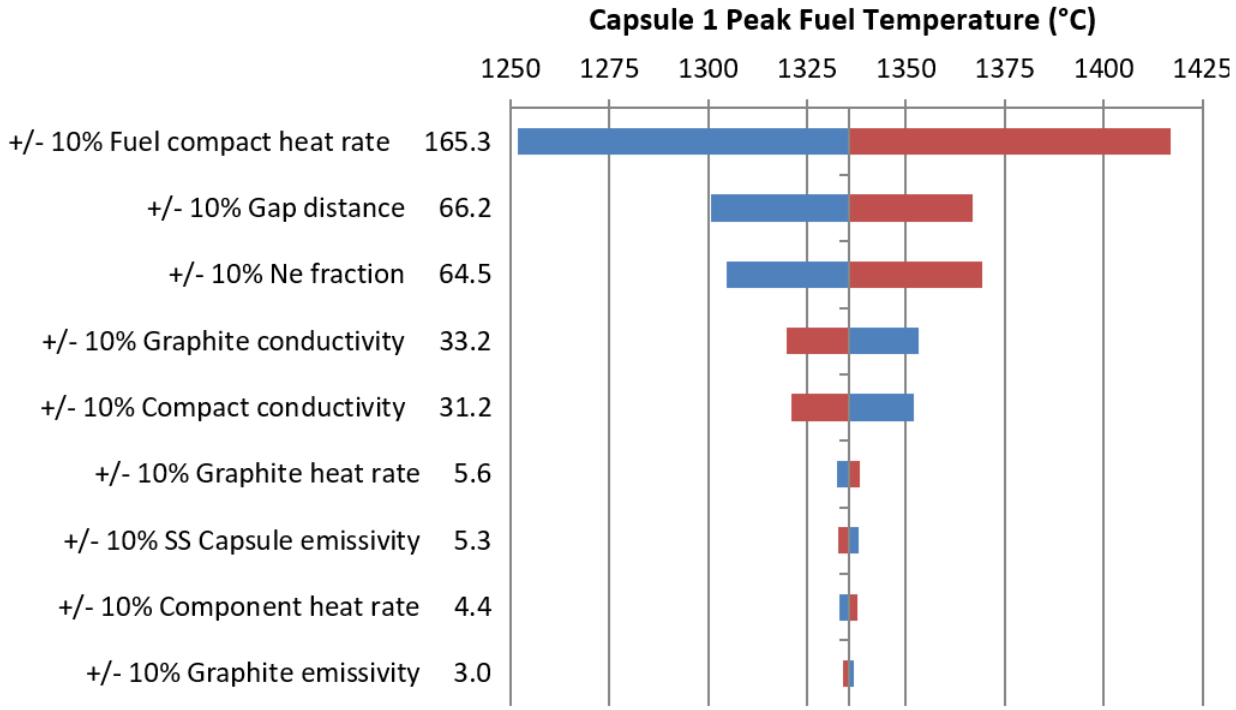

Figure 12. Parameter sensitivities for Capsule 1 peak fuel temperature (red bars are changes in the calculated temperature for a positive 10% input change, and the blue bars are for a negative 10% input change).

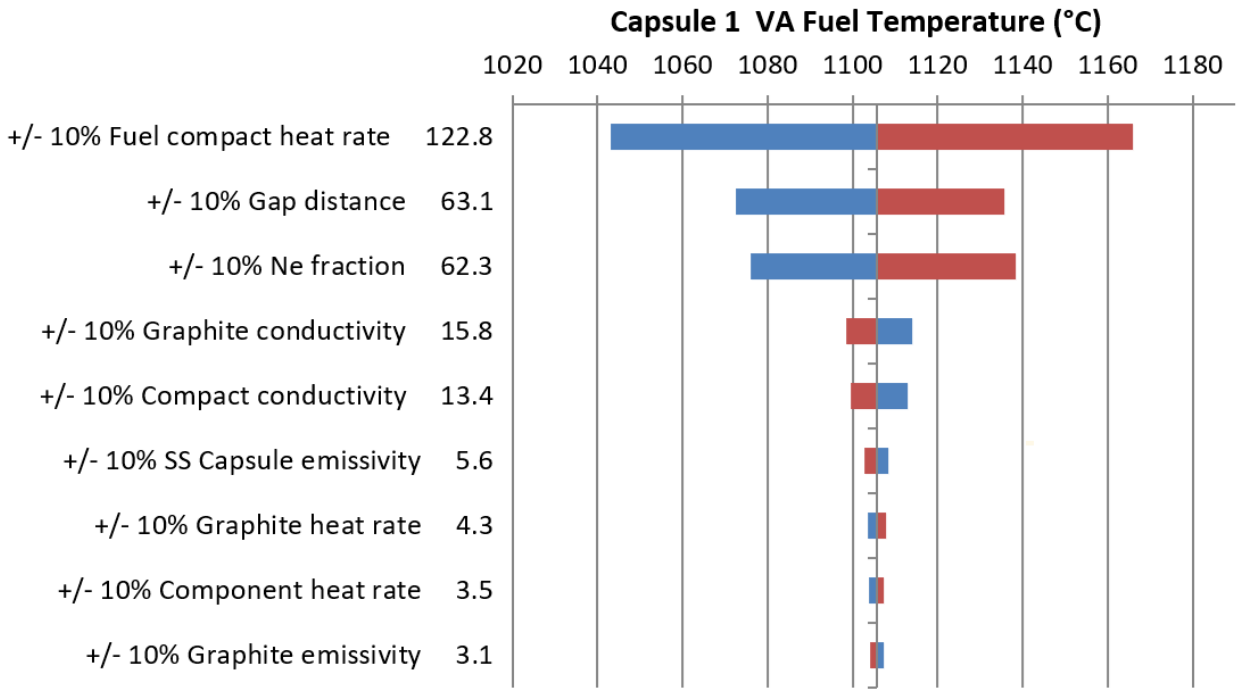

Figure 13. Parameter sensitivities for Capsule 1 volume-averaged fuel temperature (red bars are the change in calculated temperature for a positive 10% input change, and the blue bars are for a negative 10% input change).

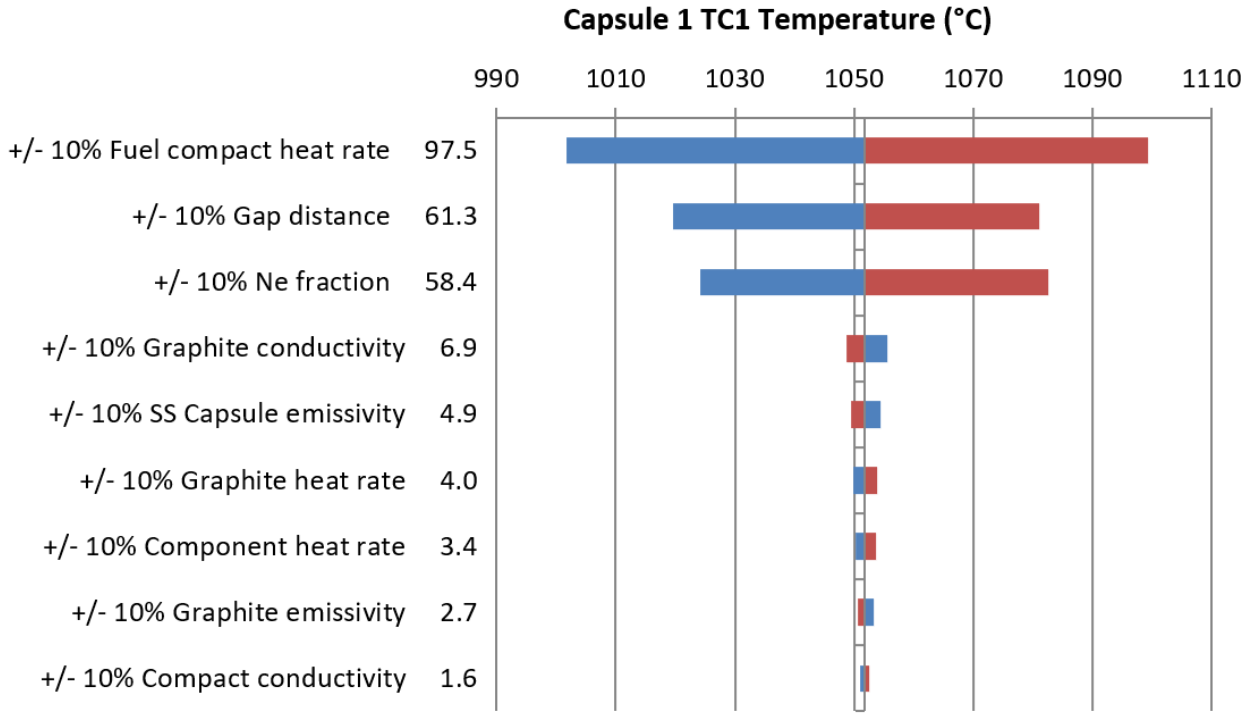

Figure 14. Parameter sensitivities for Capsule 1 calculated TC1 temperature (red bars are the change in calculated temperature for a positive 10% input change, and the blue bars are for a negative 10% input change).

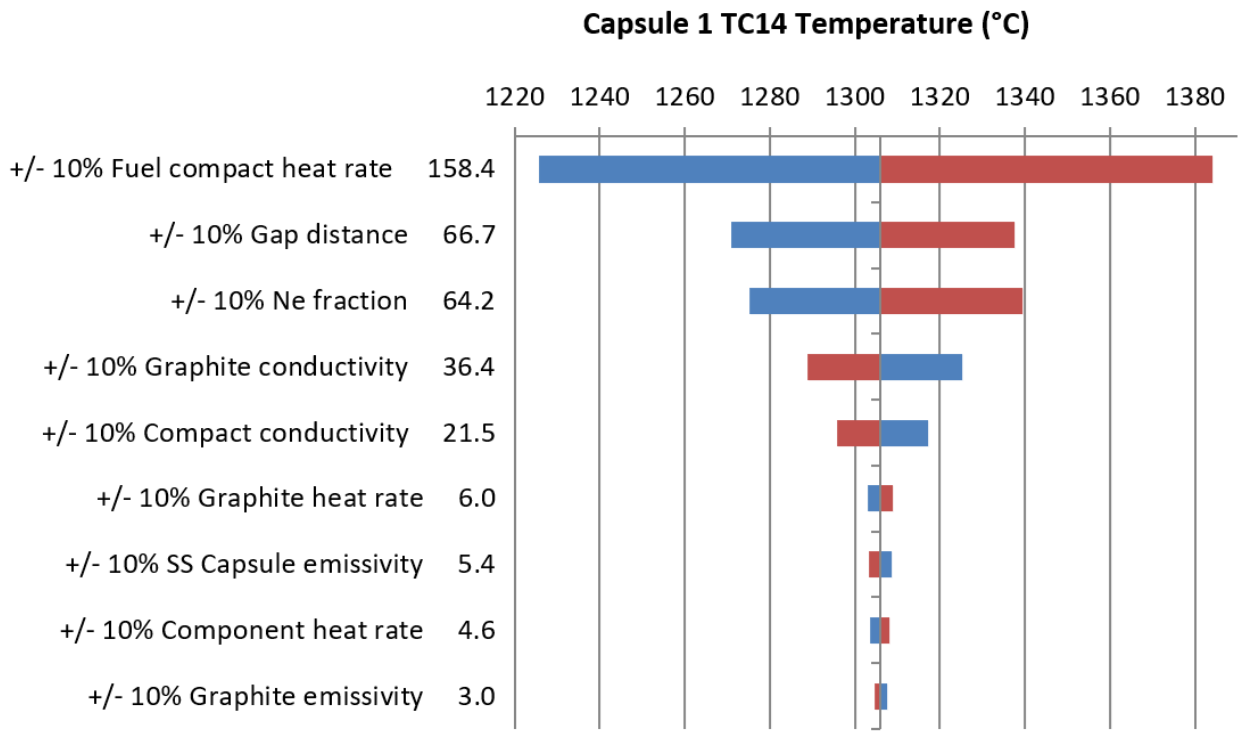

Figure 15. Parameter sensitivities for Capsule 1 calculated TC14 temperature (the red bars are the change in calculated temperature for a positive 10% input change, and the blue bars are for a negative 10% input change).

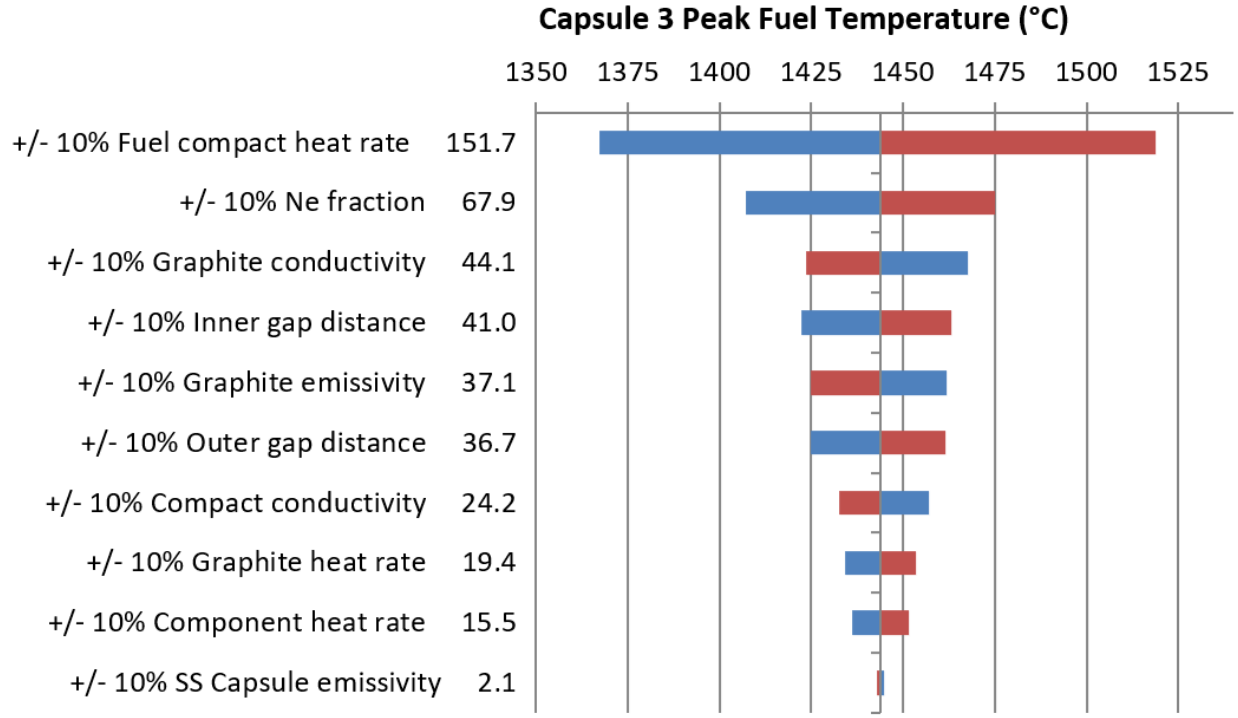

Figure 16. Parameter sensitivities for Capsule 3 peak fuel temperature (red bars are the change in calculated temperature for a positive 10% input change, and the blue bars are for a negative 10% input change).

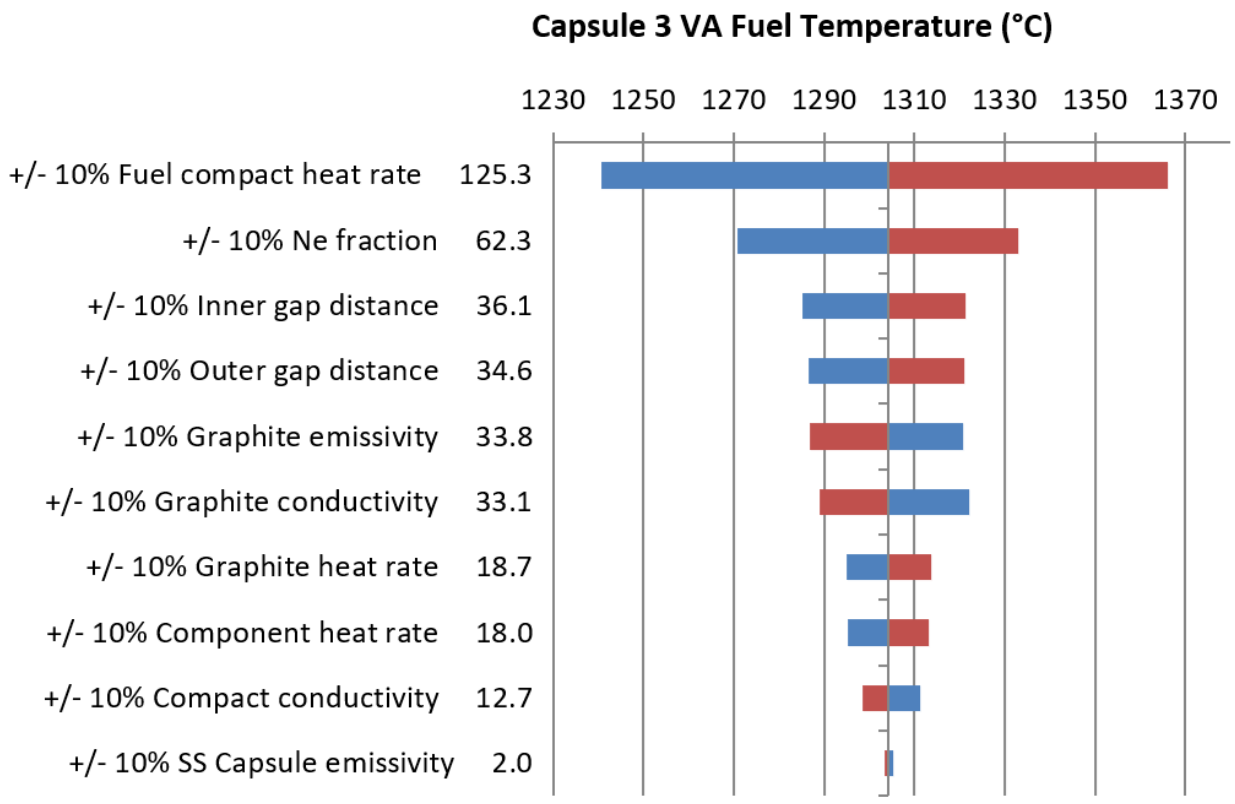

Figure 17. Parameter sensitivities for Capsule 3 volume-averaged fuel temperature (the red bars are the change in calculated temperature for a positive 10% input change, and the blue bars are for a negative 10% input change).

4.3.2 Input Uncertainties

Table 3 summarizes the uncertainties for the most influential input parameters in terms of impact on calculated temperatures, as determined by ART AGR experts. However, the input uncertainties over the course of irradiation are dynamic, accounting for the effects of unplanned events and changes in the thermal properties of capsule components (e.g., changes in the gas gap sizes or gas flow issues) over extended exposure to high temperatures and fast neutron irradiation. This section lays out the basis for determining the input uncertainty for the seven selected parameters for each time step over the entire AGR-5/6/7 irradiation.

4.3.2.1 Gas Gap Width

Heat that is mainly produced in the fuel compacts but also in the graphite holders is transferred through the gas gaps surrounding the compacts and graphite holders via a gap-conductance model, using the gap width and conductivity of the sweep gas.

At the start of irradiation (SOI), the following factors lead to uncertainty in the gas gap width: (1) dimensions are based on nominal values in design drawings, rather than on post-fabrication measurements; (2) the thermal expansion coefficient for the graphite holders is a function fitted to empirical data; (3) the offset of the holder is uncertain, due to the 0.005 in. clearance between the outside of the nubs and the capsule shell; and (4) in the calibration process, a Neolube thickness was estimated for each capsule (0.0381 mm in Capsules 1–4 and 0.0457 mm in Capsule 5).

Based on previous irradiation experiments, graphite is expected to shrink during irradiation until reaching a threshold value of neutron fluence, and then begin to swell. The AGR-5/6/7 experiment did not enter the swelling regime. Thus, gas gaps were modeled as changing linearly with time in response to the IG-430 graphite dimensional change with fast neutron fluence, as shown in 18 (Hawkes 2021). The temperature-control gap width between the outside of the graphite holders and the stainless-steel capsule wall is calculated as:

$$gap = \{(r_0 - t_{neolube})[\alpha(T_i - T_0) + 1]\}_{ss} - \left\{r_0\left[1 + \alpha(F,T)(T_i - T_0) + \frac{\Delta r \cdot F}{r}\right]\right\}_{holder} \quad (5)$$

where

i = is the instantaneous day
r_0 = is the original radius at room temperature
$\Delta r/r$ = is the slope of dimension change (18)
$\alpha(F,T)$ is the coefficient of thermal expansion as function of fluence and temperature
$t_{neolube}$ is the thickness of the Neolube layer.

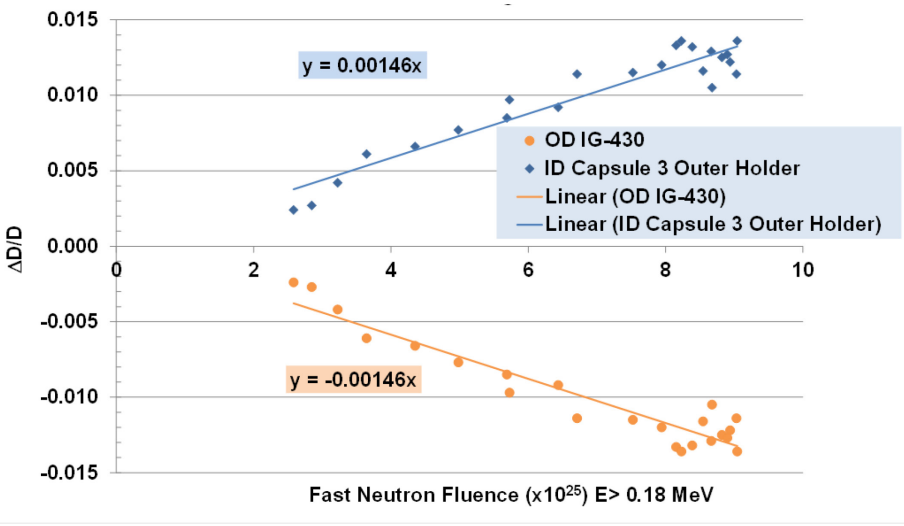

Figure 18. Inner (ID) and outer (OD) diameter change in the IG-430 holder as function of fast neutron fluence (Hawkes 2021).

Gas gap width uncertainty at the beginning of irradiation

The as-fabricated compact and graphite holder diameters are used to estimate the "cold" SOI gas gap width. Then, the cold gas gap sizes are adjusted to account for the graphite thermal expansion as the capsule temperatures increase during irradiation, resulting in so-called hot gaps (Table 4).

As designed, the graphite holders would be held off the capsule walls by small nubs of graphite every 90°. However, an error in capsule design led to a radial clearance of as much as 0.127 mm (or 0.005 in. according to the drawings) between the outside of the nubs and the capsule wall (nub-to-shell clearance) in all capsules, which could allow the holder to shift inside the capsule shell more than intended. Capsule 1 TC readings, in fact, were lower than the calculated temperatures on its southeast side (Figure 19), suggesting that an asymmetric offset may have affected its temperature distribution (Figure 19) (Stempien 2022). The current model does not accommodate asymmetry in the offset, so the uncertainty associated with an asymmetric offset was not explored directly. Instead, the range of likely values was input as a uniform offset. Because that does not produce compensatory changes in temperature from one side of the capsule to the other, the results should be a conservative estimate of the temperature uncertainty. Further studies are planned to determine whether application of an asymmetric gas gap produces a temperature distribution more consistent with that of the TCs.

When the capsules reach high operating temperature, the holders are expanded, leading to a much narrower gas gap. Thus, the gap width can vary only within the narrower "hot" clearance. Assuming a uniform distribution of gap width changes within that range, the gap width uncertainty due to the offset (σ_{offset}) is:

$$\sigma_{offset} = \frac{[t_{offset} - (gap_{fab} - gap_{hot})]}{\sqrt{3}} \quad (6)$$

where

gap_{fab} and gap_{hot} are the as-fabricated and hot gap widths, respectively

$t_{offset} = 0.127\ mm$ is the as-fabricated clearance.

Thus, gap width uncertainty due to the clearance is dependent on capsule temperature (Table 4).

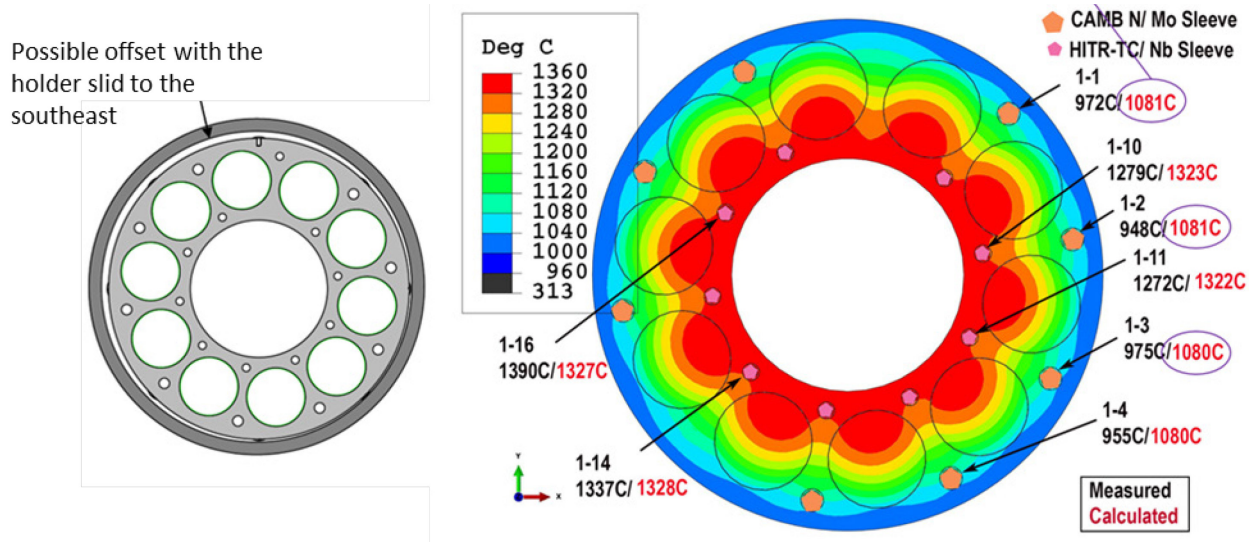

Figure 19. Capsule 1 possible offset caused by the loose fit between the fuel holder and capsule shell.

The SOI gas gap size uncertainty (σ_SOI) is calculated as a combination of three uncertainties: fabrication measurement uncertainty, graphite TE coefficient uncertainty, and holder offset:

$$\sigma_{SOI} = \sqrt{\sigma_{fab}^2 + \sigma_{exp}^2 + \sigma_{offset}^2} \quad (7)$$

where

σ_{fab} = 0.0254 mm is the fabrication dimensional measurement uncertainty and

σ_{exp} = 0.006 mm is the 20% uncertainty on the graphite thermal expansion coefficient (Pham et al. 2016).

The variation in the hot offset clearances between the graphite holder and the capsule shell leads to variation in the gap width uncertainty in capsules at the start of irradiation, as shown in (Table 4). Notably, σ_{offset} is the dominant factor in the gap width uncertainty for AGR-5/6/7 capsules. The as-fabricated gas gap in Capsule 1 is 0.007 in. (Table 4) and the nub height is 0.003 in. (according to the drawings), which indicate the nub-to-shell clearance could be only 0.004 in. instead of 0.005 in. as indicated by the drawings. To be more conservative, the nub-to-shell clearance of 0.005 in. is use in this temperature uncertainty quantification because of the absence of actual measurement of the nub height.

Table 4. AGR-5/6/7 gas gap width uncertainty at the start of irradiation.

Capsule	As-fabricated gap, mm	Hot gap, mm	Uncertainty due to clearance offset, mm	Gap width uncertainty, mm	Gap width uncertainty, %
5	0.2601	0.1976	0.0372	0.0455	23.0%
4	0.2264	0.1551	0.0321	0.0414	26.7%
3	0.1762	0.1176	0.0395	0.0473	40.2%
2	0.1848	0.1194	0.0394	0.0441	37.0%
1	0.1782	0.1023	0.0295	0.0394	38.5%

Gas gap size uncertainty over the course of irradiation

As irradiation progresses, the graphite holders are expected to contract due to exposure to fast neutron fluence, which would increase the gap width over time. Additionally, during post-irradiation examination, a series of discrete deposits were observed on the outside of the Capsule 1 holder. Figure 20 shows the three main columns of deposits on the outside of the holder, which appear to have thicknesses greater than those of the machined nubs (0.003 in.) (Stempien 2022). These deposits would have the opposite effect as the holder contraction, effectively decreasing the gap width around the deposit locations. Neither of these effects were incorporated in the thermal model, and uncertainties in their magnitudes adds to the overall uncertainty in gas gap width, which also increases with time. For this analysis, the uncertainty in gap width was assumed to have gradually increased over time from the SOI uncertainty to a 50% increase at the end of irradiation (EOI):

$$\sigma_{EOI} = 1.5 \times \sigma_{SOI} \tag{8}$$

The absolute gap width uncertainty at time i (σ_{GGi}) is expressed as:

$$\sigma_{GGi} = \sigma_{SOI} + 0.5 * \sigma_{SOI} * \frac{EFPD_i}{EFPD_{EOI}} \tag{9}$$

Even though the absolute gap width uncertainty is increasing over time, the relative gap width uncertainties were decreasing (Figure 21). This is because the gap width increases faster than its estimated uncertainty.

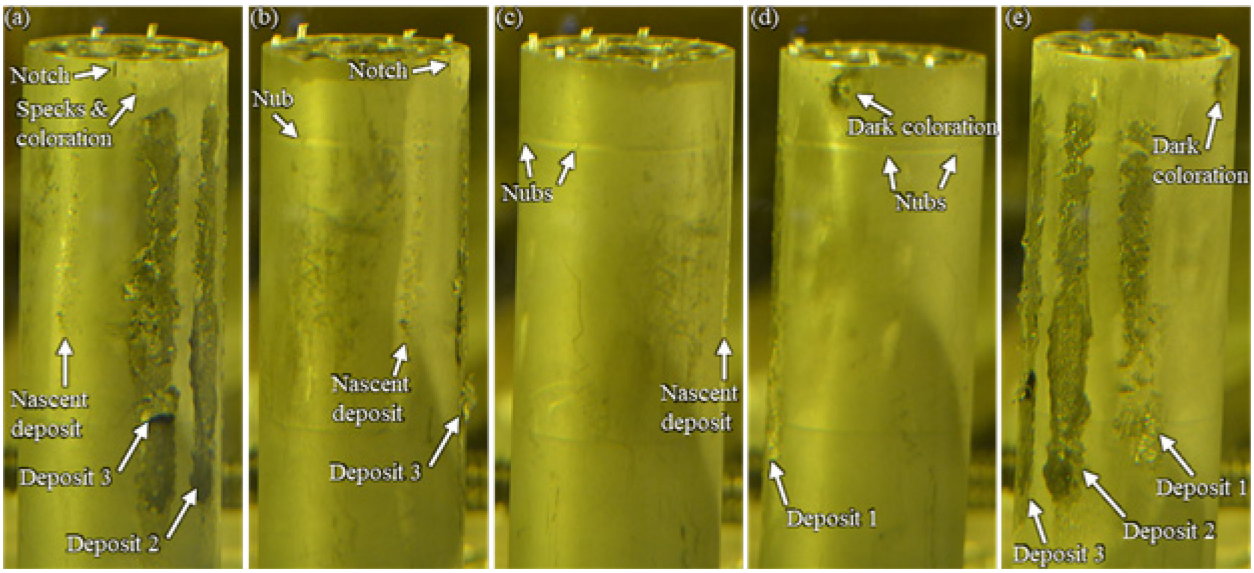

Figure 20. Series of photos of the Capsule 1 holder. Photos (b) through (e) were taken after rotating the holder counterclockwise (Stempien 2022).

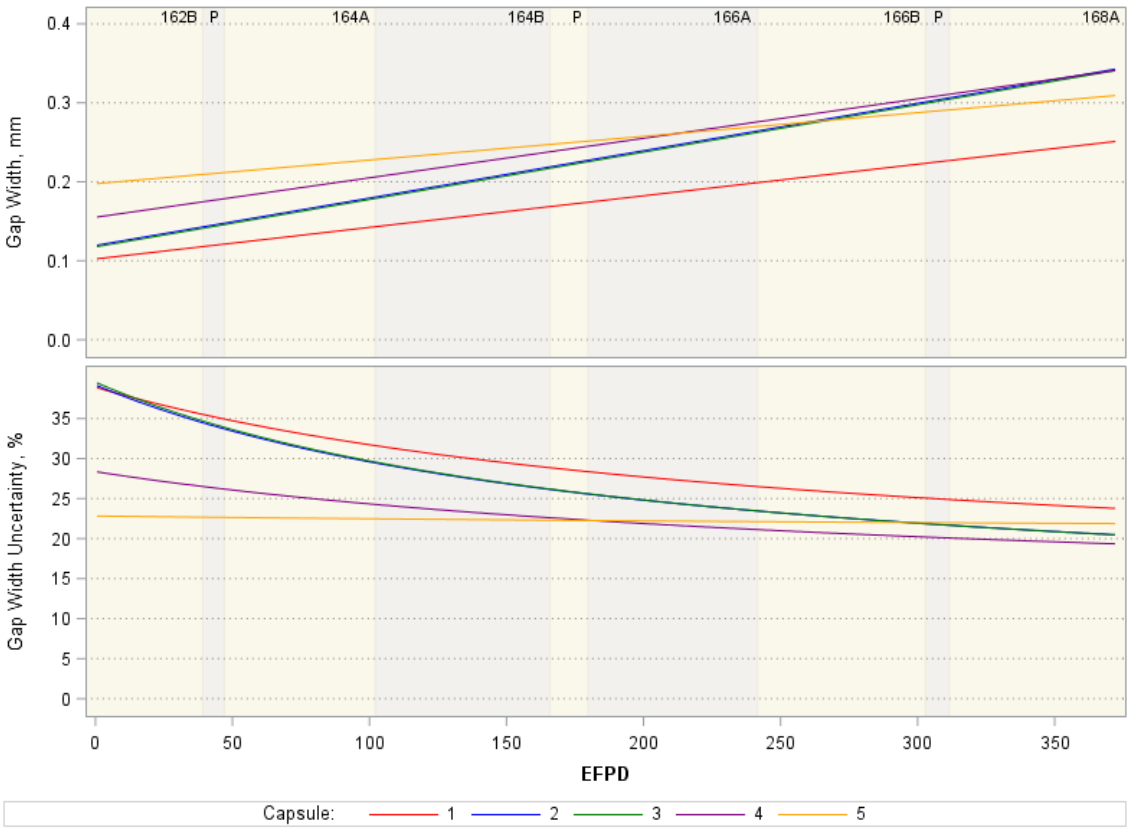

Figure 21. Daily hot gas gap width and uncertainty for AGR-5/6/7 capsules (P is a PALM cycle).

4.3.2.2 Neon Fraction

Heat produced mainly in the fuel compacts and graphite rings transfers through the control gas gaps via a gap conductance modeled as a function of gas gap size and the conductivity of the sweep gas (Hawkes 2014). The neon fraction of the capsule control gas mixture is, in turn, used in the correlation taken from a report from Brown University (Kestin, et al 1984) in order to determine the gas mixture conductivity (Hawkes 2021). As designed, the capsule gas lines do not cross-talk with each other either before or after gas enters an individual capsule, and the amount of gas leaking from a capsule gas line to the leadout is negligible; any gas leaking into a capsule is assumed to come only from the leadout flow. As a result, the calculation formula for the neon fraction in each capsule, including potential gas leakage to and from the leadout flow, is expressed as:

$$Fr_{Ne} = \frac{Q_{Ne} + \max(Q_{outlet} - Q_{Ne+He}, 0) * \dfrac{Q_{Neleadout}}{Q_{Ne+Heleadout}}}{\max(Q_{outlet}, Q_{Ne+He})} \tag{10}$$

where

Fr_{Ne} = neon fraction
Q = gas flow in sccm.

The main source of neon fraction uncertainty is measurement error in the gas flow meters, which have a 1-sccm tolerance (Table 3), based on engineering assessment. A neon fraction simulation of Equation (10), with neon and helium flows taken randomly from a normal distribution with a mean value and standard deviation of 1 sccm, was performed for different neon fraction levels. The neon fraction uncertainty for each neon fraction level equals the standard deviation calculated from 100,000 random neon fraction results. Figure 22 in the Microsoft Excel platform was used to estimate a function that results in a good fit to the data ($R^2 = 0.9924$). Therefore, the relative neon fraction uncertainty in terms of one standard deviation can be expressed as a function of neon fraction as:

$$\sigma_{Fr_{ne}} = \frac{2.5487}{Fr_{Ne}^{1.047}} \tag{11}$$

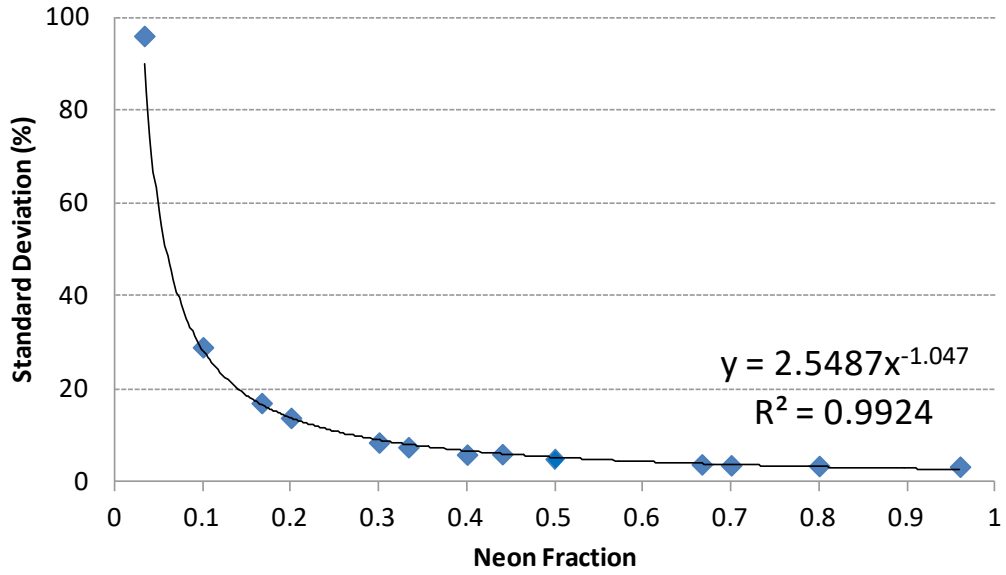

Figure 22. Neon fraction relative uncertainty and trend line.

Neon fraction uncertainty is well estimated using a power function of neon fraction. Thus, the relative uncertainty is high at low neon fraction (about 100% at 0.03 neon fraction) because of the high relative uncertainty of the mass flow controllers at lower neon flow rates. However, when AGR-5/6/7 runs on pure helium (i.e., capsule neon flow rate of 0 sccm), the neon fraction approaches zero, causing the neon fraction uncertainty to drop to about 3% due to the 1 sccm uncertainty of the neon flow rate over the 30 sccm total flow rate (±1/30). Conversely, when the capsule and leadout gas flows are pure neon (i.e., capsule neon flow rate of 30 sccm), the neon fraction approaches one, and the neon fraction uncertainty is near 0% [about 1/(30*30)], due to the lower relative uncertainty of the neon flow rate (1/30).

An obstruction developed in the Capsule 1 outlet line during Cycle 164B, altering the as-designed gas flow regime for all capsules. As irradiation progressed, the Capsule 1 gas line condition worsened and gas flow to Capsule 1 was isolated during the last three cycles, 166B–168A (Pham et al. 2021). These problems in the Capsule 1 gas line complicated the neon fraction calculation for Capsule 1, especially during the total isolation of gas flow to Capsule 1 for the last cycle, Cycle 168A. During this time, the Capsule 1 neon fraction was unknown, being somewhere between the zero-neon fraction of the Capsule 1 inlet gas before isolation and the estimated neon fraction in the leadout as a gas mix from the leadout inlet gas and any excess gas vented from Capsules 2–5 through the leadout. Fortunately, during this time, the neon fraction for Capsules 2–5 equaled the fraction of the capsule inlet flow, since gas from these capsules was vented to the leadout.

4.3.2.3 Fuel and Graphite Heat Rates

Heating rates for fuel compacts and graphite rings were taken from the as-run physics calculation (Sterbentz 2020), which provides a detailed heat rate distribution for each fuel compact for each day in order to accommodate the highly detailed thermal model (Figure 24). The uncertainty in the calculated fuel heat rate results from multiple factors, including ATR-measured parameters that go into the physics calculation, and statistical uncertainties associated with other inputs to the Monte Carlo simulations. However, results from the AGR-1 experiment, which was of a similar design, demonstrated good agreement between the burnup calculated by the physics depletion model and PIE measurements (Figure 23) (Harp 2014). In that comparison, the greatest difference, per compact, was less than 10%. This suggests that the instantaneous (daily) fuel fission power uncertainty should be small. Uncertainties in inputs to the physics calculations that are generally independent include:

- ATR total core or lobe power of ±4.1%
- Fuel compact uranium beginning-of-life number densities of ±0.5%
- Calculated irradiation flux of ±1.0%
- Calculated reaction rates or a one-group cross section of ±2.0%
- Power normalization factors of ±1.0%
- Outer shim control cylinder hafnium and beryllium reflector poison number densities of ±1.0%
- Outer shim control cylinder rotational position of ±0.5%.

Based on these values, as well as experience with similar physics calculations, the overall fuel heat rate uncertainty is estimated at ±5.0% for all capsules and all cycles, and that value is used for the fuel heat rate uncertainty in this analysis.

The graphite holder heat rates are significantly lower than the fuel heat rates (Figure 25). However, the total volume of the graphite holders in each capsule is much larger than the total volume of the four fuel compacts, leading to significant influence of the graphite heat rate on calculated temperatures, especially at TC locations in the graphite holders. Thus, the heat rate of the graphite holder(s) is included in this calculated temperature uncertainty.

The heat rate uncertainty in the graphite rings surrounding the compacts should be much smaller than the uncertainty in the compact heat rates. This is because the graphite heating is due primarily to ATR core neutron and gamma radiation interaction, the calculated transport of which is relatively straightforward, accurate, and directly scalable to the ATR core power. As a result, the heat rates in the graphite holders are also relatively constant over time, whereas the fission compact heat rates are a complex function of burnup, ATR core heating radiation, and fission from the compacts themselves that does not deposit all fission radiation components in the compacts. To account for those differences, the uncertainty in the compact heat rates is estimated to be a factor of two greater than that of the graphite holders. Therefore, for this uncertainty quantification, the graphite heat rate uncertainty is estimated to be to ±3.0% for all capsules and all cycles.

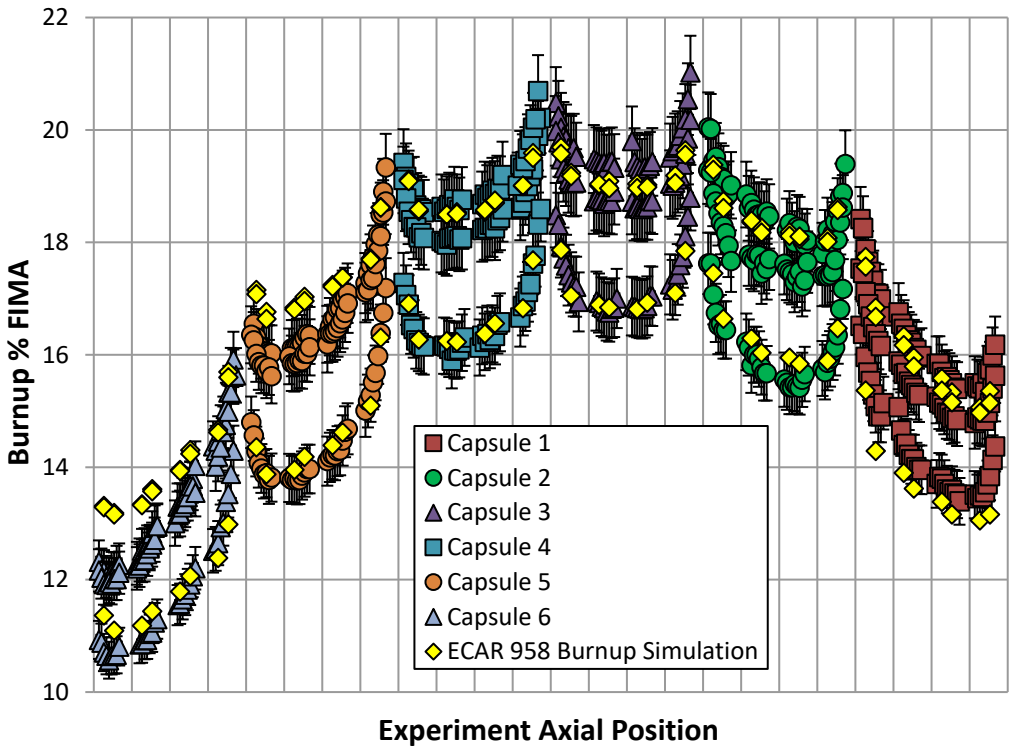

Figure 23. Burnup derived from the Cs-134/Cs-137 activity ratio for each measured precision gamma scanner slice for all AGR-1 capsules and compared to simulations. Each vertical tick mark represents a separate level in each capsule (Harp 2014).

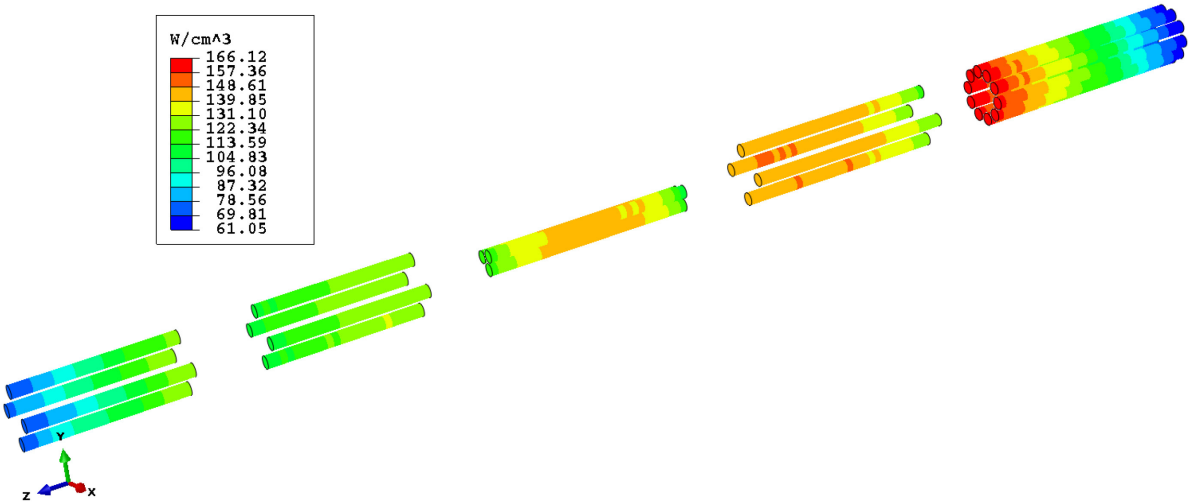

Figure 24. Compact heat rates (Capsule 5 on the far left and Capsule 1 on the far right) for Cycle 162B, day 20 (Hawkes 2021).

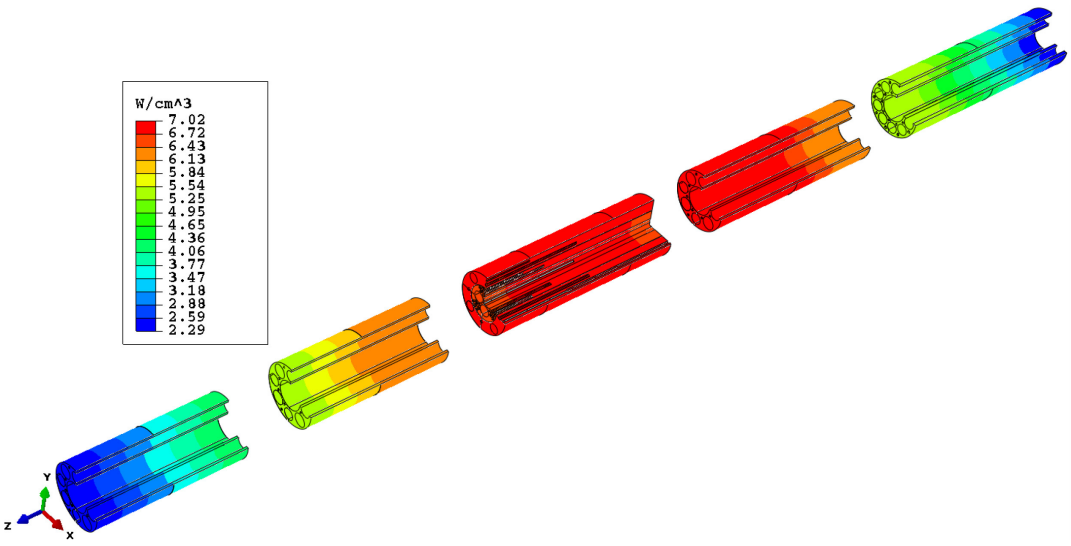

Figure 25. Graphite holders heat rates (Capsule 5 on the far left and Capsule 1 on the far right) for cycle 162B, day 20 (Hawkes 2021).

4.3.2.4 Fuel Compact Thermal Conductivity

The thermal conductivity of fuel compacts was taken from fitted equations describing its relationships with temperature, temperature of heat treatment, neutron fluence, and TRISO-coated particle packing fraction (Gontard and Nabielek 1990). These equations incorporated adjustments to account for differences in fuel compact density and packing fraction. The packing fraction for compacts in Capsules 1 and 5 was measured at 0.393, and for Capsules 2, 3, and 4 at 0.261, resulting in correction factors for packing fraction of 0.602 and 0.726, respectively. Also, the given equations were developed for a fuel compact matrix density of 1.75 g/cm^3, whereas the compact matrix used in AGR-5/6/7 has a density of 1.728 g/cm^3 for Capsules 1 and 5, and 1.757 for Capsules 2, 3, and 4, resulting in correction factors for matrix density close to 1 (0.987 and 1.004, respectively). Thus, the thermal conductivities for AGR-5/6/7 compacts were scaled according to the ratio of densities in order to correct for these differences. Figure 26 shows plots of the fuel compact thermal conductivity varying with fluence and temperature. While the relationships used to describe thermal conductivities are believed to provide reasonably accurate values, the lack of experimental data on AGR-5/6/7 fuel compact thermal properties leads to high uncertainty in these values, which we estimate this uncertainty to be 20% for the entire AGR-5/6/7 irradiation (Table 3).

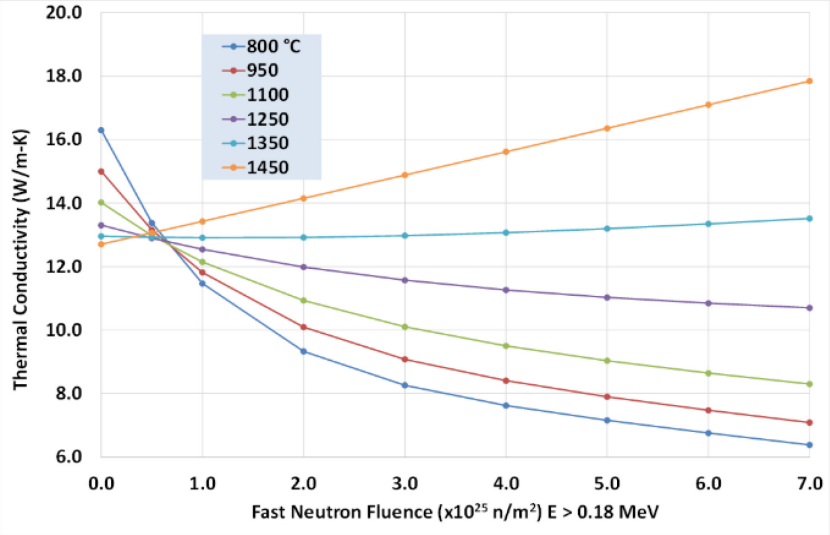

Figure 26. Thermal conductivity varying with fluence and temperature for 40%-packing-fraction fuel compacts (Hawkes 2021).

4.3.2.5 Graphite Thermal Conductivity

The AGR-5/6/7 graphite holders are made of IG-430 nuclear-grade graphite. Material properties for unirradiated graphite IG-430 were determined as follows: (1) specific heat, as a function of temperature, was taken from the American Society for Testing and Materials (ASTM 2014); (2) density and expansion coefficients (measured at 20°C) were taken from Windes (2012) and Swank et al. (2010); and (3) thermal diffusivities for the temperature range of 20–1000°C (left plot in Figure 18) were taken from Windes et al. (2013). Unirradiated thermal conductivity as a function of temperature was calculated as the product of the diffusivity, specific heat, and density. The effect of irradiation on graphite thermal conductivity was accounted for by incorporating multipliers for thermal conductivity, expressed as a function of temperature and fast neutron fluence. This multiplier was taken from the Japanese multiplier data (Shibata et al. 2010) and used to adjust the thermal conductivity of the graphite holders under actual irradiation conditions. The resulting thermal conductivity of the IG-430 graphite as function of temperature and fast neutron fluence is plotted in Figure 27. Based on analyses of previous AGR experiments, the uncertainty of the empirical equations describing graphite thermal conductivity is estimated at 15% for the entire AGR-5/6/7 irradiation, as shown in Table 3.

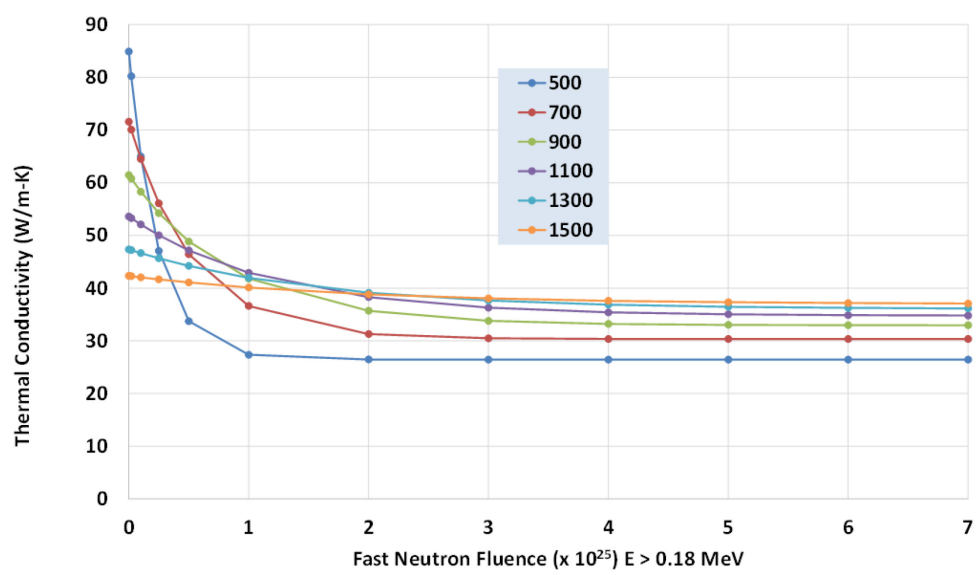

Figure 27. Thermal conductivity of IG-430 varying with temperature (°C) and fast neutron fluence.

4.3.2.6 Graphite Emissivity

Radiative heat transfer occurs across all gas gaps, with heat flux influenced by the emissivity of the surface. An emissivity of 0.9 was assumed for the IG-430 graphite holder surfaces of the AGR-5/6/7 experiment, with an estimated uncertainty of 10% (Table 3).

4.3.3 Input Parameter Sensitivity

The governing equations for the steady-state conduction and radiation heat transfer models (Equations [1 and [2) used for the AGR-5/6/7 capsule temperature calculation show complex nonlinear relationships between the output temperature and input parameters over the wide variety of experimental conditions. This makes it impossible to derive a unique analytical formula for calculating output uncertainty from the input variations over the whole experimental condition domain. Additionally, the standard Monte Carlo technique is impractical due to requiring hundreds of thousands of simulations in order to accurately estimate the overall output temperature uncertainty. The AGR-5/6/7 thermal model sensitivity analysis results given in Section 4.3.1 represent parameter sensitivities within only a small experimental condition domain of ±10% of the nominal values used in the analysis. Also, the existing sensitivity analysis in Hawkes et al.'s conference paper (2015) does not include an investigation of the interactive effects of input variables.

To be computationally efficient, a statistical experimental design was used to develop the set of simulation runs necessary to estimate all main effects and pairwise interactions of the selected seven important input variables. To account for the nonlinearity of the temperature function (e.g., Equation [1]), the AGR-5/6/7 thermal condition domain is divided into multiple smaller ranges, where the output temperature can be estimated as a linear combination of selected input variables. Consequently, the temperature uncertainty can be calculated from given input uncertainty by using standard error propagation of the linear combination (Ostle and Mensing 1975).

4.3.3.1 Statistical Experimental Design for Sensitivity Analysis

Table 5 lists the 74 runs of the ABAQUS code that were completed for each of the 15 scenarios in Table 6. These scenarios cover a wide range of input parameters (e.g., fuel heat rate, neon fraction, and fast neutron fluence [and consequently, fuel compact and graphite holder conductivities, and graphite holder emissivity]) in the five capsules.

Table 5. Experimental design matrix for AGR-5/6/7 thermal model sensitivity analysis (N is nominal and +/- are plus and minus 10% of inputs).

Run	Neon Fraction	Graphite Conductivity	Fuel Conductivity	Fuel Heat Rate	Graphite Heat Rate	Gas Gap Width	Graphite Emissivity
Base (0)	N	N	N	N	N	N	N
1 – 2	+/-	NN	NN	NN	NN	NN	NN
3 – 4	NN	+/-	NN	NN	NN	NN	NN
5 – 6	NN	NN	+/-	NN	NN	NN	NN
7 – 8	NN	NN	NN	+/-	NN	NN	NN
9 – 10	NN	NN	NN	NN	+/-	NN	NN
11 – 12	NN	NN	NN	NN	NN	+/-	NN
13 – 16	+/-/+/-	-/+/+/-	NNNN	NNNN	NNNN	NNNN	NNNN
17 – 20	+/-/+/-	NNNN	-/+/+/-	NNNN	NNNN	NNNN	NNNN
21 – 24	+/-/+/-	NNNN	NNNN	-/+/+/-	NNNN	NNNN	NNNN
25 – 28	+/-/+/-	NNNN	NNNN	NNNN	-/+/+/-	NNNN	NNNN
29 – 32	+/-/+/-	NNNN	NNNN	NNNN	NNNN	-/+/+/-	NNNN
33 – 36	NNNN	+/-/+/-	-/+/+/-	NNNN	NNNN	NNNN	NNNN
37 – 40	NNNN	+/-/+/-	NNNN	-/+/+/-	NNNN	NNNN	NNNN
41 – 44	NNNN	+/-/+/-	NNNN	NNNN	-/+/+/-	NNNN	NNNN
45 – 48	NNNN	+/-/+/-	NNNN	NNNN	NNNN	-/+/+/-	NNNN
49 – 52	NNNN	NNNN	+/-/+/-	-/+/+/-	NNNN	NNNN	NNNN
53 – 56	NNNN	NNNN	+/-/+/-	NNNN	-/+/+/-	NNNN	NNNN
57 – 60	NNNN	NNNN	+/-/+/-	NNNN	NNNN	-/+/+/-	NNNN
61 – 64	NNNN	NNNN	NNNN	+/-/+/-	-/+/+/-	NNNN	NNNN
65 – 68	NNNN	NNNN	NNNN	+/-/+/-	NNNN	-/+/+/-	NNNN
69 – 72	NNNN	NNNN	NNNN	NNNN	+/-/+/-	-/+/+/-	NNNN
73 – 74	NN	NN	NN	NN	NN	NN	+/-

Table 6. Thermal conditions of 15 cases for sensitivity analysis.

Case	Capsule	ATR Cycle	Time Step	EFPDs	Neon Fraction	Fluence, 10^{25}n/m^2	Fuel Heat Rate, w/cm^3	Graphite Heat Rate, w/cm^3	Gas Gap, mm
1	1	162B	20	20	0.87	0.15	115.3	4.1	0.274
2	1	164B	65	162	0.64	1.33	109.8	4.6	0.327
3	1	166A	60	300	0.90	2.55	98.4	4.7	0.383
4	2	162B	20	20	0.84	0.23	138.1	6.7	0.239
5	2	164B	65	162	0.72	2.07	112.5	7.2	0.322
6	2	166A	60	300	0.90	4.02	92.7	7.6	0.411
7	3	162B	20	20	0.78	0.25	133.3	6.8	0.197
8	3	164B	65	162	0.84	2.21	107.5	7.1	0.283
9	3	166A	60	300	0.86	4.30	89.5	7.6	0.376
10	4	162B	20	20	0.77	0.21	118.3	6.0	0.200
11	4	164B	65	162	0.90	1.88	99.6	6.3	0.275
12	4	166A	60	300	0.90	3.62	85.2	6.7	0.354
13	5	162B	20	20	0.69	0.12	99.6	3.3	0.184
14	5	164B	65	162	0.90	1.08	95.1	3.6	0.226
15	5	166A	60	300	0.90	2.06	86.8	3.7	0.269

4.3.3.2 Parameter Sensitivity Analysis

From the ABAQUS output for each of the 15 scenarios, multiple temperatures of interest were obtained, such as VA FT, peak FT, and TC temperatures. These results were used for a sensitivity analysis of the input parameters on model calculated temperatures. The JMP® module "Fit Model" (JMP® 13.0.0) of SAS® (SAS® 2009) was used to build a surrogate response surface model for each of the calculated temperatures in order to determine which input terms have significant impacts. The parameter coefficients are treated as sensitivities that estimate the rate of change of temperature regarding the input. Consequently, they can be used to propagate the parameter uncertainty to the output temperatures.

As stated in the previous section, seven thermal model input parameters are included in this sensitivity analysis: fuel heat rate (FHR), graphite ring heat rate (GHR), width of the gas gap (GG), neon fraction (NeF) of the capsule gas mixture, fuel thermal conductivity (FC), graphite thermal conductivity (GC), and graphite emissivity (GE). The experimental design provides an estimation of the main input effects and second-order term effects (noted as $Term^2$), which are pairwise interactions among the inputs and square terms of the inputs. The following response surface model containing 29 terms was constructed and studied for each of the calculated temperature response measures as a ratio between the relative change in temperature in response to a 10% change in each input, using the JMP® platform:

$$f_T = a_0 + a_1 FHR + a_2 GHR + a_3 GG + a_4 Nef + a_5 FC + a_6 GC + a_7 GE + \sum_{i=8}^{28} a_i \, Term^2 \qquad (12)$$

where

$f_T = \frac{\Delta T}{T_{Base}}$, and

T_{Base} is temperature for the base set of inputs.

Both input variables and output responses are transformed into a relative value (0.9 is 10% less, 1.0 is nominal, and 1.1 is 10% more) by dividing by the nominal values prior to fitting the response surface model. This transformation does not impact the parameter sensitivities. The results of Case 1 (Table 6) are plotted here for discussion because they are similar to resemble those of the other cases. Figure 28 presents the actual relative temperature change of the simulation, versus its predicted temperature change using Equation (12) for VA FT, indicating a near-perfect fit of the response surface regression model (R-square-d is nearly 1).

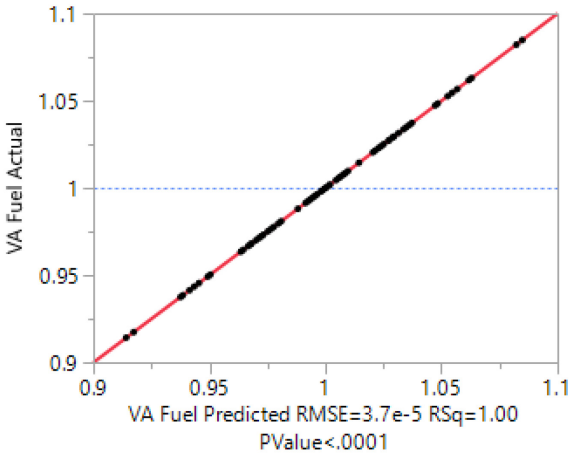

Figure 28. Actual versus predicted relative calculated temperature change for VA FT for Case 1.

Figure 29 lists all parameter estimates (a_1 to a_{28} in Equation [12]), sorted from largest to smallest, for VA fuel temperature in Case 1 (they are almost in the same order for other temperatures and other cases). Many coefficients (parameter estimates) in the model are significantly different from zero. However, the bar chart showing the parameter estimates for each term (or sensitivity coefficient) indicates that most main effects are significant, except for graphite emissivity, which is only sensitive for Capsule 3 temperatures. The most significant among the second-order terms (namely, the square of the gas gap) has a negligible influence on output temperature.

Term	Estimate	Std Error	Prob>|t|
FHR	0.5556259	0.000082	<.0001 *
Gap	0.2852241	0.000082	<.0001 *
Nef	0.2815083	0.000082	<.0001 *
GC	-0.071303	0.000082	<.0001 *
FC	-0.060383	0.000082	<.0001 *
GHR	0.0195443	0.000082	<.0001 *
(Gap-1)*(Gap-1)	-0.142896	0.001198	<.0001 *
(Nef-1)*(Nef-1)	0.139228	0.001198	<.0001 *
(FHR-1)*(FHR-1)	-0.099275	0.001198	<.0001 *
GEMI	-0.014132	0.000272	<.0001 *
(GC-1)*(GC-1)	0.0537055	0.001198	<.0001 *
(FC-1)*(FC-1)	0.0468767	0.001198	<.0001 *
(FHR-1)*(GC-1)	-0.070594	0.001923	<.0001 *
(FHR-1)*(FC-1)	-0.067066	0.001923	<.0001 *
(Nef-1)*(FHR-1)	0.0655287	0.001923	<.0001 *
(Gap-1)*(FHR-1)	0.0604863	0.001923	<.0001 *
(FC-1)*(GC-1)	0.0259356	0.001923	<.0001 *
(FHR-1)*(GHR-1)	-0.008208	0.001923	<.0001 *
(Gap-1)*(Nef-1)	0.007281	0.001923	0.0004 *
(Gap-1)*(FC-1)	-0.003256	0.001923	0.0971
(Gap-1)*(GC-1)	-0.002804	0.001923	0.1516
(GHR-1)*(GHR-1)	-0.001563	0.001198	0.1987
(Nef-1)*(GC-1)	-0.002284	0.001923	0.2410
(Nef-1)*(GHR-1)	0.0022159	0.001923	0.2551
(Gap-1)*(GHR-1)	0.0022159	0.001923	0.2551
(GHR-1)*(GC-1)	-0.001967	0.001923	0.3116
(Nef-1)*(FC-1)	-0.001945	0.001923	0.3171
(GHR-1)*(FC-1)	-0.001334	0.001923	0.4913

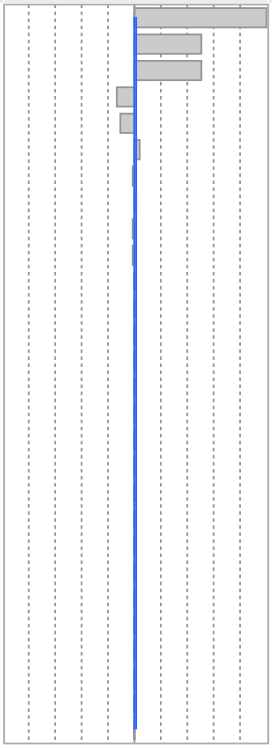

Figure 29. Parameter estimates (Equation [12]) sorted from largest to smallest in terms of volume-averaged fuel temperature of Case 1.

For the seven main effects (variables) and squared gas gap for VA FT, Figure 30 shows leverage plots illustrating the impact of adding each term to the model of Equation (12). The significant slopes of fuel heat rate, gas gap, and neon fraction are further indications of their influence on VA FT variation, while the small slope of the graphite emissivity (bottom right) indicates its negligible influence. Although the estimate of the squared gas gap term is significantly different from zero, its contribution to fuel temperature variation is small, as shown by the almost horizontal line in its leverage plot. All other second-order terms in the regression model in Equation (12) have even smaller contributions to the capsule temperature variations.

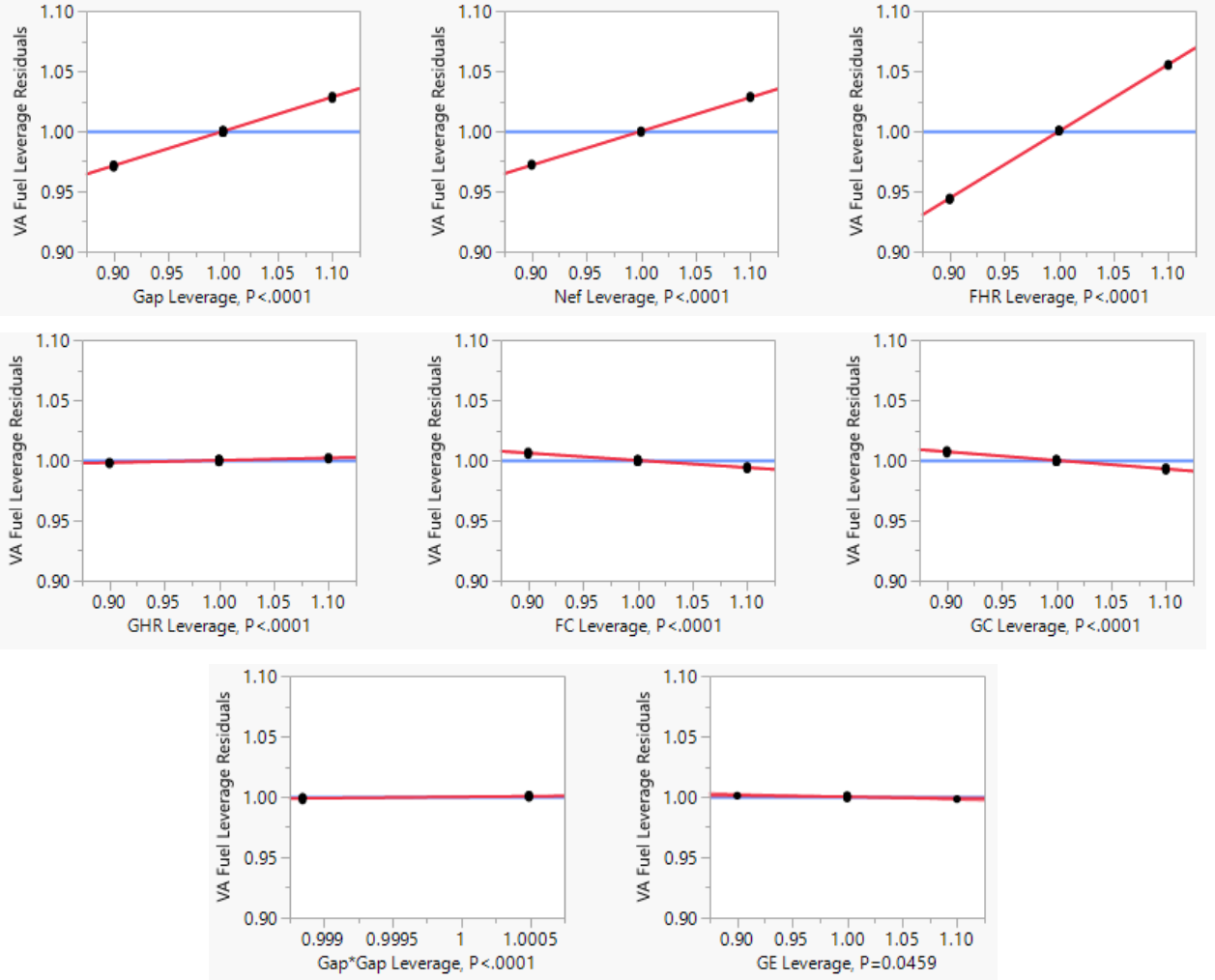

Figure 30. Leverage plots for the seven main effects and square term of gap width for VA fuel temperatures for Case 1 (parameters are relative ratios to their nominal values and in order of sensitivity from largest to smallest indicated by the slope of the plots).

Prediction profilers in the JMP "fit model" platform display (Figure 31) the profile traces for each independent variable for fuel, graphite (-VA and peak), and TC temperatures. A profile trace is the predicted response when one variable is changed but the others are maintained at their current values. The absence of curvature in the prediction profiles for all variables supports the use of a linear relationship between the response measures and the input variables within 10% of input variations. The bar plots in Figure 32 show the parameter sensitivities of seven inputs for all calculated temperatures of interest for Case 7 (Capsule 3) and these sensitivities resemble those for other capsules for all inputs, except for the sensitivity of graphite emissivity, which is only significant for temperatures in Capsule 3.

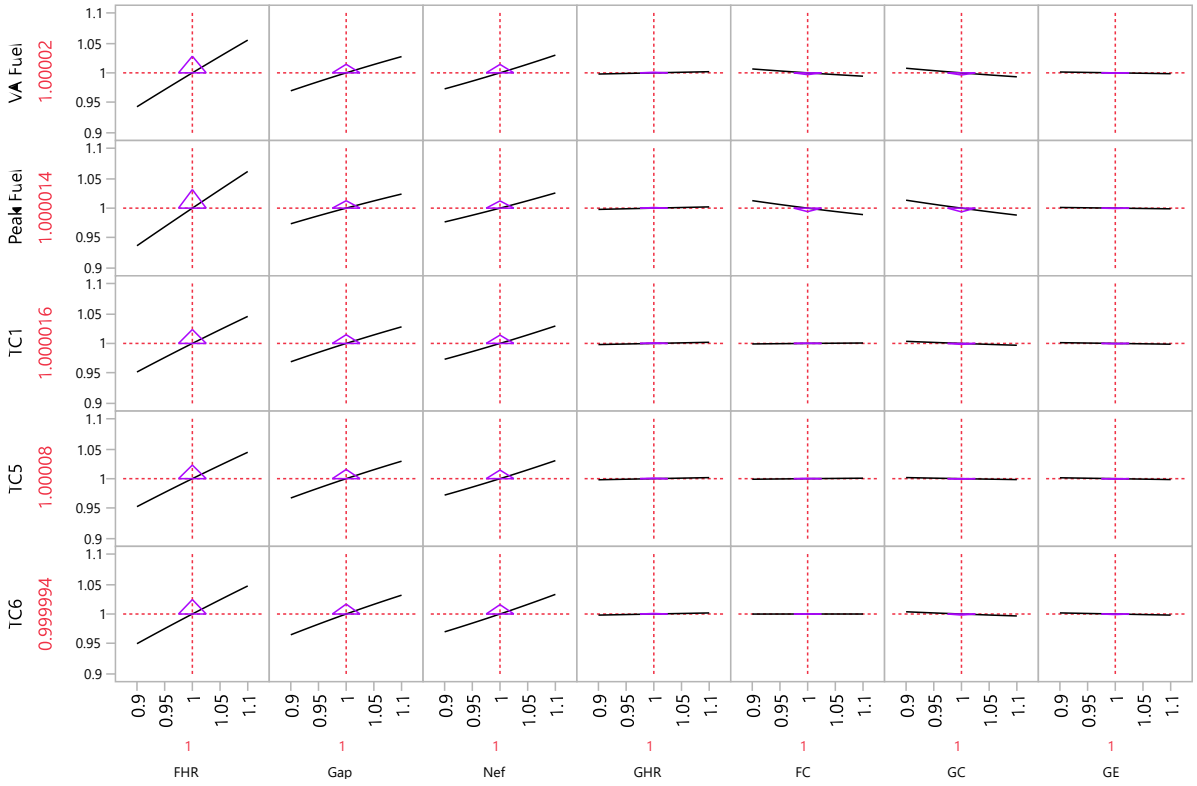

Figure 31. Prediction profiles of functions for fuel VA, peak, and TC temperatures for Case 1.

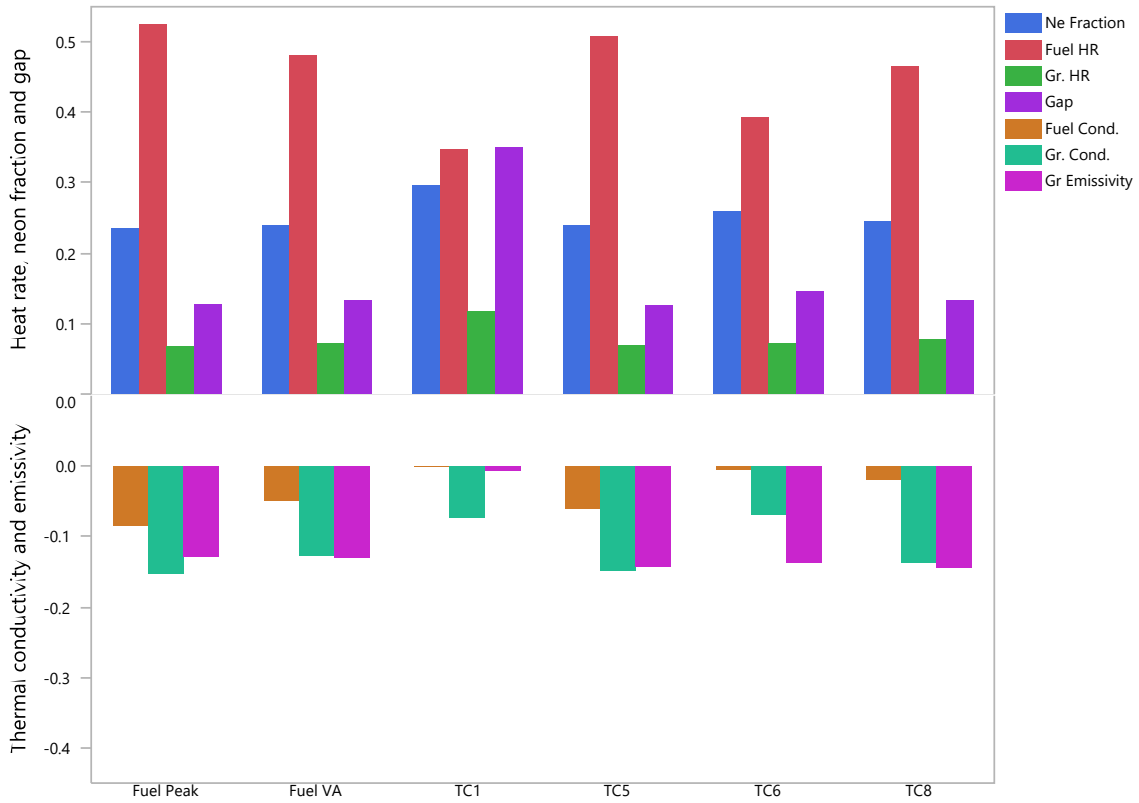

Figure 32. Sensitivity coefficients for fuel peak, VA, and TC temperatures for Capsule 3.

The sensitivity analysis results presented in Figure 29, Figure 30, and Figure 31 allow for exclusion of all second-order terms (square terms of seven variables and their pairwise interactions) in the regression model of Equation (12) because of their relatively negligible contributions to temperature variation. As a result, the regression model of Equation (12) can be reduced to a linearized approximation of model temperature:

$$f_T = a_0 + a_1 FHR + a_2 GHR + a_3 GG + a_4 Nef + a_5 FC + a_6 GC + a_7 GE \quad (13)$$

All calculated temperature results were provided by Grant Hawkes (Hawkes 2022), and the resulting sensitivity coefficients of the seven selected inputs for the 15 scenarios listed in Table 6 were committed to the NDMAS subversion repository (\\isasapp\NGNP_Data\AGR567\PHY\Calc_temperature\Sensitivity\).

4.3.3.3 Sensitivity Coefficients

For each capsule, the 74 runs (Table 5) were performed for 3 different days (Table 6). For each case (i.e., each day and each capsule) and each temperature of interest (i.e., VA FT, peak FT, and TC temperatures), a set of seven sensitivities (as coefficient estimates (a_1–a_7) for Equation [13]) are calculated based on the 74 runs. As a result, we will have three sensitivity values for each of seven inputs for each capsule and each temperature of interest that are plotted in Figure 33 through Figure 39. For each capsule and each temperature of interest, the three sensitivity data points for each input show a clear linear relationship with corresponding input values, as seen in the regression lines in Figure 33 through Figure 35. Therefore, each input sensitivities for other time steps are estimated for each capsule and each temperature of interest via interpolation using linear regression functions from these three data points.

Figure 33 through Figure 35 present sensitivity coefficients and regression lines of the three most sensitive inputs (i.e., fuel heat rate, neon fraction, and gas gap) for both fuel and TC calculated temperatures in the capsules. The remaining less-sensitive inputs have different influences on different temperatures of interest.

The fuel heat rate sensitivity is highest, and similar for all temperatures of interest, reaching a value of 0.6 for TC14 in Capsule 1 (Figure 33).

The three sensitivities in each capsule are well -fit with a linear function of neon fraction with an intercept of zero, which ensures that the interpolated sensitivity always remains positive (Figure 34). The neon fraction sensitivity is greatest for Capsule 5, due to this capsule having the largest gas gap. The different behavior of neon fraction sensitivity in Capsule 3, relative to other capsules, might be caused by the different design of Capsule 3, which had two gas gaps instead of one.

The control gas gap sensitivity (Figure 35) is also highest for Capsule 5 (up to 0.4 for TC6) and lowest for Capsule 3 fuel VA and peak temperatures (~0.1), since its fuel compacts are housed in the inner holder and relatively far removed from the control gas gap.

Figure 36 and Figure 37 show negative sensitivity coefficients and regression lines for the two least-sensitive inputs: fuel and graphite thermal conductivities. Their sensitivities are plotted as a function of fast fluence, which is the main factor in conductivity variation. Both fuel and graphite conductivity sensitivities are stable within an individual capsule but vary significantly across capsules and the temperatures of interest. Most sensitivities for the fuel thermal conductivity are low (absolute sensitivity is less than 0.1, as shown in Figure 36). Sensitivities for the graphite conductivity are slightly higher, ranging between -0.15 and -0.04 (Figure 37).

The graphite heat rate sensitivity coefficient is low (between 0.02 and 0.15) and reached a maximum value of 0.15 for the peripheral TC1 in Capsule 3 (Figure 38).

Finally, the sensitivity coefficients for the graphite thermal emissivity (Figure 39) are only significant (up to -0.25) for fuel and TC temperatures in Capsule 3. This is explained by the large temperature drop (~800°F) across the gap between the inner and outer holders in Capsule 3. This is why the graphite emissivity is included in the list of influential inputs for the AGR-5/6/7 calculated temperature uncertainty. For the other four capsules, the temperature drop between the graphite holder and capsule shell is much smaller (~200°F), leading to lower sensitivity of the graphite emissivity for these capsules.

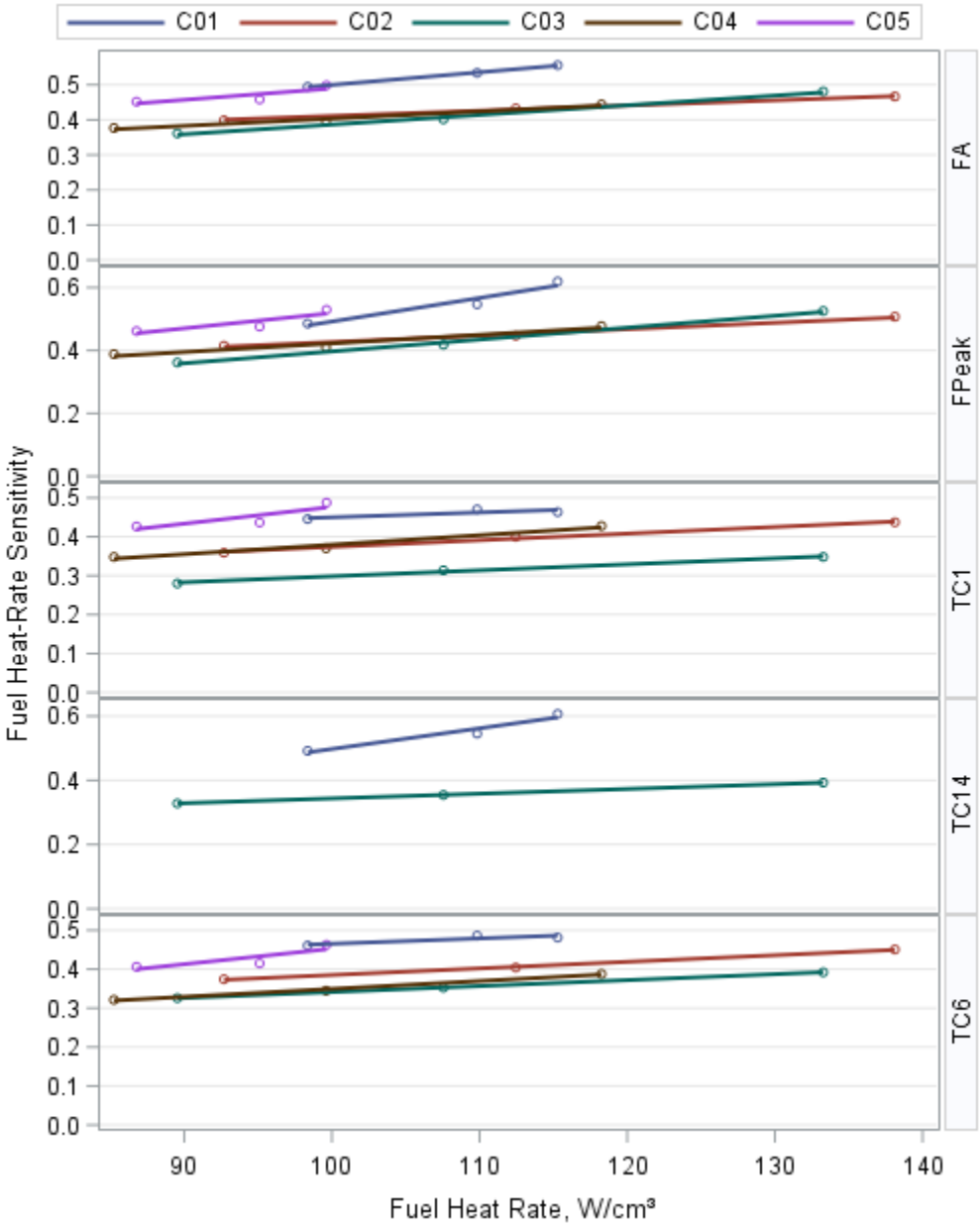

Figure 33. Sensitivity coefficients of the fuel heat rate in the five capsules.

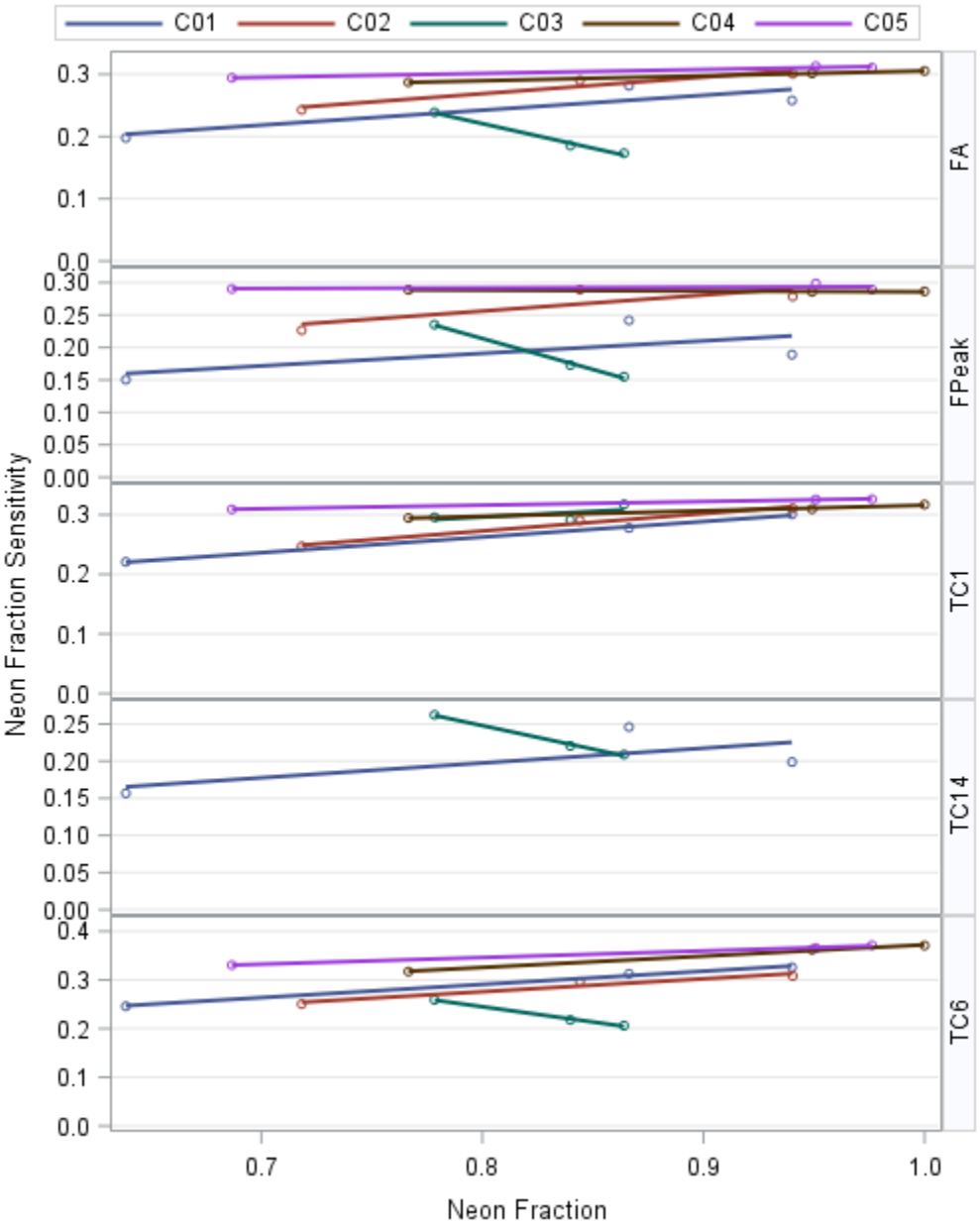

Figure 34. Sensitivity coefficients of the neon fraction in the five capsules.

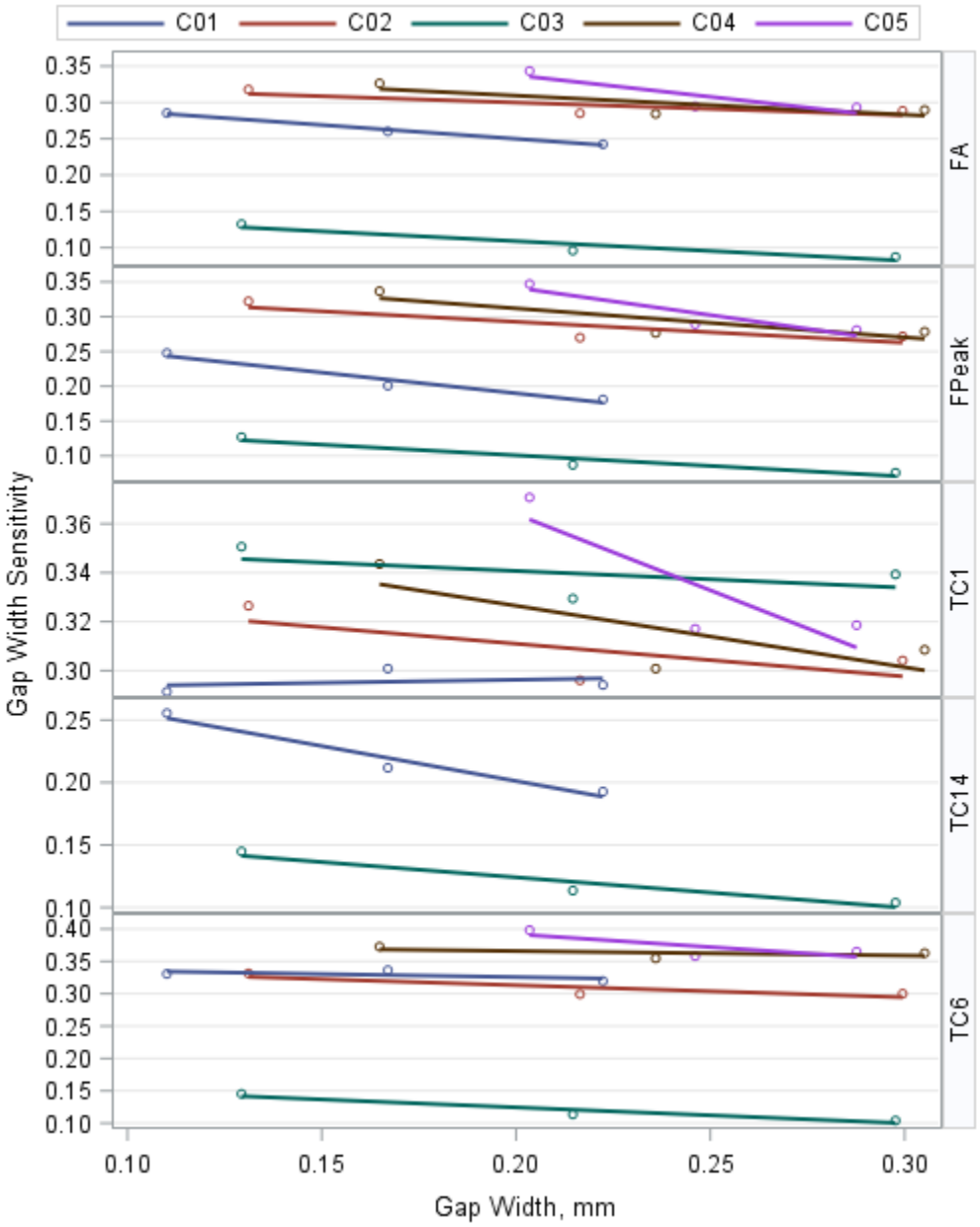

Figure 35. Sensitivity coefficients of the temperature-control gas gap width in the five capsules.

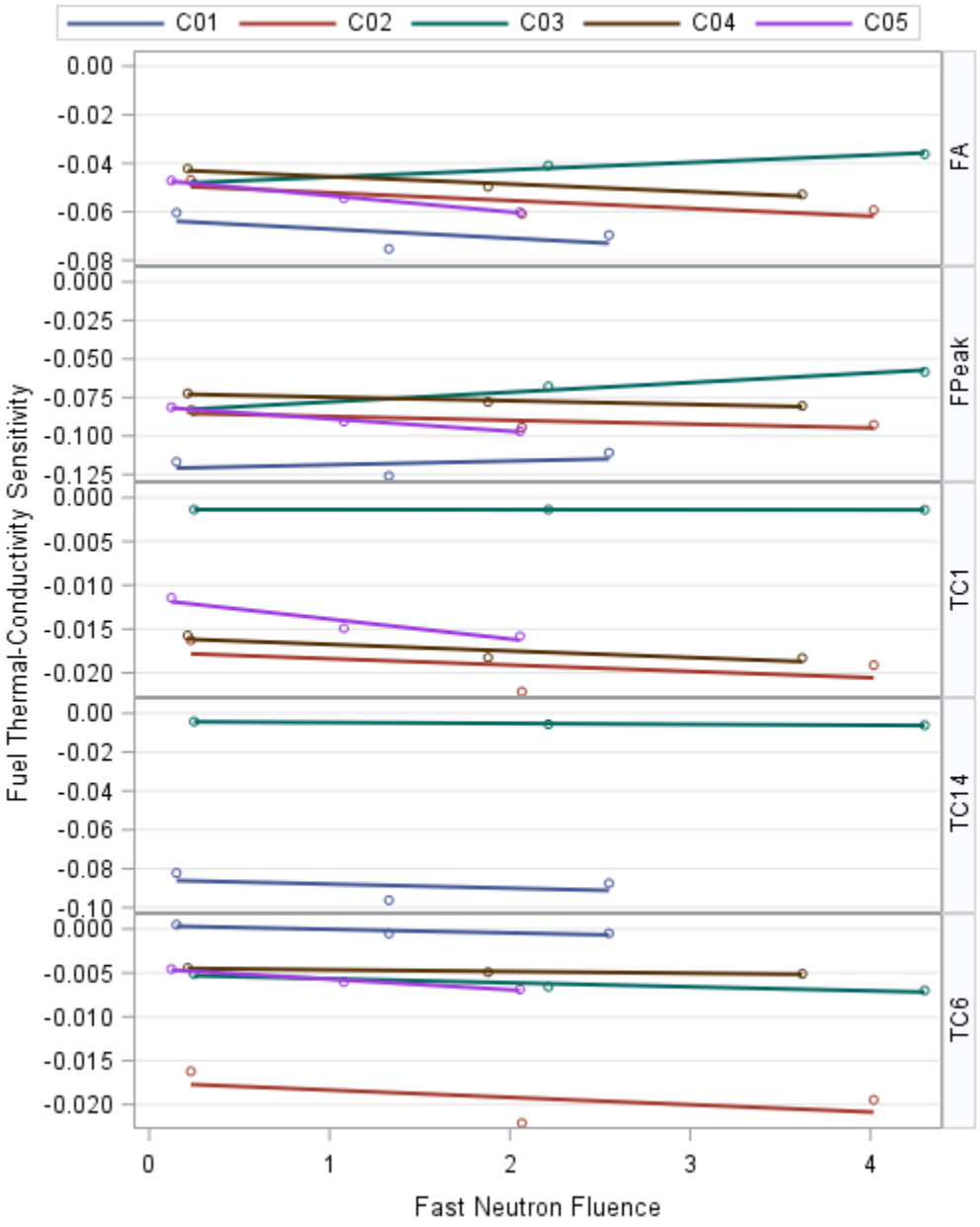

Figure 36. Sensitivity coefficients of the fuel conductivity in the five capsules.

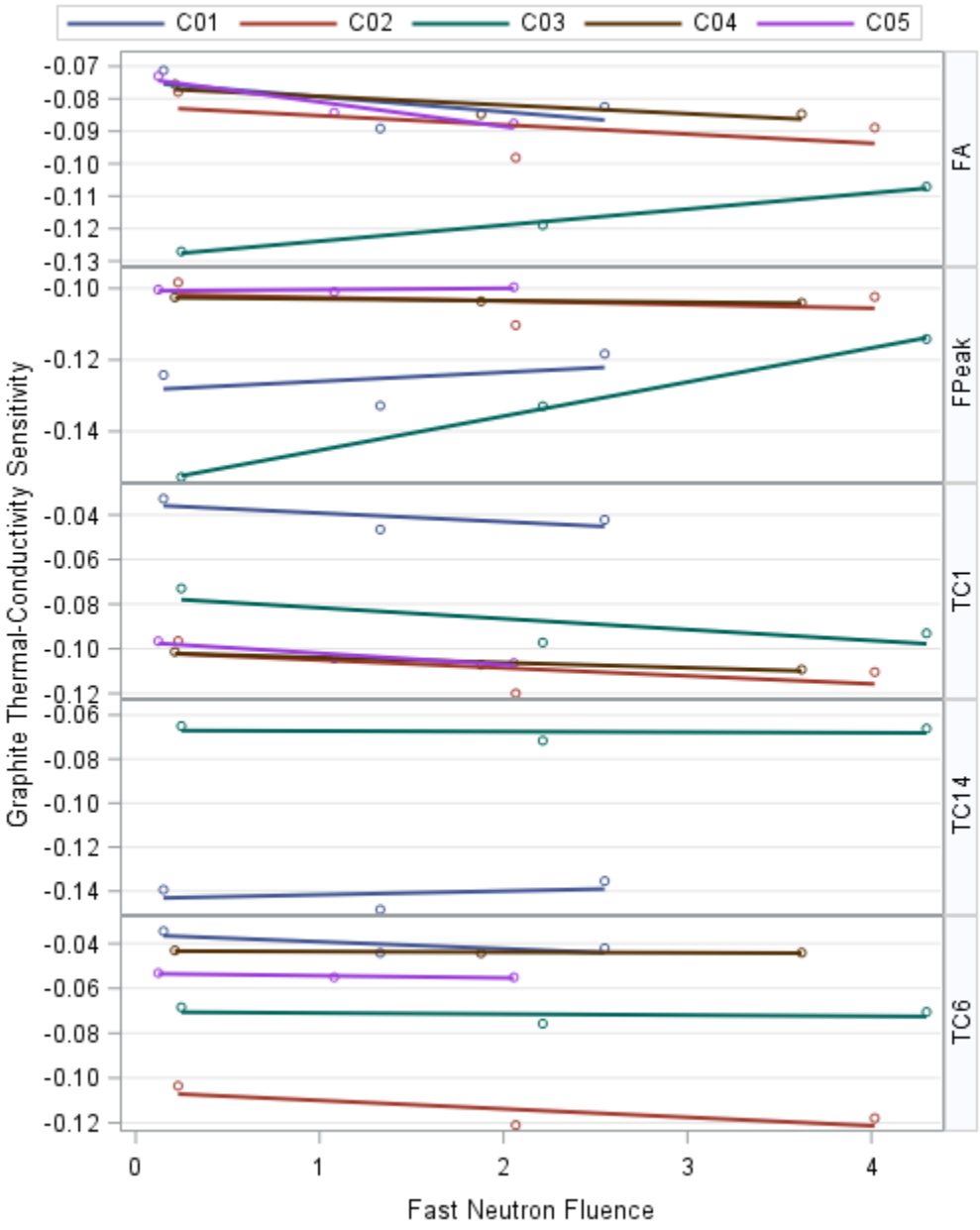

Figure 37. Sensitivity coefficients of the graphite conductivity in the five capsules.

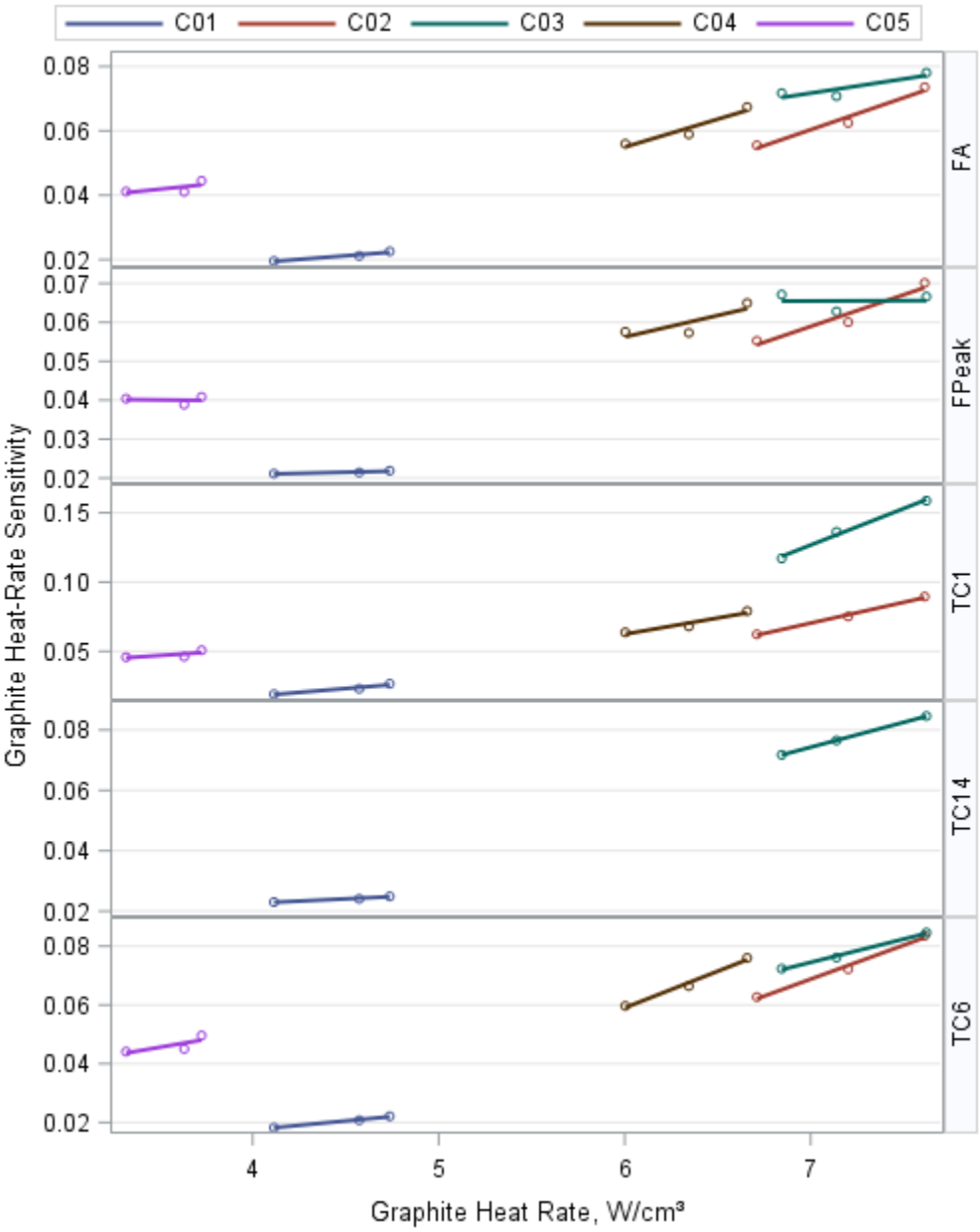

Figure 38. Sensitivity coefficients of the graphite heat rate in the five capsules.

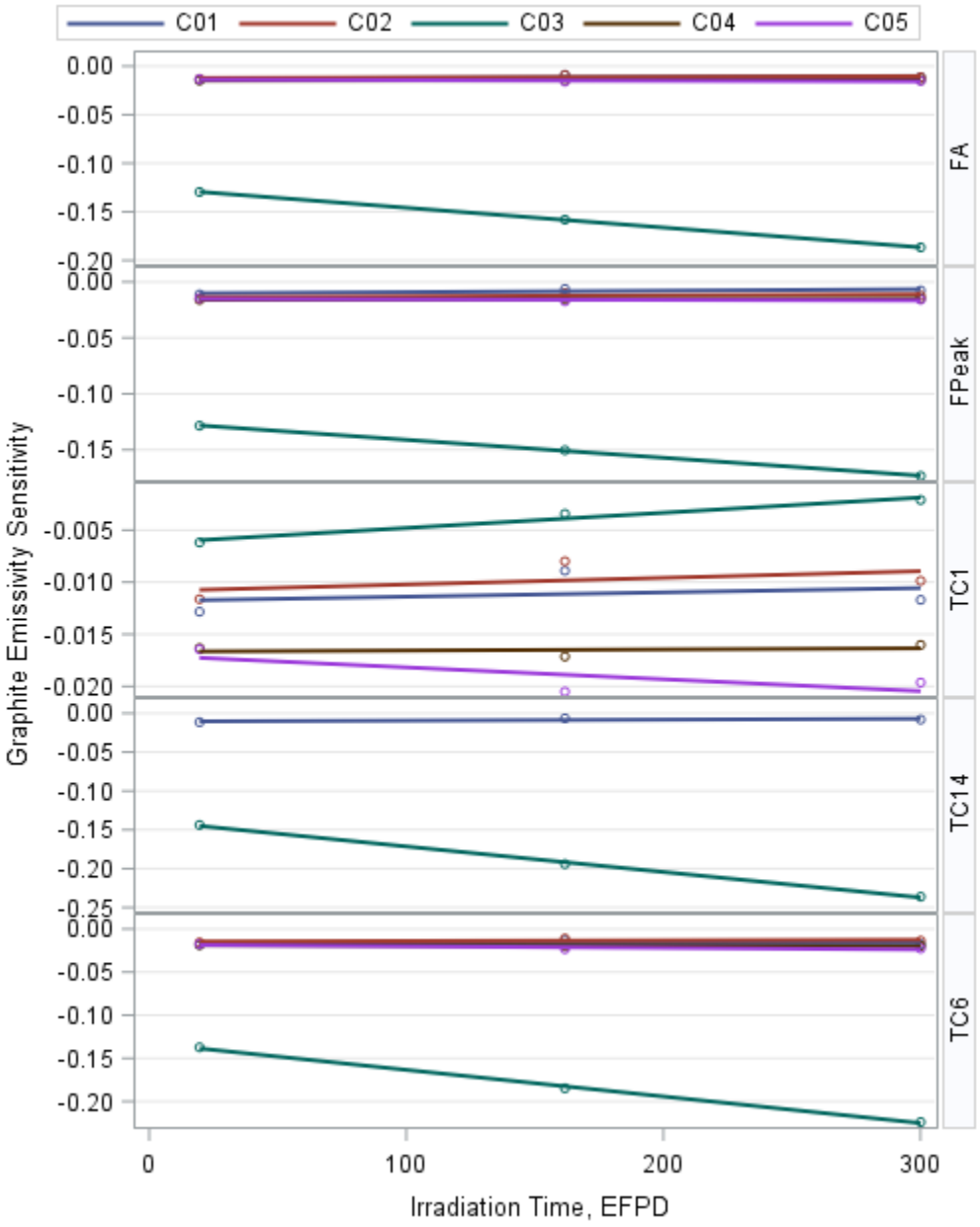

Figure 39. Sensitivity coefficients of the graphite thermal emissivity in the five capsules.

4.3.4 Correlation Coefficients of Thermal Model Input Parameters

4.3.4.1 Uncorrelated Parameters

The correlation coefficient between two input parameters equals zero when their error sources are independent or uncorrelated. In other words, the variation of one parameter does not affect the variation of the other. For example, initial gas gap size and neon fraction are determined using different tools and procedures. The flow rate is measured by the flow meter, and the control gas gap is based on measuring the physical dimensions of the capsule components. Therefore, the uncertainty of the gas gap measurement does not affect the uncertainty in the flow rate measurement; thus, these errors are considered independent. As a result, the correlation coefficient between the neon fraction and gas gap size is zero. For the same reason, correlation coefficients between the two measured parameters (gas gap size and neon fraction) and the four calculated parameters (fuel heat rate, graphite and fuel compact thermal conductivities, and graphite emissivity) are zero.

4.3.4.2 Correlated Parameters

This section estimates the correlation coefficients between the error sources of three calculated parameters: fuel heat rate, graphite conductivity, and fuel compact conductivity. The error associations of these calculated parameters are due to the fact that their formulas contain common factors such as temperature and fast neutron fluence.

Fuel and Graphite Compact Thermal Conductivities

The fuel compact thermal conductivity plot varying with temperature and fast fluence (expressed in neutrons per square centimeter or equivalent displacements per atom) is presented in Figure 26 and the graphite holder thermal conductivity plot is given in Figure 27. From the available data provided by the look-up tables for fuel compact and graphite conductivities as functions of fast fluence and temperature (Hawkes et al. 2014), the relationship between the fuel compact and graphite thermal conductivities as functions of fast fluence (converted into displacements per atom) and temperature (T) were constructed using JMP®. The functional relationship given for fuel compact thermal conductivity is:

$$\begin{aligned} FC = {} & 3.72 \cdot 10^{-5} + 4.07 \cdot 10^{-8} T - 9.44 \cdot 10^{-6} dpa + 3.74 \cdot 10^{-11} (T - 2030)^2 \\ & + 2.31 \cdot 10^{-8} (T - 2030)(dpa - 1.82) + 2.85 \cdot 10^{-6} (dpa - 1.82)^2 \end{aligned} \tag{14}$$

And for graphite holder thermal conductivity:

$$\begin{aligned} GC = {} & 3.36 \cdot 10^{-4} - 3.85 \cdot 10^{-8} T + 1.02 \cdot 10^{-8} (T - 1449.5)(\log(dpa) + 5.05) \\ & - 4.499 \cdot 10^{-5} \log(dpa) - 2.36 \cdot 10^{-6} (\log(dpa) + 5.05)^2 \end{aligned} \tag{15}$$

Using JMP®, 100,000 data points were collected from normal distributions of FT (1500 ± 200 K), graphite temperature (1200 ± 200 K), and displacements per atom (μ_{dpa} ± 10%) for five levels of the mean displacements per atom, μ_{dpa} = 0.5, 1, 2, 3, 4, corresponding to fast neuron fluence. The multiplier used to convert fast fluence to displacements per atom is 0.823×10^{-25} dpa/(n/m^2) (Hawkes 2015).

To compute the correlation coefficient between random variations of fuel and graphite conductivities, the fuel compact and graphite temperatures of one data point (a pair of temperatures and displacements per atom) were sampled with the same noise components. The sampled displacements per atom and temperature values were inserted in Equation (14) and Equation (15) to compute the fuel compact and graphite thermal conductivities for each data point. The correlation coefficient between the graphite and the fuel compact thermal conductivities was estimated using the JMP® "multivariate" function. Figure 40 shows the scatter plot matrix of FT, displacements per atom, fuel compact, and graphite thermal conductivities, along with their distribution and correlation coefficients, for each pair of variables for displacements per atom levels 0.5 and 2.0.

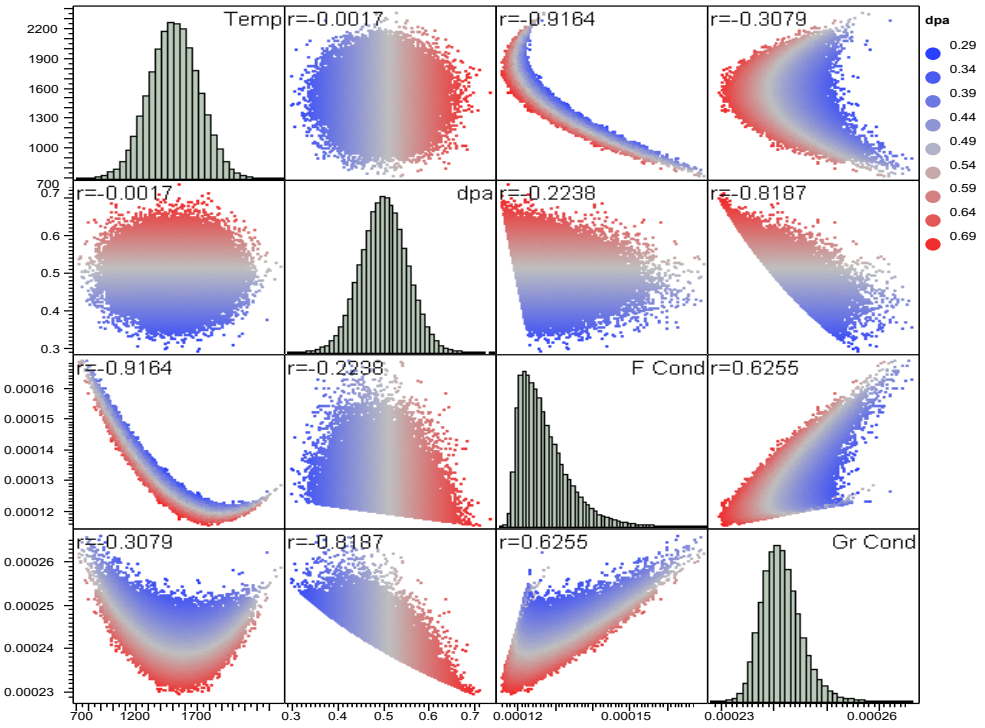

$$\mu_{dpa} = 0.5$$

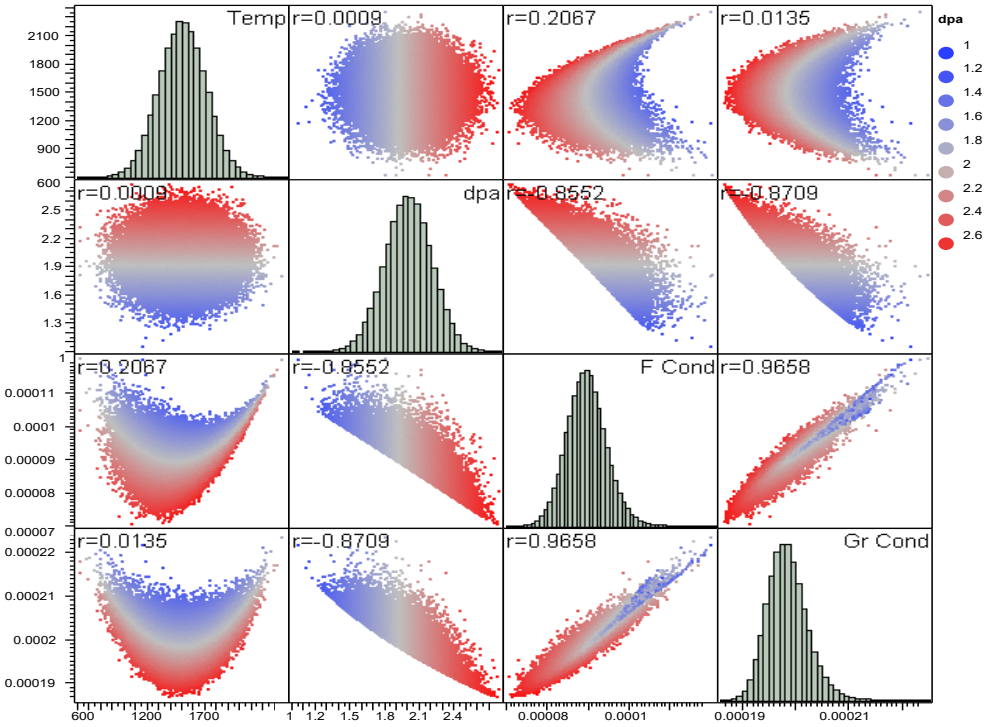

$$\mu_{dpa} = 2.0$$

Figure 40. Scatter plot matrix showing the correlation between the fuel compact and the graphite thermal conductivities at one fuel temperature and two displacements per atom levels (0.5 and 2.0).

The noise correlation coefficients between the fuel compact and the graphite thermal conductivities $\rho_{FC,GC}$ for five levels of fast neutron fluence (converted from displacements per atom) are presented in Table 7 and Figure 41. The second-order polynomial function of the fast fluence (f) in n/m^2 × 10^{25} was used to fit the correlation coefficients in Table 7.

$$\rho_{FC,GC} = -0.0708f^2 + 0.3585f + 0.4464 \quad (16)$$

Table 7. Correlation coefficients between the fuel compact and the graphite thermal conductivities.

Fast fluence (n/m2 × 1025) [E > 0.18 MeV]	0.6075	1.215	2.430	3.645	4.860
Correlation coefficient	0.6255	0.7739	0.9658	0.7355	0.544

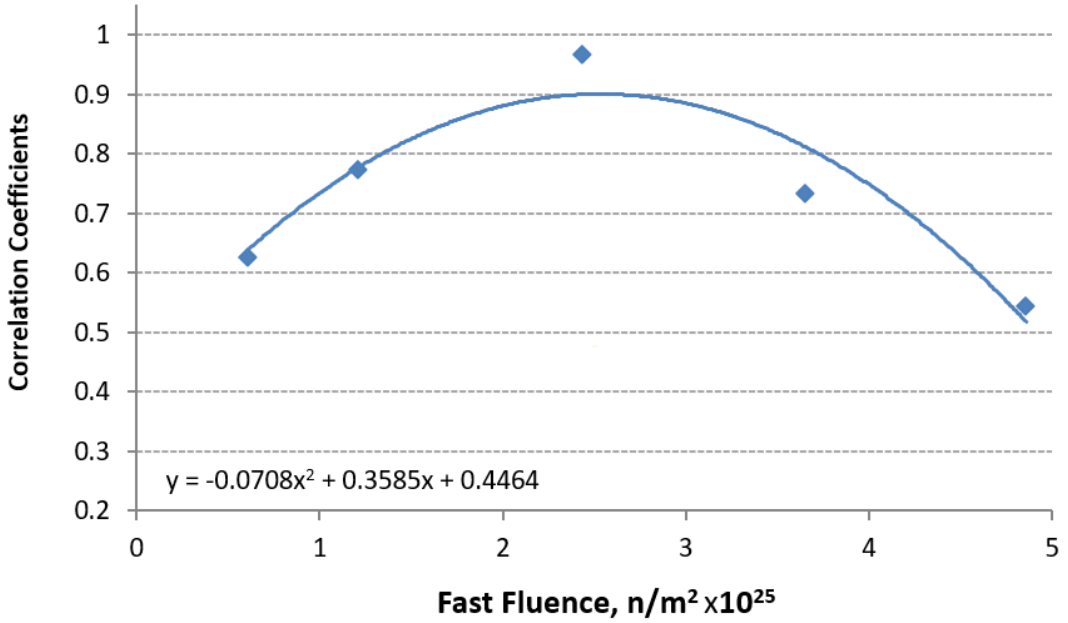

Figure 41. Correlation coefficients between the fuel compact and the graphite thermal conductivities varying with fast neutron fluence.

Fuel Compact/Graphite Thermal Conductivity and Fuel Compact/Graphite Heat Rate

The value of the fuel compact heat rate (Q) depends on the daily neutron flux, FT, and material properties such as cross section and fuel burnup. The graphite and fuel compact thermal conductivities, as mentioned earlier, are a function of temperature and fast neutron fluence. Based on the functional dependence of the fuel compact and graphite thermal conductivity and fuel heat rate on the fast neutron fluence and neutron flux, it is reasonable to assume that the correlation coefficient between their noises should be smaller than that between the graphite and fuel conductivities. Since the fuel compact and graphite thermal conductivities and fuel heat rate are impossible to simulate, their noise correlation coefficients are assumed to be half of the correlation coefficient between the fuel and graphite conductivities.

Fuel Compact/Graphite Heat Rate

The fuel compact and graphite heat rates are directly defined by fast neutron fluence; therefore, their correlation coefficient should be very high. In this study, this correlation coefficient is conservatively assumed to be 1.

4.3.5 Quantify the Uncertainty for Instantaneous Temperatures

The variation of parameter estimates across the three thermal condition scenarios in the five capsules presented in Figure 31 through Figure 39 reflects the variation in parameter sensitivities over the entire input domain for the AGR-5/6/7 capsules. This reflects the nonlinear response of the thermal model to variation in the input variables. However, within a small enough input range (e.g., from [nominal*(1−10%)] to [nominal*(1+10%)]), the calculated temperatures can be estimated by a linear combination of seven input variables, as presented in Equation (13). Consequently, the standard parameter error propagation of the linear summation (Ostle and Mensing 1975) can be used to calculate the overall output temperature uncertainty from the variance/-covariance matrix of input variables for an input range close to the nominal values. The expression of output variance for each output, *T*, is given in Equation (4).

The input parameter uncertainties are estimated in terms of relative standard deviations (%) in Section 4.3 and the sensitivity coefficients are estimated in Section 4.3.3. Section 4.3.4 addresses the correlation coefficients of each variable pair. The correlation coefficient of a variable pair is a measure of the degree (or intensity) of association between the two variables (Ostle and Mensing 1975). For each capsule, the AGR-5/6/7 thermal model parameter uncertainty quantification for daily average temperatures (TC temperature, VA FT, or peak FT) is performed.

4.3.5.1 Daily Input Parameter Uncertainties (σ_i)

The daily input parameter uncertainties in terms of relative standard deviation for the seven significant input variables are estimated via the manner discussed in Section ***4.3***. The details of the daily uncertainty calculations are:

- The parameter uncertainties for fuel heat rate, fuel compact thermal conductivity, graphite holder thermal conductivity, and graphite holder emissivity are assumed to be constant random errors for all time steps and the five capsules, as presented in Table 3. Therefore, their plots as a function of EFPDs are flat lines for all three parameters in all capsules.
- The daily parameter uncertainties for gas gap width (σ_{GG_i}) are based on the error of the gas gap width in Equation (9), as described in Section 4.3.2.
- The daily parameter uncertainty for the neon fraction (σ_{Nef_i}) is calculated for each time step and each capsule by substituting the actual capsule neon fraction at that time step, using Equation (10) (representing a functional relationship between neon fraction uncertainties and neon fraction values). Since the capsule neon fractions vary with time to maintain the capsule specified FT, the daily uncertainties of the neon fraction also vary with EFPDs.

4.3.5.2 Daily Parameter Sensitivities (a_i)

The daily parameter sensitivities, a_i, of seven significant input variables at time step (i) were estimated using the functional relationships between the sensitivity coefficients and corresponding input parameters that were established in Section 4.3.3 for each output temperature in each capsule. Since the inputs to the thermal models vary with time, so do the resulting daily parameter sensitivities.

4.3.5.3 Daily Correlation Coefficients (σ_{FC,GC_i})

The daily correlation coefficients between the fuel compact and graphite thermal conductivities, $\rho_{FC,GC}$, at time step (i) are calculated using the function of fast neutron fluence given in Equation (16) and shown in Figure 41. Since the neutron fluence varies with time, so do the daily correlation coefficients.

4.3.5.4 Quantify Parameter Uncertainty ($\sigma_{P_i}^2$)

The parameter uncertainty (in terms of variance) of the thermal model output temperature at time step (i) is calculated using Equation (4). Since the input sensitivity, correlation coefficient, and uncertainty all vary with time, so does the calculated temperature uncertainty.

4.3.6 Quantify the Uncertainty for Time-Averaged Fuel Temperatures

The capsule TA, VA, FT, and TA peak FT at day (*i*) are calculated from the daily average temperatures as:

$$T_{TA_i} = \frac{\sum_{k=1}^{i} T_k \cdot t_k}{\sum_{k=1}^{i} t_k} \tag{17}$$

where

T_k and t_k = daily average calculated temperature and time step at day (k).

Time step t_k equals 1 for most time steps and t_k <1 for the startup or power--down days. The uncertainty of the TA temperatures is calculated using the standard formula for error propagation of the linear combination of daily average temperatures. Assuming that changes in daily averaged calculated temperatures are independent from each other, the uncertainty of the TA FT (VA or peak) is calculated as:

$$\sigma_{T_{TAi}} = \sqrt{\frac{\sum_{k=1}^{i} t_k \sigma_{T_k}^2}{\sum_{k=1}^{i} t_k}} \tag{18}$$

5. RESULTS

The overall model temperature uncertainty is estimated using the uncertainty quantification procedure described in the previous sections. The daily uncertainty (in terms of relative and absolute standard deviation at each time step) is estimated for the following calculated temperatures: all TCs, instantaneous VA FT, and peak FT. The uncertainty of the corresponding -TA fuel temperatures is calculated from uncertainties for instantaneous temperatures, using Equation (18).

As stated in Section 4.3, the uncertainties of fuel heat rate, graphite heat rate, fuel thermal conductivity, graphite thermal conductivity, and graphite emissivity are assumed constant over the entire irradiation and are the same for all capsules. Therefore, they are plotted as horizontal lines as a function of EFPDs. Among these, fuel conductivity has the highest uncertainty (20%), followed by the graphite conductivity (15%) and graphite emissivity (10%). The uncertainty for the fuel heat rate (5%) is higher than that for the graphite heat rate (3%) because of the added complexity of fuel depletion. On the other hand, the uncertainties of the gas gap width and neon fraction are dynamic over the irradiation time because they are a function of the input variations, as described in Section 4.3.2. The gas gap width uncertainties are highest due to the 0.005 in. clearance between the holder and capsule shell. For the neon fraction, the uncertainties are unusually large for a few time steps at the beginning and end of each ATR cycle, when the neon fractions were close to zero.

The uncertainty results include the dominant parameter of the calculated temperature uncertainty, that contributes most to temperature variance. That variance is the square of the product of the sensitivity coefficient and the standard deviation for a parameter$(a_i\sigma_i)^2$. The dominant parameter varies depending on the magnitude of the parameter uncertainty (e.g., fuel heat rate, neon fraction) and sensitivity to that parameter. The results given in the following sections identify the dominant parameter and quantify its influence on the overall uncertainty. The overall uncertainties in terms of standard deviation are given both as a range (maximum/minimum) over EFPDs for instantaneous temperatures and at the end of irradiation for -TA temperatures. Note that only data for full days at full power (EFPD = 1) are included in these plots because temperatures are much lower during start-up and power-down periods and are of minor importance in model uncertainty. Also, the values in the summary tables below (Table 8 through Table 12) were calculated excluding two low-power PALM cycles (163A and 167A) and the days around startups and power-downs, when temperatures in all capsules were low.

The results of the uncertainty analysis for each capsule are summarized below, in separate subsections, starting with the capsule at the top of the experiment test train. Those sections also contain plots comparing measured TC values to the model-calculated values and their corresponding 1-σ uncertainty, allowing a comparison of apparent model error to estimated model uncertainty. Additional plots that provide that comparison for each TC, including an estimated TC uncertainty, are contained in Appendix A.

5.1 Temperature Uncertainty Results for Capsule 5

Table 8 summarizes the temperature uncertainty results for Capsule 5. Figure 42 shows the daily uncertainty in terms of relative standard deviation for the selected inputs, together with sensitivity coefficients for VA fuel temperature (similar for peak fuel temperature) and TC1 temperature (representative for other TCs). The daily uncertainty results are presented in Figure 43 for peak and VA fuel temperature, and in Figure 44 for TC temperatures.

Table 8. Summary of temperature uncertainty results for Capsule 5 (excluding Cycles 163A and 167A).

	Peak Fuel	Volume-Averaged Fuel	Peak Fuel	Volume-Averaged Fuel	TCs
Instantaneous Temperature – Minimum/Maximum	6.9 – 9.9%	6.9 – 9.8%	46 – 76°C	38 – 65°C	55 – 70°C
Time-Averaged Temperature – At End of Irradiation	7.8%	7.7%	66°C	57°C	N/A

The following results of calculated temperature uncertainty are observed:

- *Input uncertainty* (Figure 42): The gas gap has the highest input uncertainties (up to 22% at SOI) and slightly changes over time due to increases in both the gap absolute uncertainty and gap width. The neon fraction uncertainties (green line) are mostly close to 3% for a ~1 neon fraction (near-pure neon gas mixture), with a few higher values for time steps at the beginning of each cycle, when the neon fraction is low. Uncertainties for the remaining inputs remain unchanged throughout the irradiation time.
- *Input parameter sensitivity* (Figure 42): The fuel heat rate (red line) has the highest sensitivity for both fuel and TC temperatures (up to 0.5), followed by neon fraction and gas gap (up to 0.35). The remaining four inputs (fuel and graphite conductivities, graphite heat rate, and graphite emissivity) have small sensitivity coefficients for fuel and TC temperatures: generally less than 0.1 in absolute values.

- *Weighted variance* (Figure 43 and Figure 44): Gas gap uncertainty is the dominant factor for both fuel and TC temperature, due to its high uncertainty and sensitivity. The fuel heat rate (the second dominant factor), which had the highest sensitivity but a low input uncertainty (5%), thus, had significantly less influence on the uncertainties of calculated temperatures. The remaining inputs contributed very little to the calculated temperature uncertainty.
- *Input calculated temperature uncertainty* (Figure 43 and Figure 44): The calculated temperature uncertainties are moderate compared to the other capsules, ranging between 60 and 75°C for absolute uncertainty. The moderate temperature uncertainty is caused mainly by the lower gas gap uncertainty due to the larger gap width. In terms of absolute standard deviation, the uncertainty is largest for peak fuel temperature (70°C on average). In terms of relative standard deviation, TC6, located near the control gap, had the highest uncertainty (up to 10%), due to the high sensitivity of the gap width uncertainty, whereas other TC and fuel temperatures had a similar level of uncertainty (between 7 and 9%).

  The bottom panels show daily instantaneous and TA temperatures plotted with one standard deviation. For TC temperatures (Figure 44), the measured temperatures of the three operational TCs (dots) lie below the corresponding calculated lines but are well within the one-standard-deviation uncertainty band, suggesting that the uncertainty calculations capture the influential factors for this capsule.

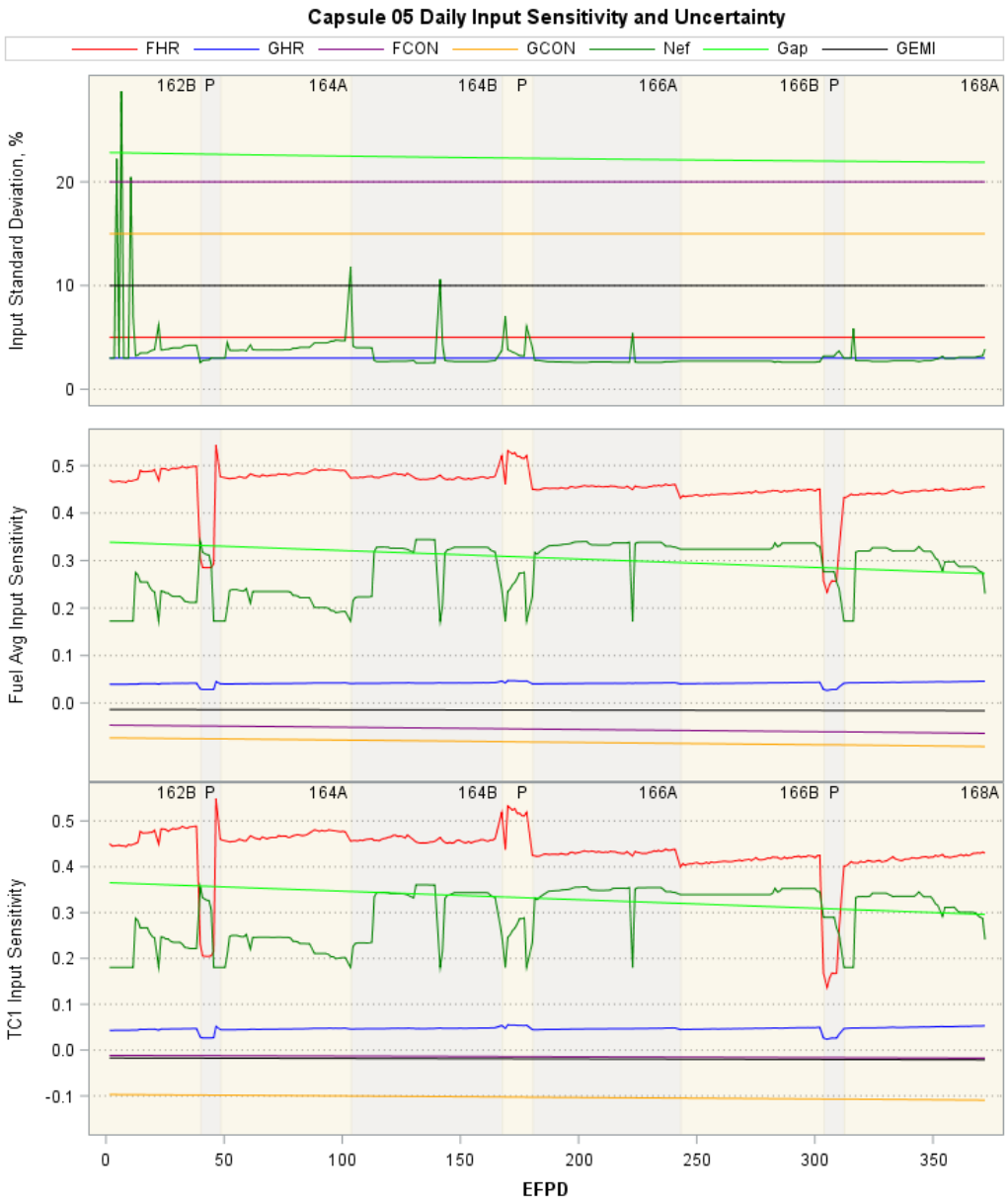

Figure 42. Daily relative standard deviations for seven inputs in Capsule 5. "P" – PALM Cycles 163A, 165A, and 167A.

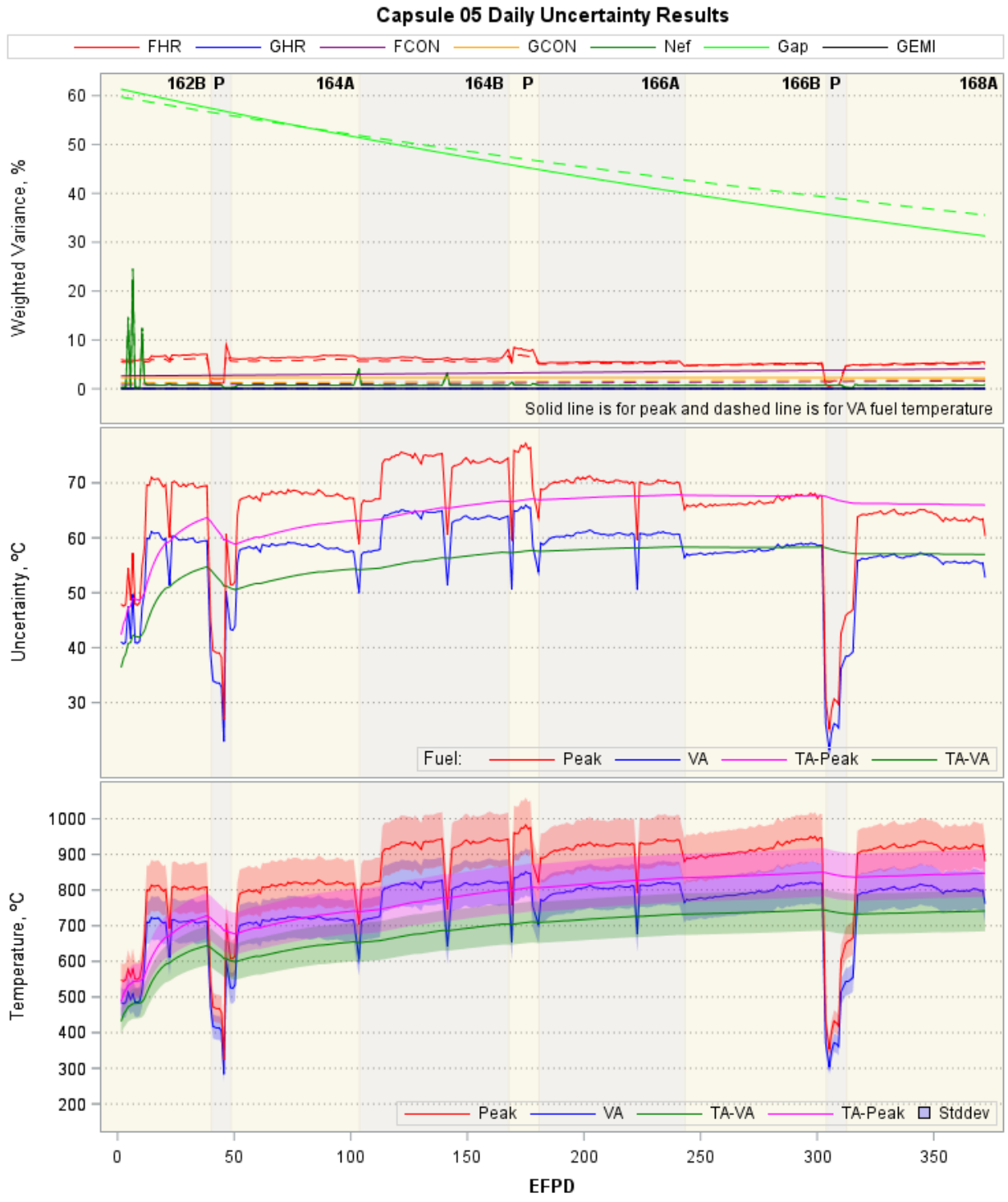

Figure 43. Daily uncertainty results for instantaneous and time-averaged peak and volume-averaged fuel temperatures in Capsule 5. “P” – PALM Cycles 163A, 165A, and 167A.

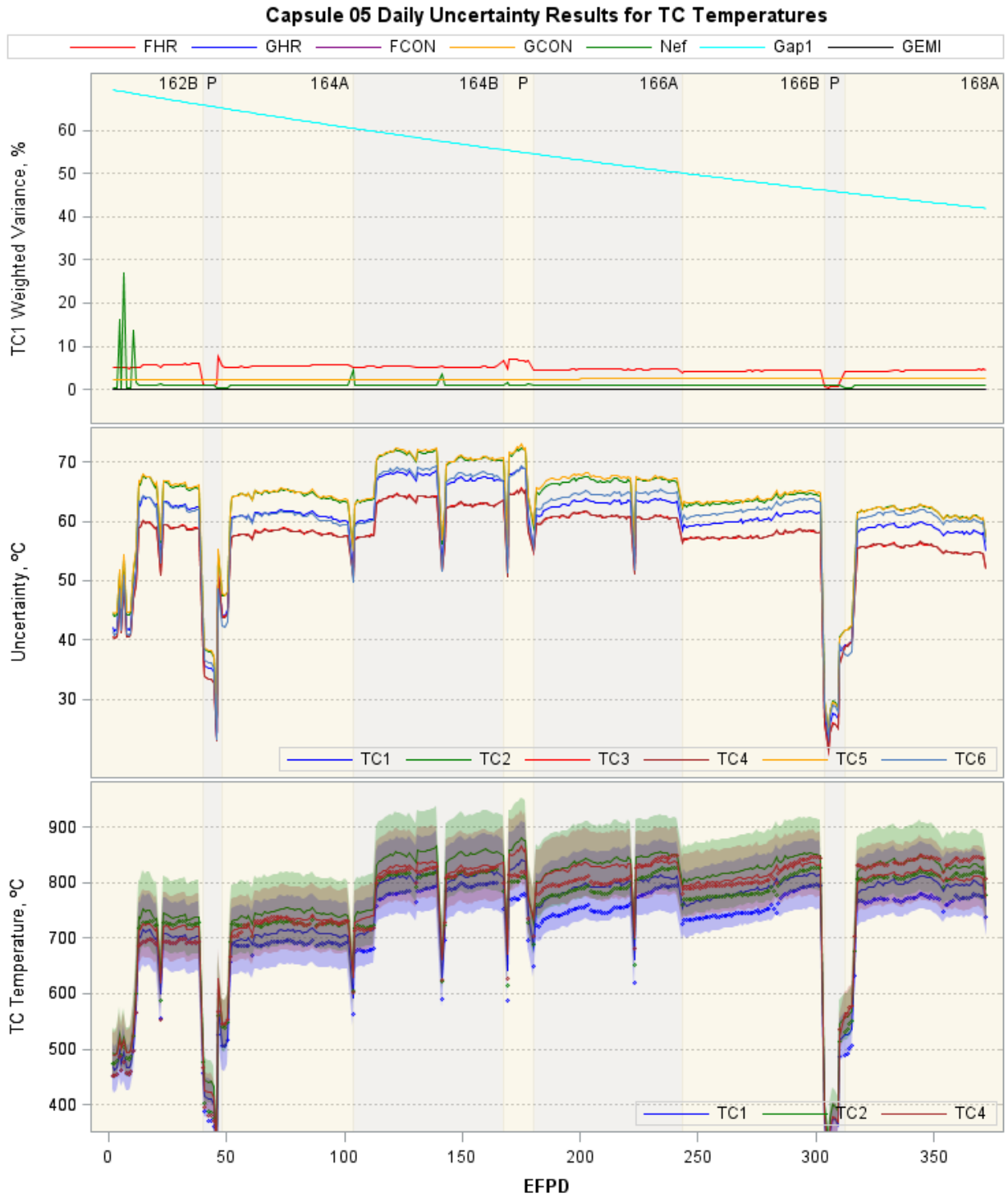

Figure 44. Daily uncertainty results for instantaneous TC temperatures in Capsule 5 (lines are calculated TCs and dots are measured TCs). TC3, TC5, and TC6 are excluded in the bottom panel because they failed early. "P" – PALM Cycles 163A, 165A, and 167A.

5.2 Temperature Uncertainty Results for Capsule 4

Table 9 summarizes the temperature uncertainty results for Capsule 4. Figure 45 shows the daily uncertainty in terms of relative standard deviation for selected inputs, together with the sensitivity coefficients for VA fuel temperature (similar for peak fuel temperature) and TC1 temperature (representative for other TCs). The daily uncertainty results are presented in Figure 46 for peak and VA fuel temperature, and in Figure 47 for TC temperatures. Since Capsules 4 and 5 have similar designs and were exposed to a similar temperature range, this led to quite similar uncertainty results for both the calculated fuel and TC temperatures.

Table 9. Summary of temperature uncertainty results for Capsule 4 (excluding Cycles 163A and 167A).

	Peak Fuel	Volume-Averaged Fuel	Peak Fuel	Volume-Averaged Fuel	TCs
Instantaneous Temperature – Minimum/Maximum	6.5 – 11.1%	6.6 – 10.8%	49 – 95°C	43 – 82°C	65 – 90°C
Time-Averaged Temperature – At End of Irradiation	8.0%	7.9%	76°C	66°C	N/A

The following results of calculated temperature uncertainty are observed:

- *Input uncertainty* (Figure 45): The gas gap has the highest input uncertainties (up to 28% at SOI) and changes over time due to increases in both the gap absolute uncertainty and gap width (~20% at EOI). The neon fraction uncertainties (green line) are mostly close to 3% for ~1 neon fraction, except a few higher values for time steps at the beginning of each cycle when the neon fraction is low. Uncertainties for the remaining inputs remain unchanged throughout the irradiation time.
- *Input parameter sensitivity* (Figure 45): The fuel heat rate (red line) has the highest sensitivity for both fuel and TC temperatures (~ 0.4), followed by the neon fraction and gas gap (~ 0.3). The remaining four inputs (fuel and graphite conductivities, graphite heat rate, and graphite emissivity) have small sensitivity coefficients for the fuel and TC temperatures: generally less than 0.1 in absolute values.
- *Weighted variance* (Figure 46 and Figure 47): The gas gap uncertainty is the dominant factor for both the fuel and TC temperature, due to both high uncertainty and sensitivity. The fuel heat rate (the second most influential factor), which had the highest sensitivity but a low input uncertainty (5%), had significantly less influence on the uncertainties of calculated temperatures. The remaining inputs contributed very little to the calculated temperature uncertainty.
- *Calculated temperature uncertainty* (Figure 46 and Figure 47): The calculated temperature uncertainties are higher than for Capsule 5 during the first half of irradiation, due to impact of higher gap width uncertainty. Uncertainties for VA and peak fuel temperatures range between 60 and 95°C. In terms of absolute standard deviation, the uncertainty is largest for peak fuel temperature (70°C on average). In term of relative standard deviation, TC6, located near the control gap, has the highest uncertainty (up to 11%), due to the high sensitivity of the gap width uncertainty, whereas other TC and fuel temperatures have a similar uncertainty of between 6 and 10%.

  The bottom panels show daily instantaneous and TA temperatures plotted with one standard deviation. Like Capsule 5, the measured temperatures of the three operational TCs (dots) are lower than the corresponding calculated lines but well within the one-standard-deviation uncertainty band (Figure 47), suggesting that the uncertainty calculation captures the primary influential factors for this capsule.

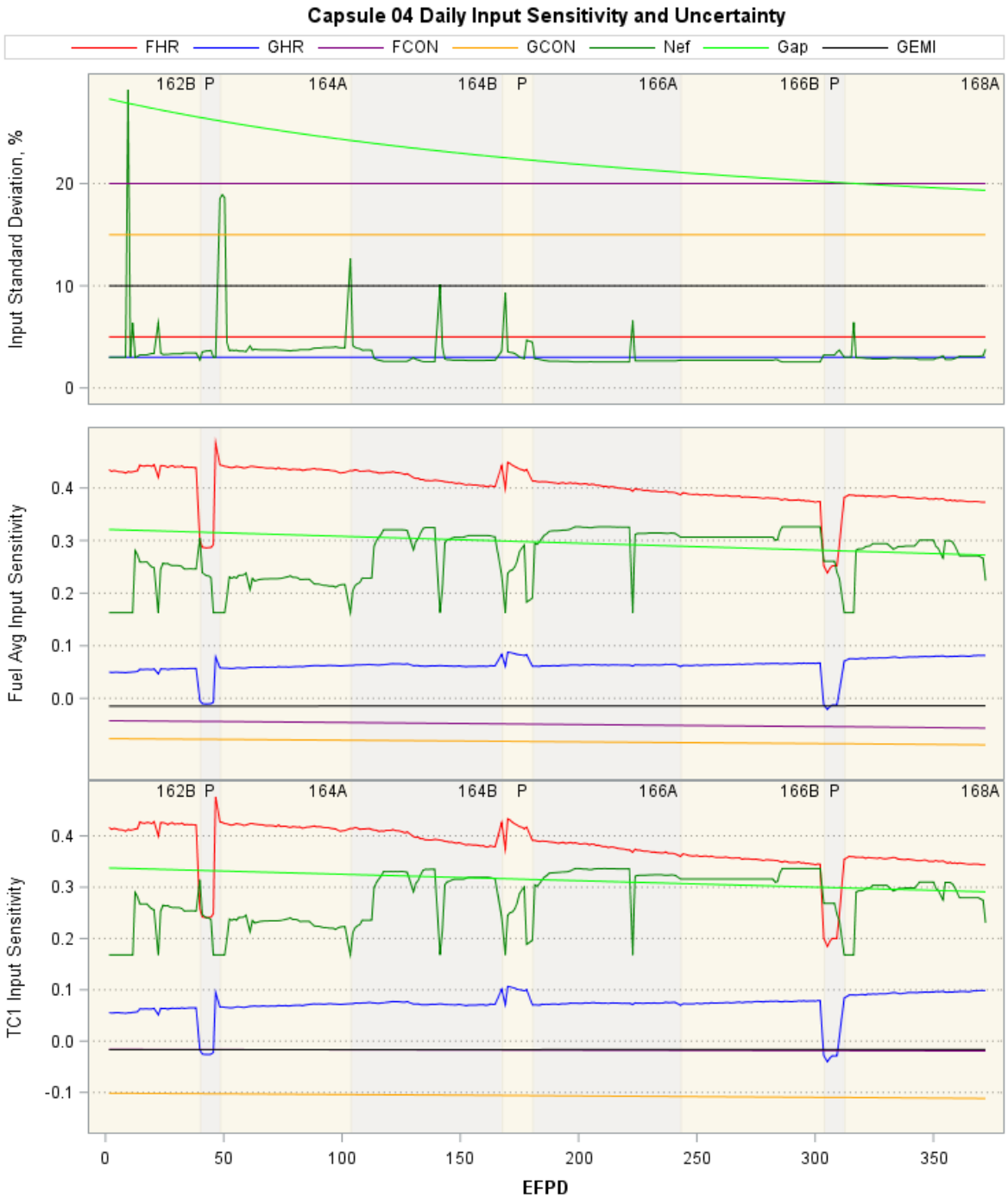

Figure 45. Daily relative standard deviations for seven inputs in Capsule 4. "P" – PALM Cycles 163A, 165A, and 167A.

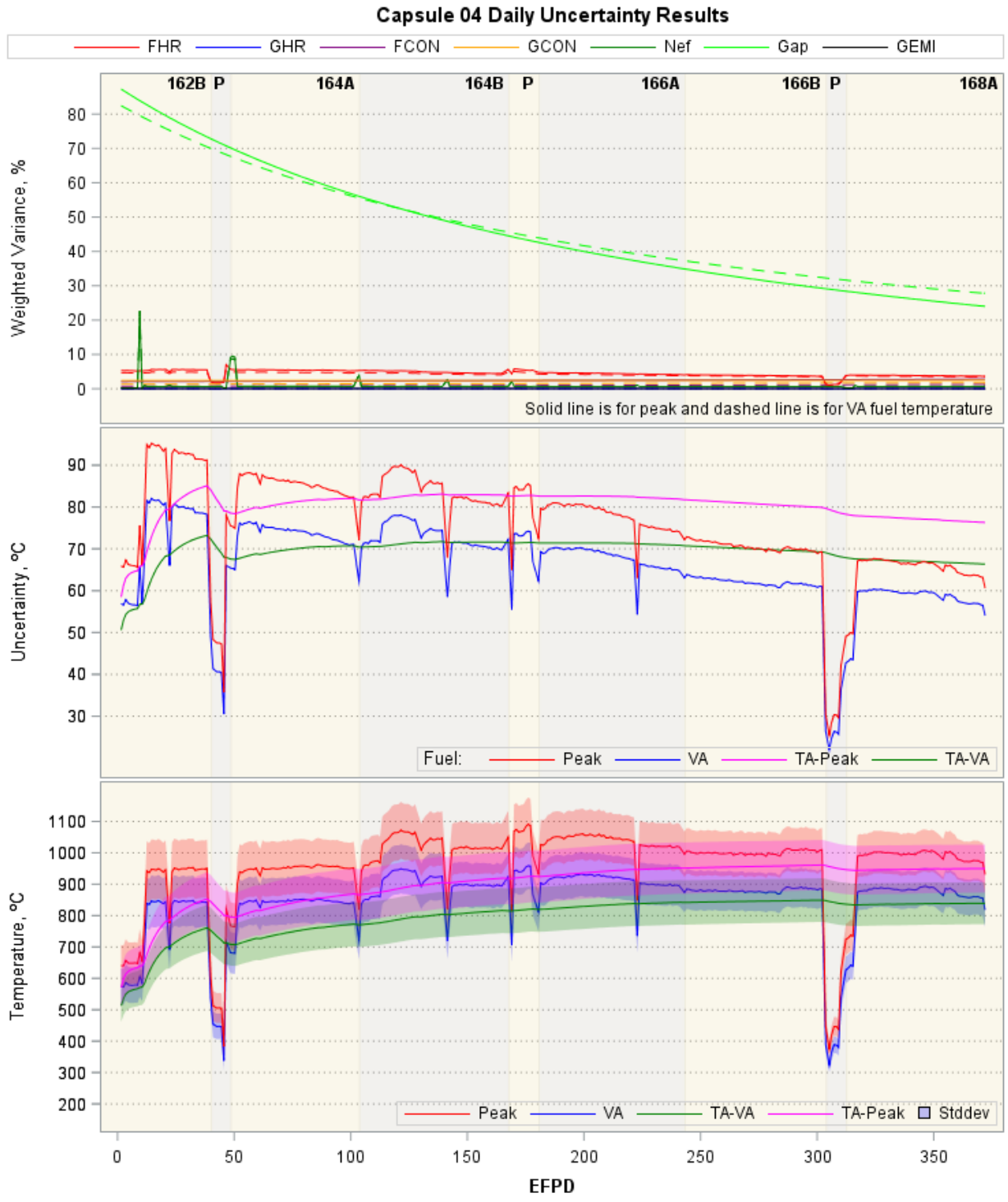

Figure 46. Daily uncertainty results for instantaneous and time-averaged peak and volume average fuel temperatures in Capsule 4. “P” – PALM Cycles 163A, 165A, and 167A.

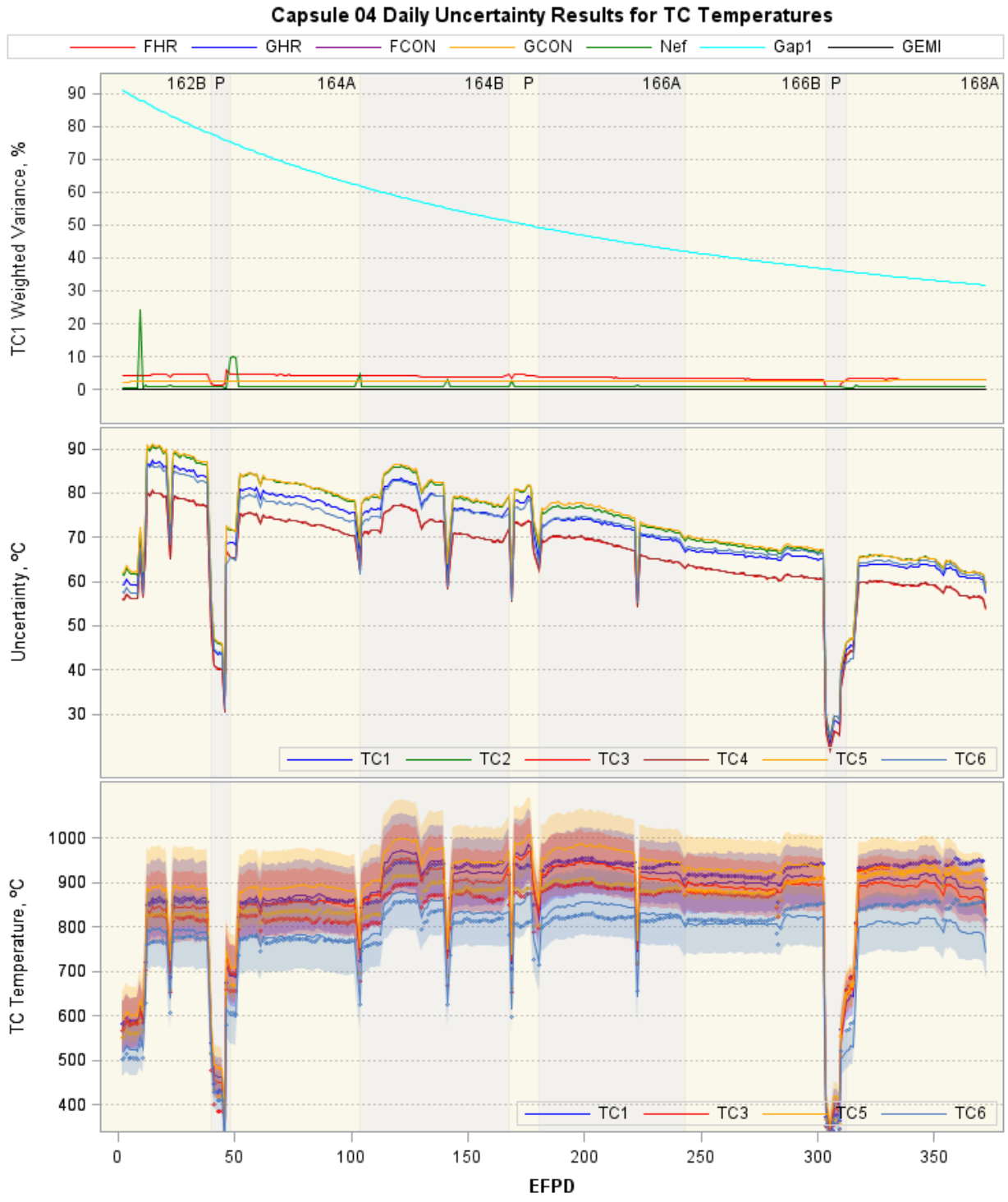

Figure 47. Daily uncertainty results for instantaneous TC temperatures in Capsule 4 (lines are calculated TCs and dots are measured TCs). Failed TC2 and TC4 were excluded in the bottom panel to make the plots less busy). "P" – PALM Cycles 163A, 165A, and 167A.

5.3 Temperature Uncertainty Results for Capsule 3

Table 10 summarizes the temperature uncertainty results for Capsule 3. Figure 48 shows the daily uncertainty in terms of the relative standard deviation for selected inputs, together with the sensitivity coefficients for VA fuel temperature (similar for peak fuel temperature) and TC1 temperature (representative of other TCs). The daily uncertainty results are presented in Figure 49 for peak and VA fuel temperature, and in Figure 50 for TC temperatures.

Table 10. Summary of temperature uncertainty results for Capsule 3 (excluding Cycles 163A and 167A).

	Peak Fuel	Volume-Averaged Fuel	Peak Fuel	Volume-Averaged Fuel	TCs
Instantaneous Temperature – Minimum/Maximum	3.5 – 8.3%	3.6 – 8.3	42 – 89	39 – 78	45 – 98
Time-Averaged Temperature – At End of Irradiation	4.5	4.4	64	57	N/A

The following results of calculated temperature uncertainty are observed:

- *Input uncertainty* (Figure 48): Like Capsules 4 and 5, gas gap width had the highest uncertainties (up to 40% at SOI, due to the smaller gap width) and changes over time due to increases in both the gap absolute uncertainty and gap width (~20% at EOI). The neon fraction uncertainties (green line) are mostly close to 3% for ~1 neon fraction (near-pure neon gas mixture), except a few higher values for time steps at the beginning of each cycle, when the neon fraction is low. Uncertainties for the remaining inputs are unchanged over irradiation time.
- *Input parameter sensitivity* (Figure 48): Capsule 3 had a different design than the other four capsules, with two graphite holders and fuel compacts housed in the inner holder (Figure 4). Therefore, fuel compact temperatures are less sensitive to the outer gap width between the outer holder and capsule shell. The fuel heat rate still has the highest sensitivity for both fuel and TC temperatures (0.35 to 0.5 for fuel temperature and ~0.3 for TCs), followed by the neon fraction (~ 0.2). But the gap sensitivity is only high (~0.3) for TC1, located in the outer holder, and is significantly lower (~0.1) for the fuel temperature inside the inner holder. Unlike Capsules 4 and 5, the graphite emissivity has a notably higher sensitivity coefficient for fuel temperatures (0.12 to 0.2) but not for TC1 temperature. The remaining three inputs have small sensitivity coefficients for fuel and TC temperatures: generally less than 0.1 in absolute values, as for the other capsules.
- *Weighted variance* (Figure 49 and Figure 50): Gas gap uncertainty is still the dominant factor for TC temperature, due to its high uncertainty and sensitivity. For fuel temperatures, the gas gap uncertainty is a dominant factor only during the first four cycles, then the fuel heat rate and graphite conductivity become the most dominant factors. The remaining inputs contributed very little to the calculated temperature uncertainty for both the fuel and TC temperatures.
- *Calculated temperature uncertainty* (Figure 49 and Figure 50): Uncertainties for VA, peak fuel, and TC temperatures range between 50 and 90°C. In terms of relative standard deviation, only TC1, located near the control gap, has the highest uncertainty (up to 14%), due to the high sensitivity of the gap width uncertainty, whereas other TC and fuel temperatures have a similar uncertainty of between 4 and 6%.

The bottom panels show daily instantaneous and TA- temperatures plotted with one standard deviation. The measured temperatures of the operational TCs (dots) are well within the one-standard-deviation uncertainty band (Figure 50) until the end of Cycle 164B, when readings of the remaining five TCs (1, 3, 4, 12, and 13) start to go beyond their uncertainty band (Figure 51). There are several

potential reasons for this type of departure in TC readings, including too narrow uncertainty bands, TC drift (i.e., TC5 shows the strongest evidence for this), and/or increased model form uncertainty (i.e., due to uncertainty in the gas gap variation model over time, which was not adequately included in the parameter uncertainty). According to the test results of TCs used in AGR-5/6/7 (Palmer et al. 2022), TCs showed only downward drift over time. Thus, the upward trend of the four TCs (1, 3, 4, and 12) relative to calculated temperatures is a strong indication that the thermal model underpredicted the temperatures for their locations.

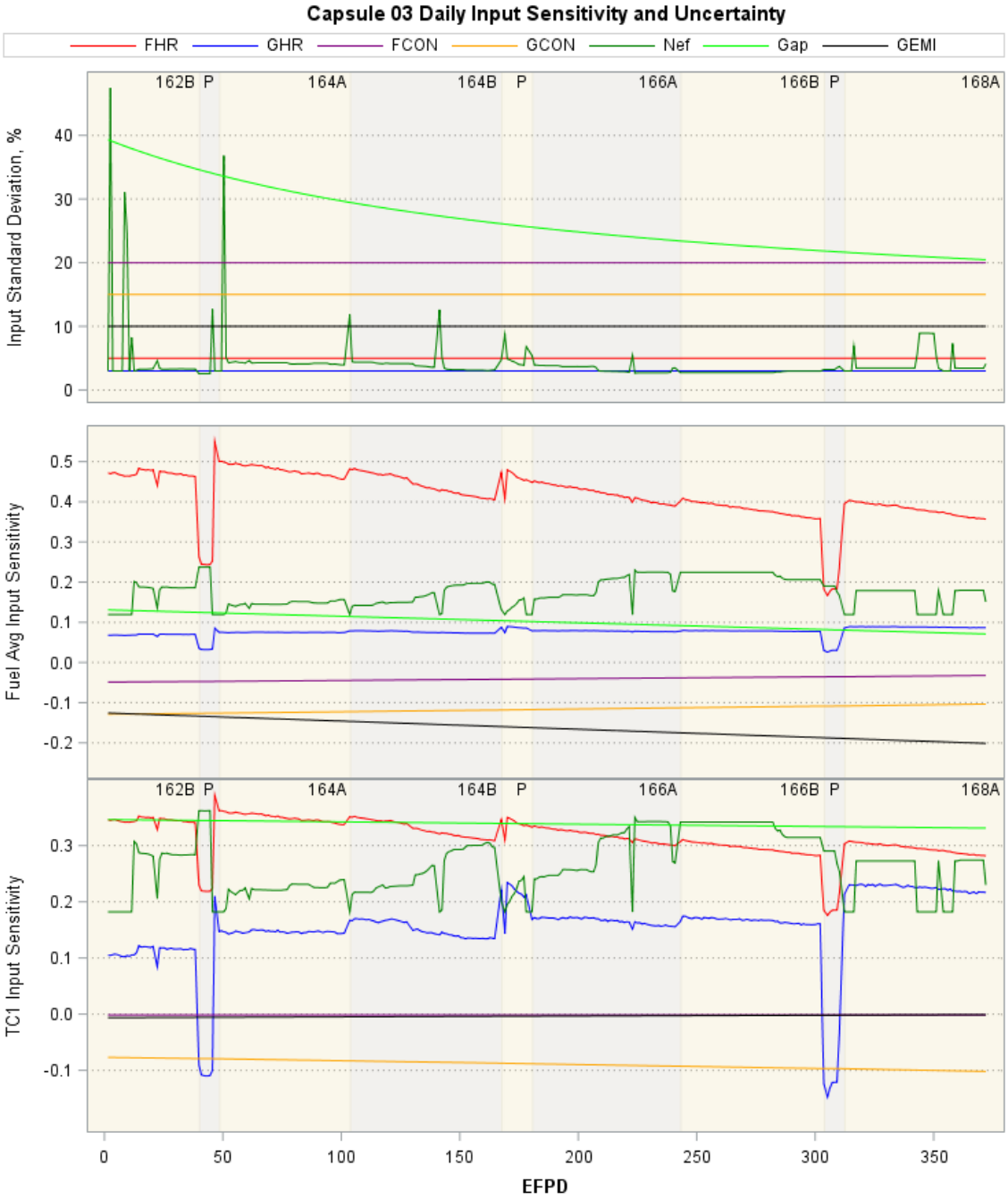

Figure 48. Daily relative standard deviations for seven inputs in Capsule 3. "P" – PALM Cycles 163A, 165A, and 167A.

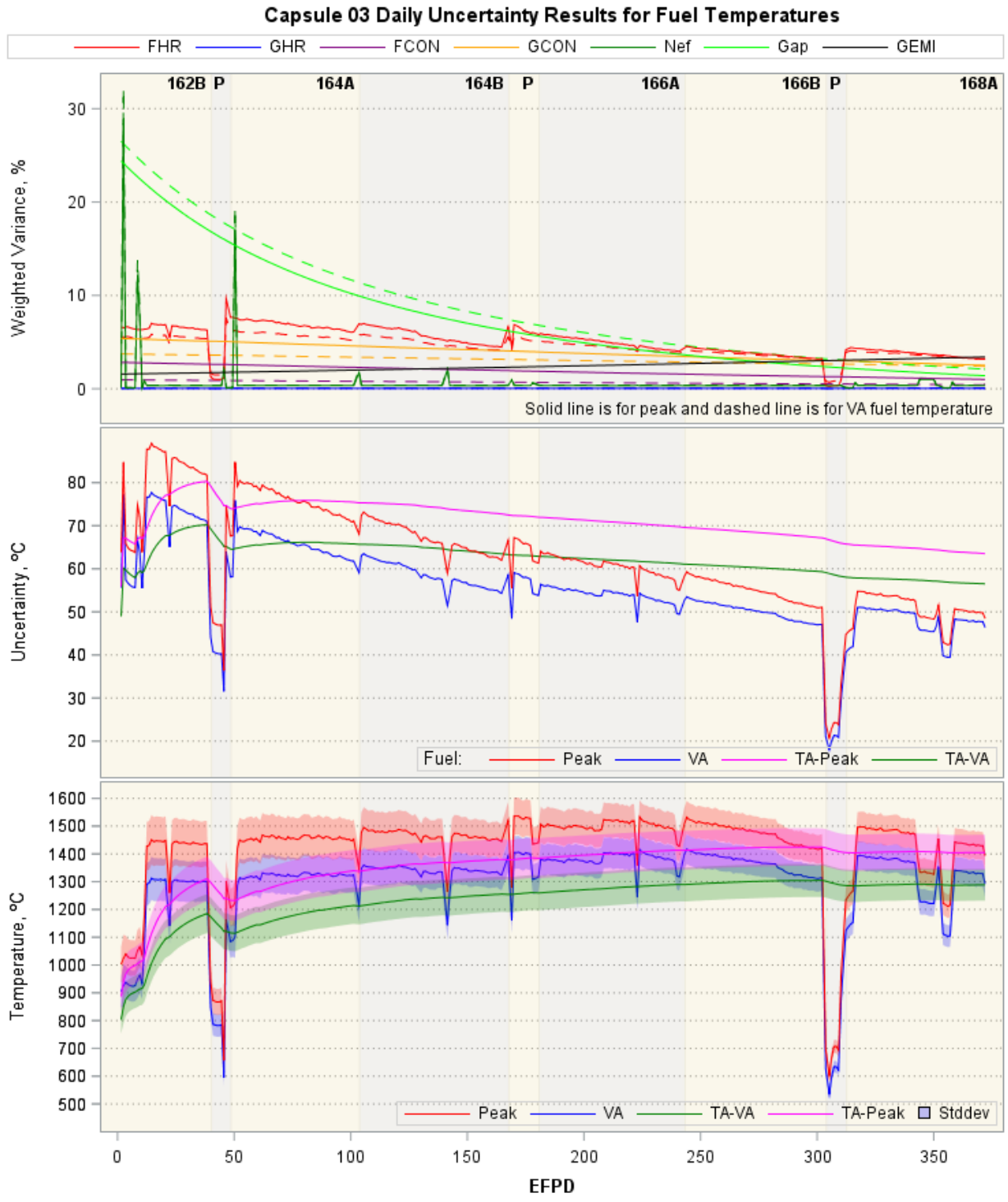

Figure 49. Daily uncertainty results for instantaneous and time-averaged peak and volume-average fuel temperatures in Capsule 3. “P” – PALM Cycles 163A, 165A, and 167A.

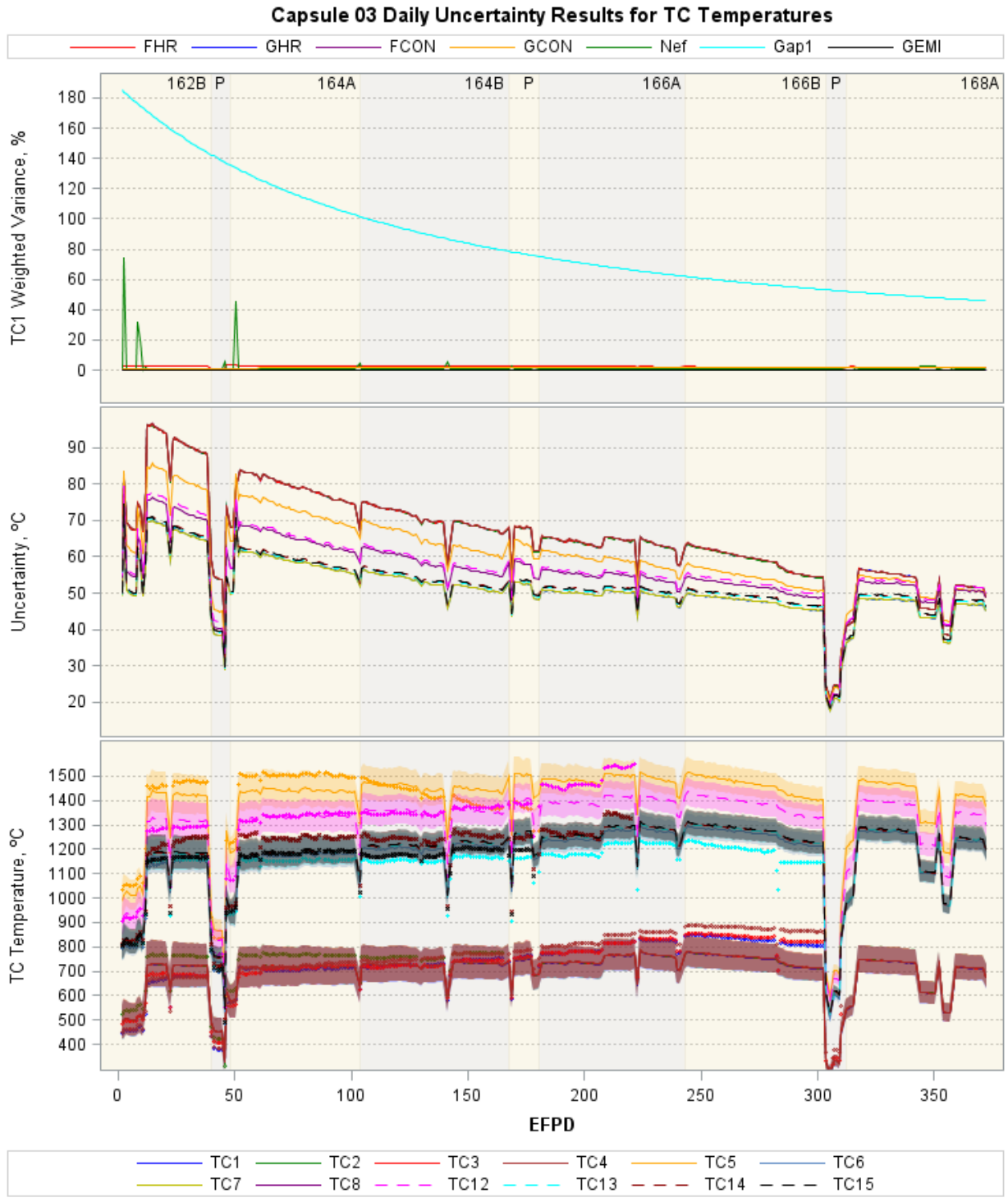

Figure 50. Daily uncertainty results for instantaneous TC temperatures in Capsule 3 (lines are calculated TCs and dots are measured TCs). Failed TCs were excluded in the bottom panel for clarity. “P” – PALM Cycles 163A, 165A, and 167A.

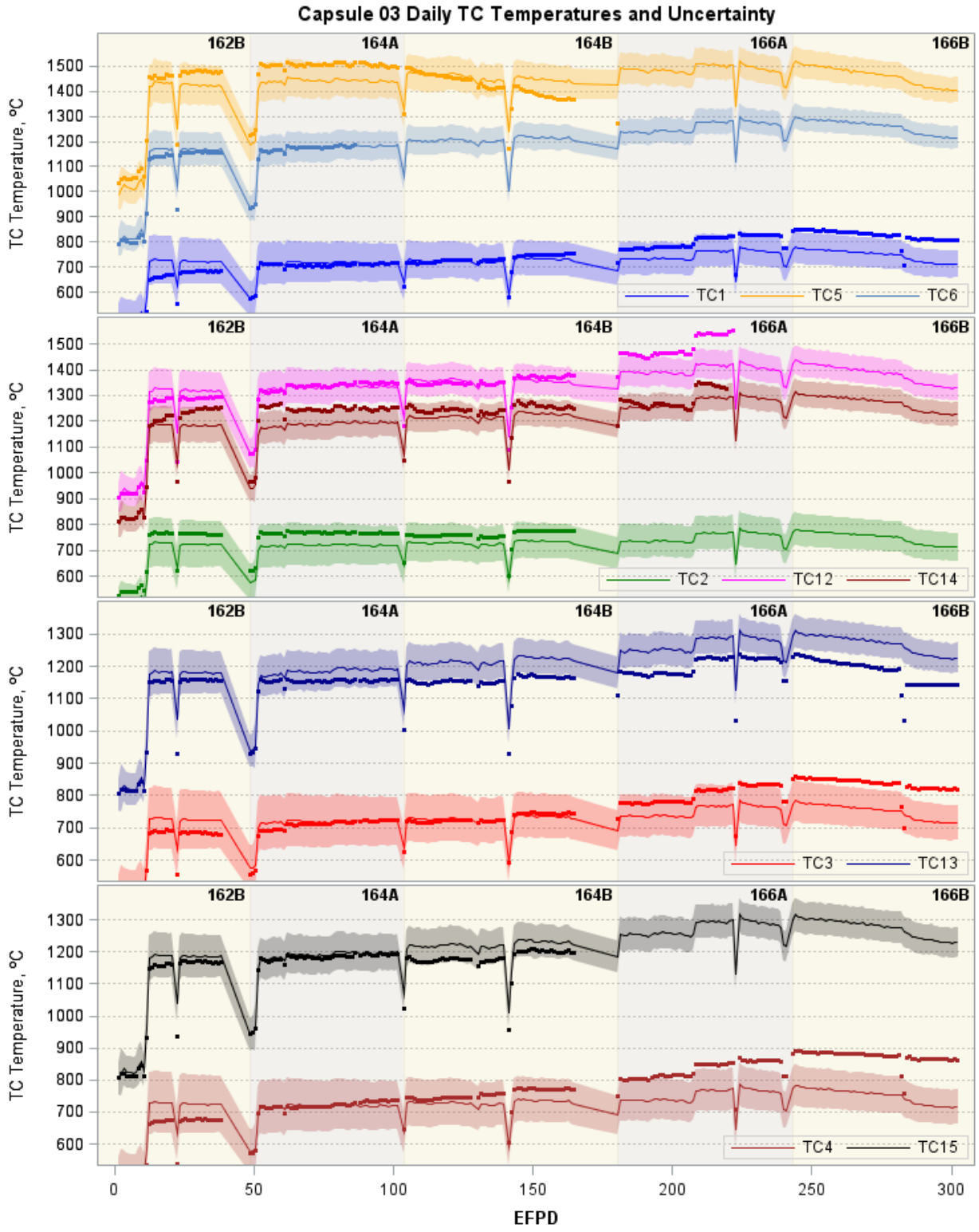

Figure 51. Daily temperatures (lines are calculated and dots are measured temperatures) and one standard deviation (shaded areas) for Capsule 3 operational TCs during the five regular cycles.

5.4 Temperature Uncertainty Results for Capsule 2

Table 11 summarizes the temperature uncertainty results for Capsule 2. Figure 52 shows the daily uncertainty in terms of relative standard deviation for the selected inputs, together with sensitivity coefficients for VA fuel temperature (similar for peak fuel temperature) and TC1 temperature (representative of other TCs). The daily uncertainty results are presented in Figure 53 for peak and VA fuel temperature, and in Figure 54 for TC temperatures.

Table 11. Summary of temperature uncertainty results for Capsule 2 (excluding Cycles 163A and 167A).

	Peak Fuel	Volume-Averaged Fuel	Peak Fuel	Volume-Averaged Fuel	TCs
Instantaneous Temperature – Minimum/Maximum	6.3 – 15.7%	6.5 – 15.8%	46 – 122°C	41 – 107°C	58 – 115°C
Time-Averaged Temperature – At End of Irradiation	8.7%	8.7%	80°C	71°C	N/A

The following results of calculated temperature uncertainty are observed:

- *Input uncertainty* (Figure 52): The gas gap has the highest input uncertainties (up to 40% at SOI) and is changing over time due to increases in both the gap absolute uncertainty and gap width (~20% at EOI). The neon fraction uncertainties (green line) are mostly close to 3% for ~1 neon fraction (near-pure neon gas mixture), except a few higher values for time steps at the beginning of each cycle, when the neon fraction is low. Uncertainties for the remaining inputs remain unchanged throughout the irradiation time.
- *Input parameter sensitivity* (Figure 52): The fuel heat rate (red line) has the highest sensitivity for both fuel and TC temperatures (0.35 to 0.5), following by the neon fraction and gas gap (up to 0.3). The remaining four inputs (fuel and graphite conductivities, graphite heat rate, and graphite emissivity) have small sensitivity coefficients for the fuel and TC temperatures: generally less than 0.1 in absolute values.
- *Weighted variance* (Figure 53 and Figure 54): Gas gap uncertainty is the dominant factor for both fuel and TC temperature due to its high uncertainty and sensitivity, especially at the SOI. The fuel heat rate (the second dominant factor), which has the highest sensitivity but a low input uncertainty (5%), had significantly less influence on the uncertainties of calculated temperatures. The remaining inputs contributed very little to the calculated temperature uncertainty.
- *Calculated temperature uncertainty* (Figure 53 and Figure 54): The calculated temperature uncertainties are higher than for Capsules 3 to 5, ranging from 70 to 120°C for absolute uncertainty. The high temperature uncertainty is caused mainly by the large gas gap uncertainty and sensitivity. In terms of relative standard deviation, the uncertainties for the fuel and TC temperatures are similar, ranging from 7 to 13%.

  The bottom panels show daily instantaneous and TA temperatures plotted with one standard deviation. For TC temperature (), the measured temperatures of the five operational TCs (dots) fall well within the one-standard-deviation uncertainty band, indicating that the uncertainty calculation is likely to include all influential uncertainty factors for this capsule as well as the thermal-model-predicted well temperatures in Capsule 2.

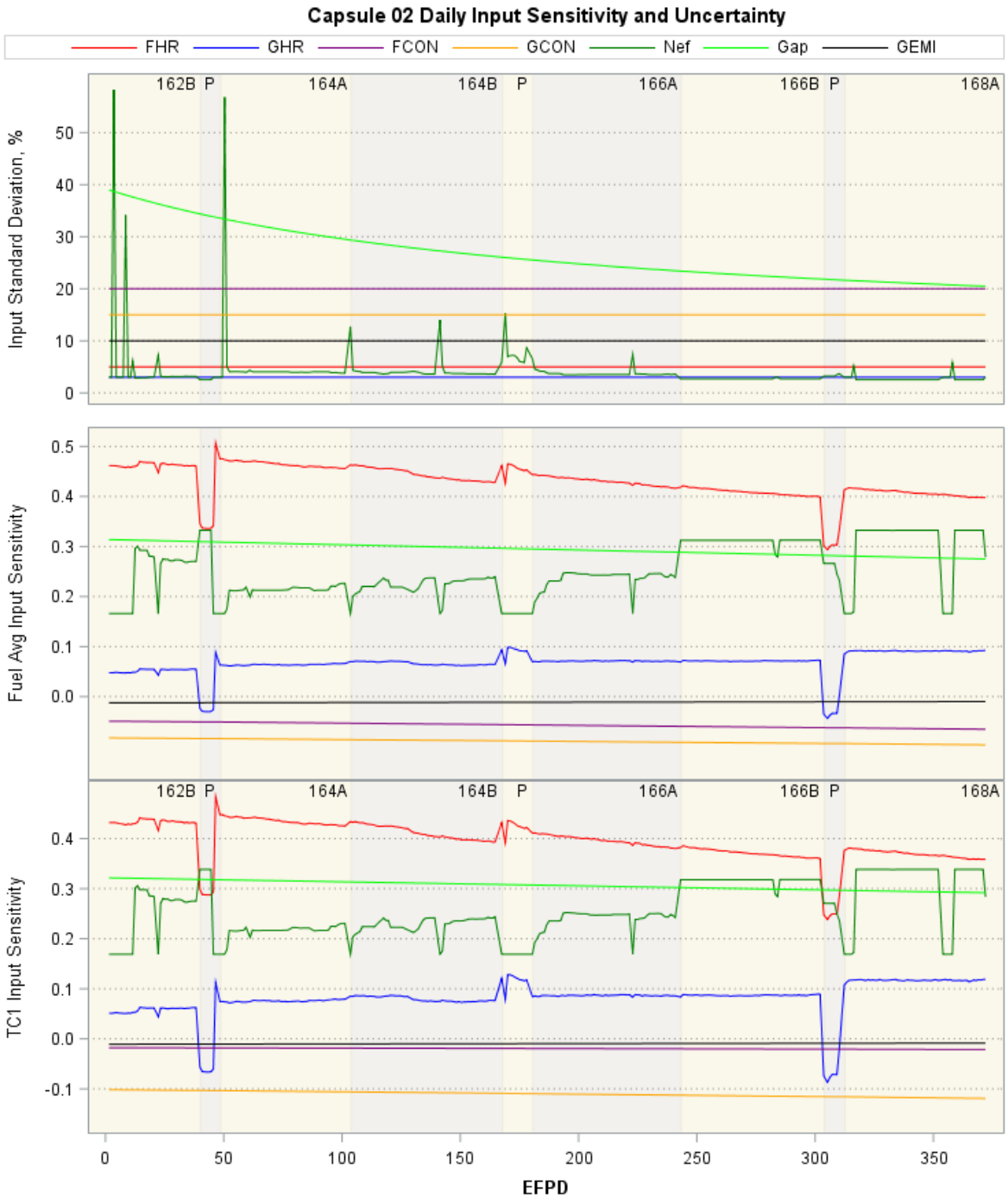

Figure 52. Daily relative standard deviations for seven inputs in Capsule 2. “P” – PALM Cycles 163A, 165A, and 167A.

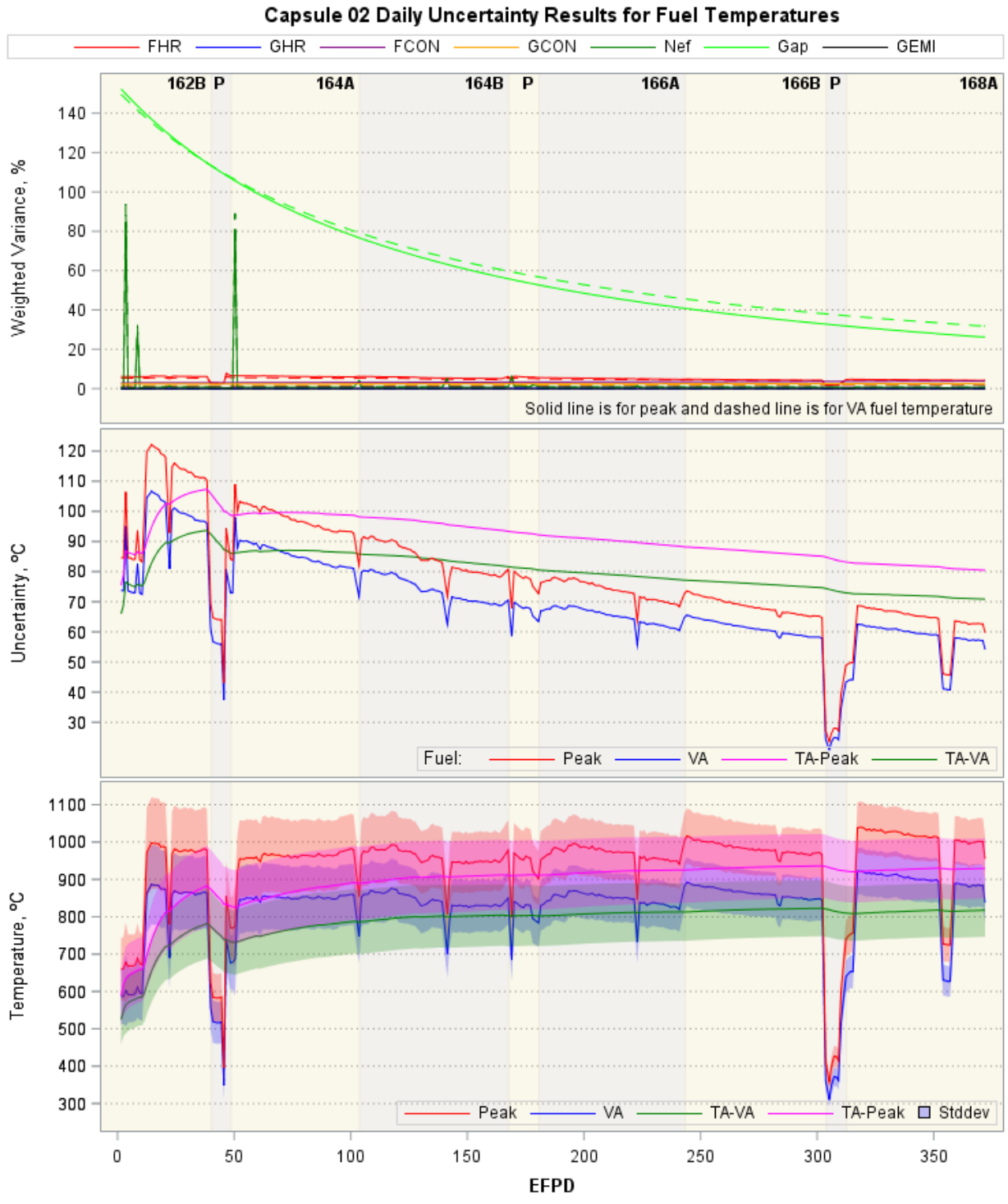

Figure 53. Daily uncertainty results for instantaneous and time-averaged peak and volume-average fuel temperatures in Capsule 2. "P" – PALM Cycles 163A, 165A, and 167A.

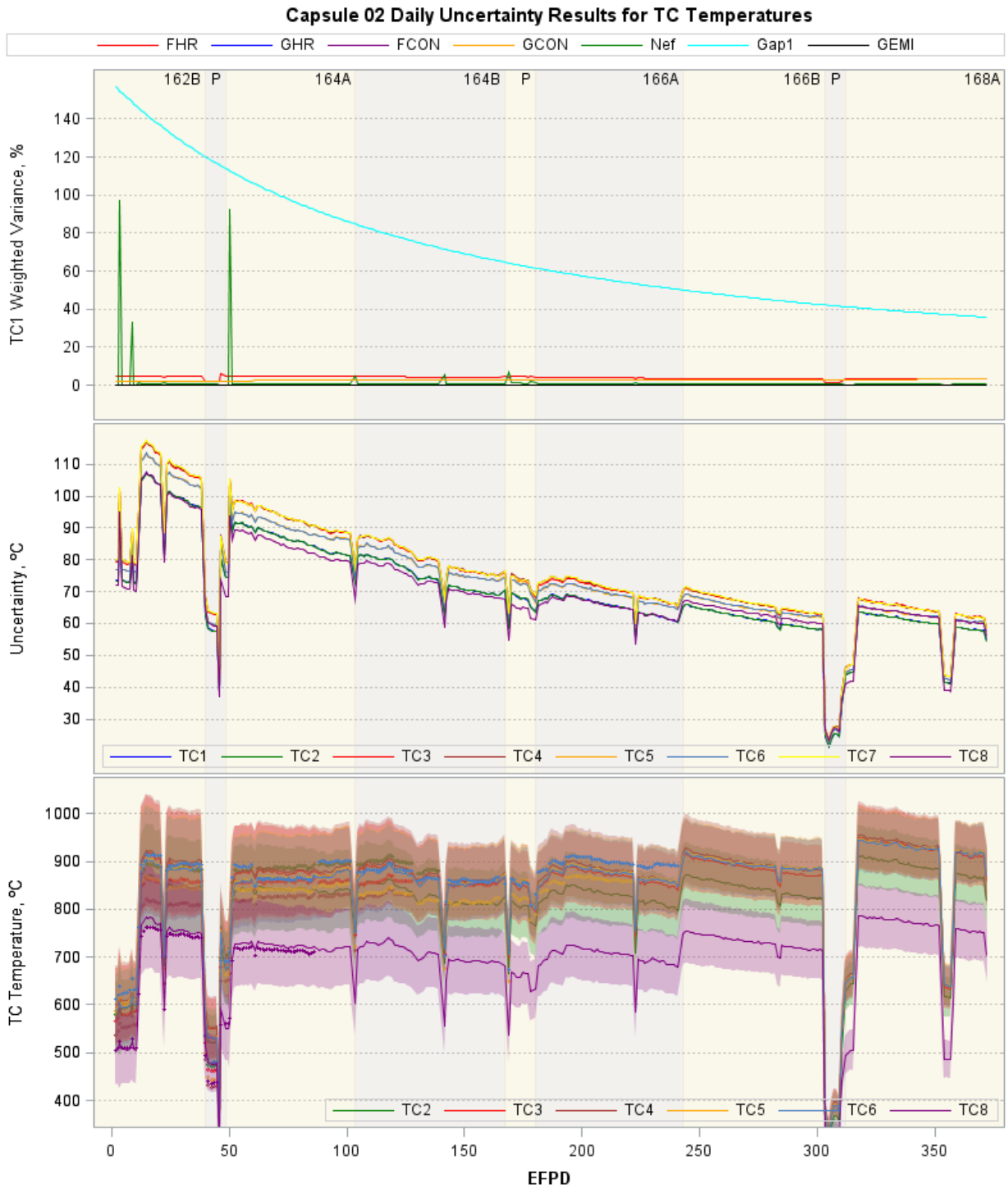

Figure 54. Daily uncertainty results for instantaneous TC temperatures in Capsule 2 (lines are calculated TCs and dots are measured TCs). Failed TC1 and TC7 were excluded on the bottom panel to make the plots less busy. “P” – PALM Cycles 163A, 165A, and 167A.

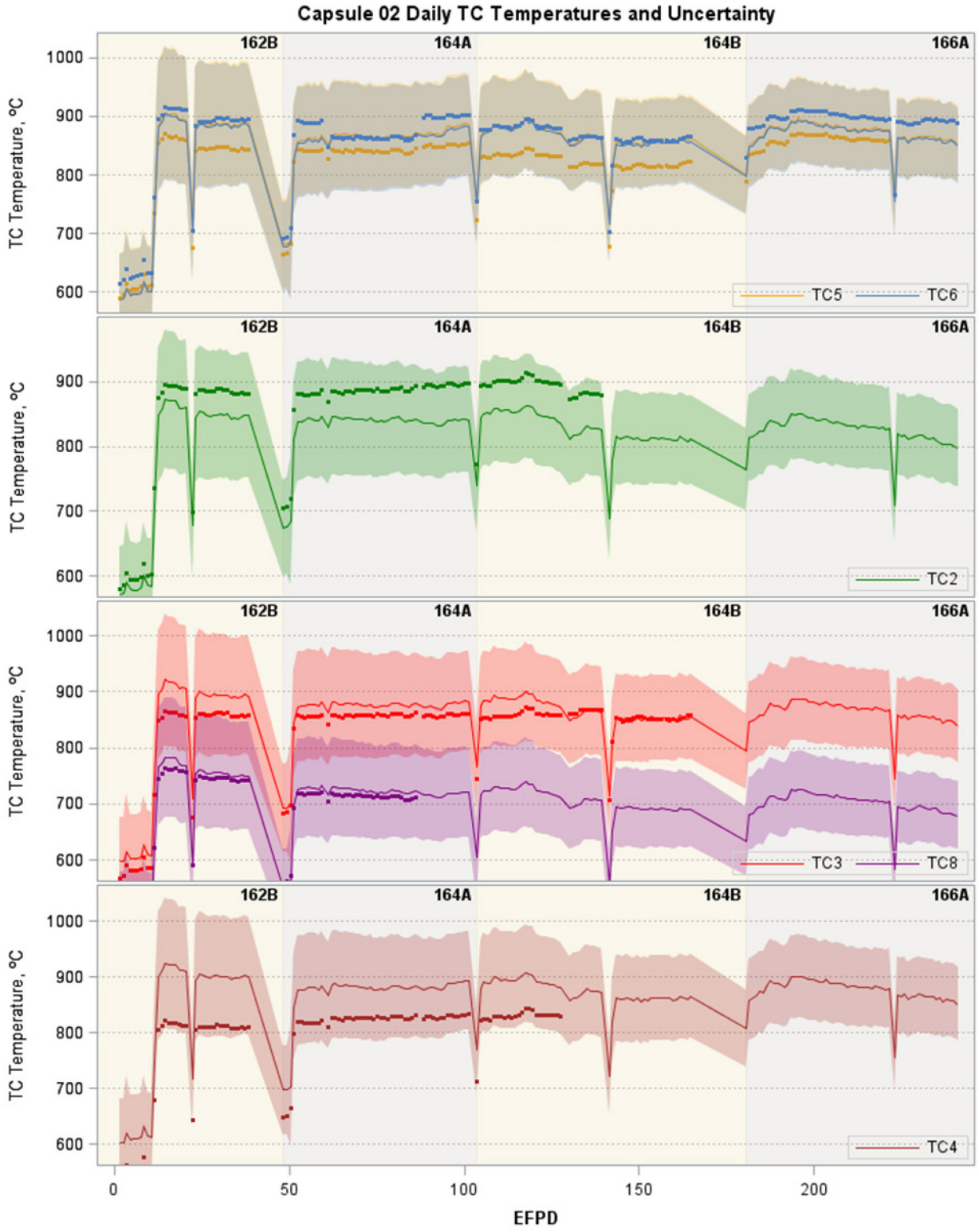

Figure 55. Daily temperatures (lines are calculated and dots are measured temperatures) and one standard deviation (shaded areas) for Capsule 2 operational TCs during the five regular cycles.

5.5 Temperature Uncertainty Results for Capsule 1

Table 12 summarizes the temperature uncertainty results for Capsule 1. Figure 56 shows the daily uncertainty in terms of the relative standard deviation for selected inputs, together with sensitivity coefficients for VA fuel temperature (similar for peak fuel temperature) and TC1 temperature (representative of other TCs). The daily uncertainty results are presented in Figure 57 for peak and VA fuel temperature, and in Figure 58 for TC temperatures.

Table 12. Summary of temperature uncertainty results for Capsule 1 (excluding Cycles 163A and 167A).

	Peak Fuel	VolumeAveraged Fuel	Peak Fuel	VolumeAveraged Fuel	TCs
Instantaneous Temperature – Minimum/Maximum	6.4 – 12.6%	7.2 – 14.4%	77 – 143°C	67 – 130°C	80 – 135°C
Time-Averaged Temperature – At End of Irradiation	8.2%	9.2%	100°C	91°C	N/A

The following results of calculated temperature uncertainty are observed:

- *Input uncertainty* (Figure 56): The gas gap had the highest input uncertainties (up to 40% at SOI) and changes over time due to increases in both the gap absolute uncertainty and gap width (~20% at EOI). The neon fraction uncertainties (green line) are mostly close to 3% for a ~1 neon fraction (near-pure neon gas mixture), except a few higher values for time steps at the beginning of each cycle, when the neon fraction is low, and during Cycle 168A, when the neon fraction uncertainty was not exactly definable and assumed to be 50%. Uncertainties for the remaining inputs remained unchanged throughout the irradiation time.
- *Input parameter sensitivity* (Figure 56): The fuel heat rate has the highest sensitivity for both the fuel and TC temperatures (~ 0.5), followed by the neon fraction and gas gap (~ 0.3). The remaining four inputs (fuel and graphite conductivities, graphite heat rate, and graphite emissivity) have small sensitivity coefficients for the fuel and TC temperatures: generally less than 0.1 in absolute values.
- *Weighted variance* (Figure 57 and Figure 58): The gas gap uncertainty is the dominant factor for both the fuel and TC temperature, due to its high uncertainty and sensitivity, except for Cycle 168A when the neon fraction uncertainty is a dominant factor. The fuel heat rate (the second dominant factor), which has the highest sensitivity but a low input uncertainty (5%), had significantly less influence on the uncertainties of calculated temperatures. The remaining inputs contributed very little to the calculated temperature uncertainty.
- *Calculated temperature uncertainty* (Figure 57 and Figure 58): The uncertainties for VA and peak fuel temperatures range from 80 to 140°C and peaked at the SOI, due to the highest gap width uncertainty. In terms of relative standard deviation, TC6, which was located near the control gap, had the highest uncertainty (up to 13%), due to the high sensitivity of the gap width. The uncertainty range for VA and peak fuel temperatures is between 7 and 11%.

  The bottom panels show daily instantaneous and TA temperatures plotted with one standard deviation. Unlike Capsule 3, the TC measured temperatures (dots) from all nine TCs are within the one-standard-deviation uncertainty band (Figure 59), indicating that the uncertainty calculation is likely to include all influential uncertainty factors for this capsule.

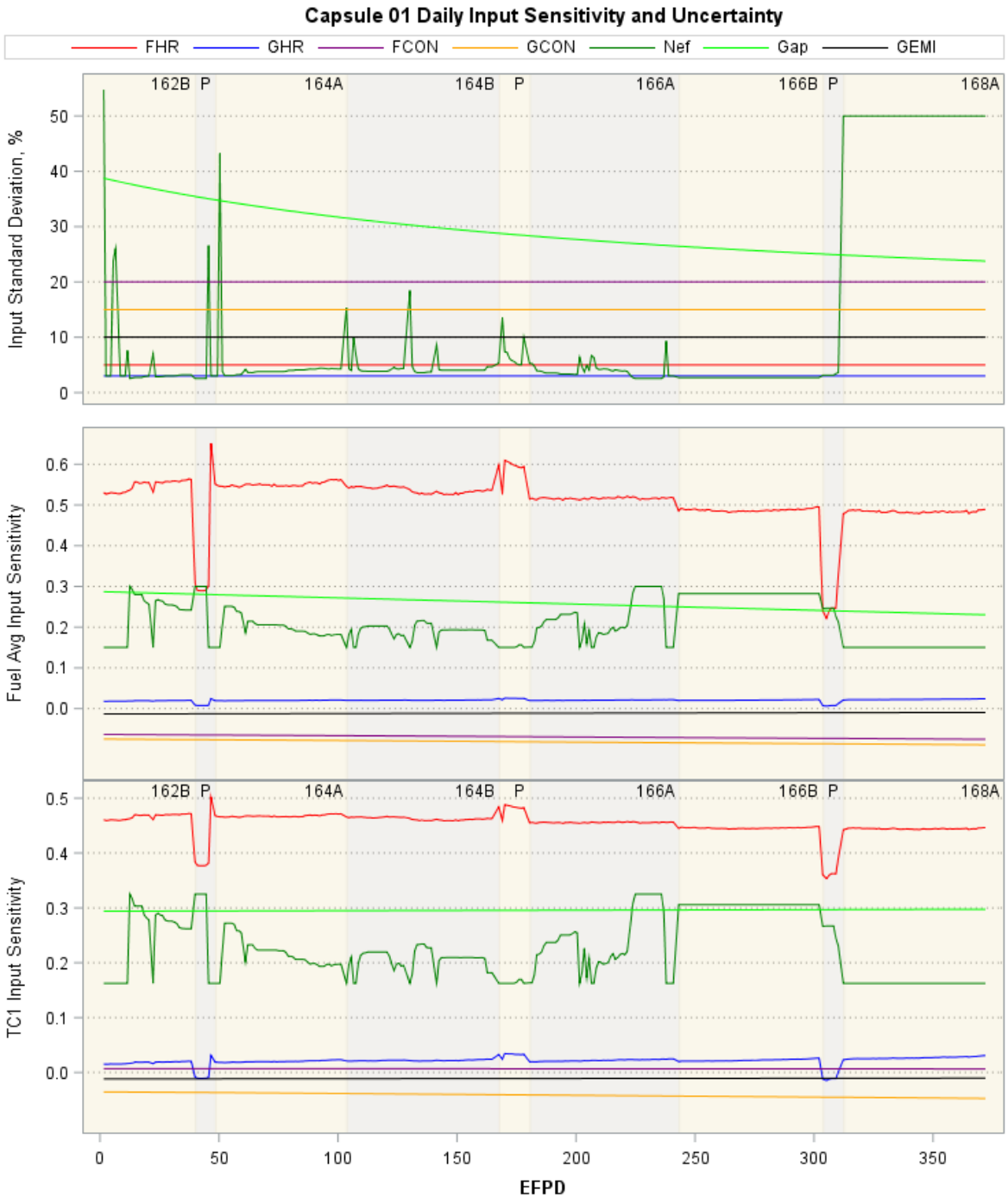

Figure 56. Daily relative standard deviations for seven inputs in Capsule 1. "P" – PALM Cycles 163A, 165A, and 167A.

Figure 57. Daily uncertainty results for instantaneous and time-averaged peak and volume-average fuel temperatures in Capsule 1. "P" – PALM Cycles 163A, 165A, and 167A.

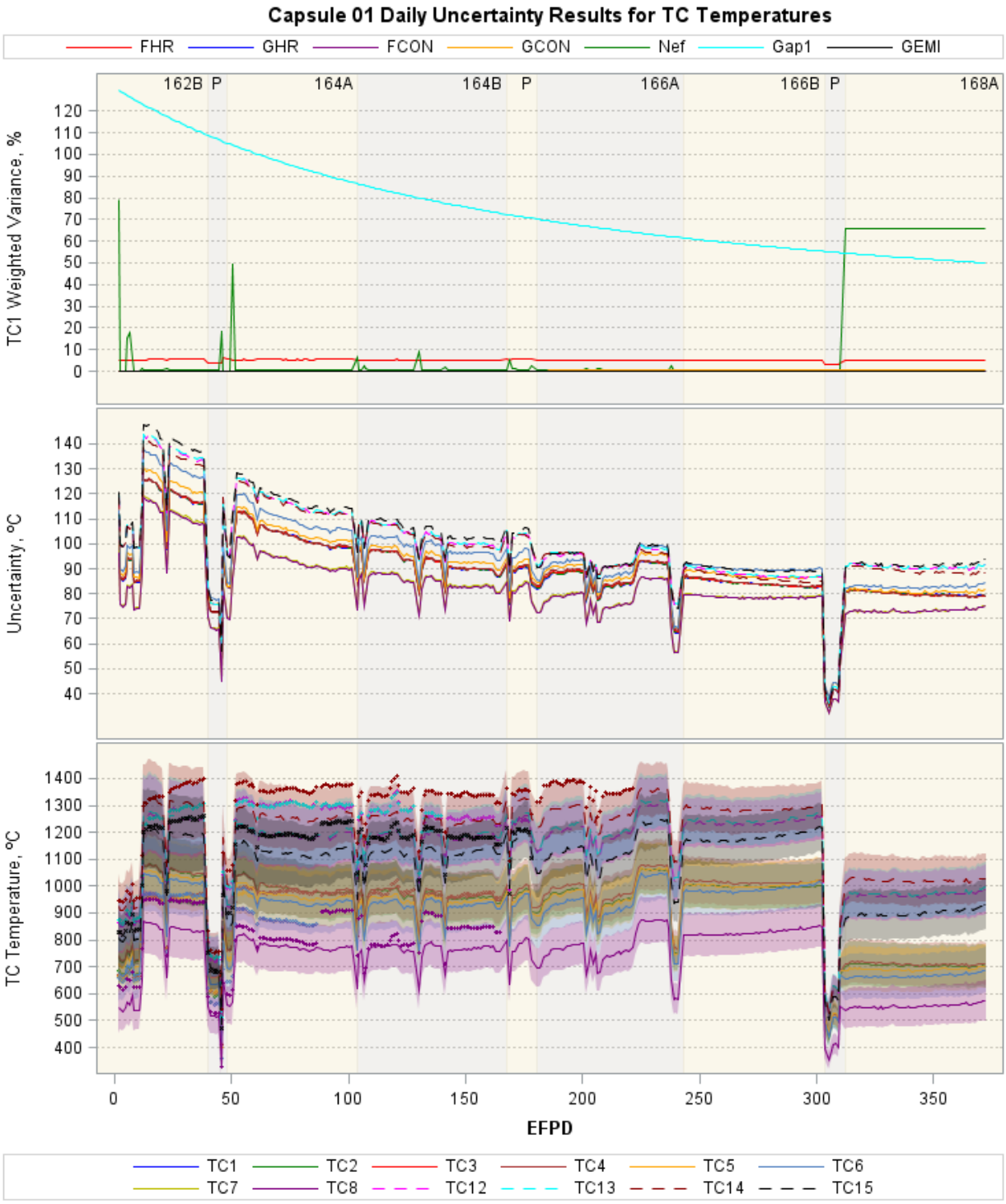

Figure 58. Daily uncertainty results for instantaneous TC temperatures in Capsule 1 (lines are calculated TCs and dots are measured TCs). Failed TCs were excluded on the bottom panel, for clarity. “P” – PALM Cycles 163A, 165A, and 167A.

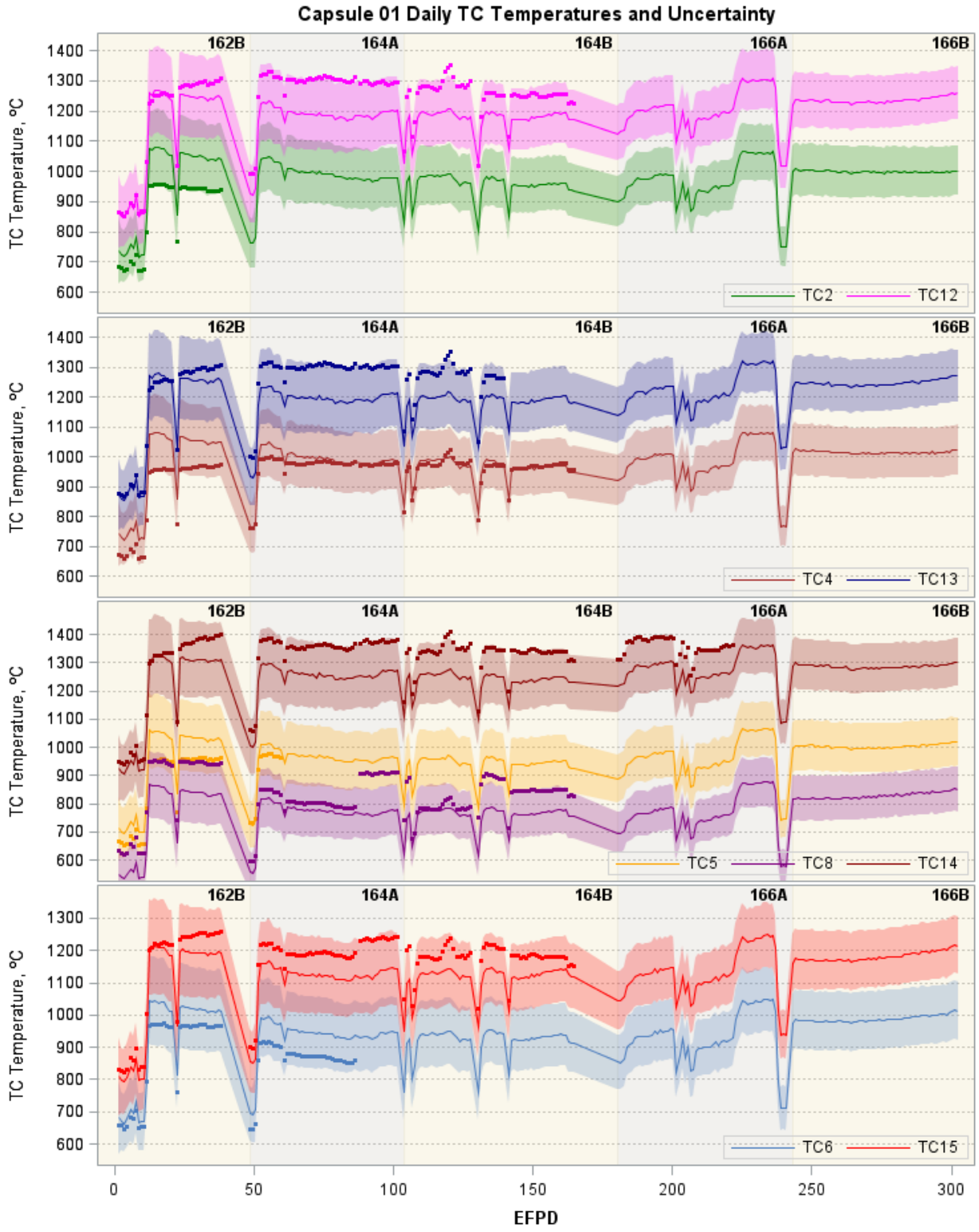

Figure 59. Daily temperatures (lines are calculated and dots are measured temperatures) and one standard deviation (shaded areas) for Capsule 1 operational TCs during the six regular cycles.

5.6 Summary and Discussion

The gas gap uncertainty is the dominant factor for both fuel and TC temperature, due to its high uncertainty (up to 40%) and sensitivity (~ 0.3). The fuel heat rate is the second most influential factor, even though its uncertainty is relatively low (5%), because the model is highly sensitive to that input. The remaining inputs (neon fraction, fuel and graphite conductivities, graphite heat rate and conductivity) contributed very little to the calculated temperature uncertainty.

The overall uncertainty in all calculated temperatures of interest ranged from 7 to 14% (excluding a few peak uncertainties associated with highly uncertain, near-zero, neon fractions). The uncertainties vary depending on irradiation time (thermal conditions), capsule, and the temperature parameter being calculated. For all capsules, the relative uncertainties decrease with time, due to the decreasing gap width uncertainty related to graphite shrinkage with increasing neutron fluence.

Table 13 summarizes the uncertainty for instantaneous temperatures of fuel compacts, averaged over the entire irradiation. The main factor leading to differences in temperature uncertainty across capsules is gas gap width uncertainty. Other notable observations include the following:

- Capsule 1 uncertainties are in the range of [6.4 to 12.6%] for peak fuel temperatures and [7.2 to 14.4%] for VA fuel temperatures.
- Capsule 2 uncertainties are similar for both peak fuel and VA fuel temperatures, ranging from 6.3 to 15.7% and 6.5 to 15.8.
- Capsule 3 has the lowest fuel temperature uncertainty (3.5 to 8.3%), thanks to lower gap width uncertainties. This is due to relatively larger gaps and lower gap width sensitivity, since the fuel compacts are in the inner holder, away from the outer gap. However, uncertainties for several TCs located in the outer holder (TC1 through TC4) are higher due to higher gap sensitivity.
- Capsules 4 and 5 have higher uncertainty (up to ~11.1% for Capsule 4 peak fuel temperatures at the start of irradiation) than Capsule 3, due to higher gas gap width uncertainties and sensitivity. Uncertainties for TC temperatures are higher (Figure 44 for Capsule 5 and Figure 47 for Capsule 4) than for fuel temperatures, because of the higher gap width sensitivity.

Table 13. Uncertainty range for instantaneous temperatures and uncertainty for TA at the end of irradiation (as relative standard deviation in % [D°C/°C]). The RMS of TC residuals in each capsule are included for comparison.

Capsule	Relative Root Mean Square of TC Residuals	Peak Fuel	Volume-Averaged Fuel	TA Peak Fuel	TA Volume-Averaged Fuel
5	2.7	6.9 – 9.9	6.9 – 9.8	7.8	7.7
4	4.0	6.5 – 11.1	6.6 – 10.8	8	7.9
3	3.2	3.5 – 8.3	3.6 – 8.3	4.5	4.4
2	4.5	6.3 – 15.7	6.5 – 15.8	8.7	8.7
1*	7.5	6.4 – 12.6	7.2 – 14.4	8.2	9.3
*Excluding cycle 168A.					

In the absence of error in the model form, input uncertainties, and inaccuracy in the TC measurements, the TC residuals should equal zero. To the extent that TC locations adequately sample the temperature distribution of the volume of interest, over the period of interest, those residuals are thus an independent measure of the minimum uncertainty of the thermal model. The relative RMS of TC residuals, averaged using Cycle 162A and 164B data, are included in Table 13 for comparison with the calculated parameter uncertainty effects. Comparisons suggest the following:

- Capsules 1, 2, and 3 contained eight to 10 operational TCs and experienced a wide range of temperatures. Thus, the relative RMS of the residuals is close to the lower end of the range for calculated temperature uncertainty. Capsule 1 TC residuals varied most across TCs, reflecting the higher uncertainty of calculated temperatures for Capsule 1. In contrast, Capsule 3 has the lowest average variation in TC residuals, as is consistent with the lower calculated temperature uncertainty for this capsule. The TC residual variation in Capsule 2 is notably smaller than the calculated temperature uncertainty.
- Capsules 4 and 5 had only a few operational TCs (4 and 3 TCs, respectively) and measured a relatively narrow range of temperatures. Therefore, the variation of TC residuals is much smaller than the calculated temperature uncertainty in those capsules, since TCs residuals are not a fully random sample of differences between the measured and calculated values, due to the limited number of TCs in Capsules 4 and 5.

6. CONCLUSIONS

Knowledge of the thermal conditions and associated uncertainties of nuclear fuel in a reactor experiment are central to interpreting the experimental results, particularly when using the experiment results for calibration and validation of nuclear fuel performance models and codes that will ultimately be used in support of the design and licensing of the new nuclear fuel. The work documented in this report supports the quantification of uncertainty in the computed thermal condition of nuclear fuels in the AGR-5/6/7 test, in which was impossible to obtain direct fuel temperature measurements. The experiment was instrumented with multiple TCs to provide temperature measurements in the graphite holders surrounding the fuel compacts. The AGR-5/6/7 TC temperatures also can be used to assess and calibrate thermal analysis models in the ABAQUS code to predict fuel temperatures (Hawkes 2021).

This study focuses on quantifying the impact of thermal model parameters of potential importance on the calculated FTs, selected based on a combination of input uncertainty and sensitivity. Expert judgment is used as a basis to specify the uncertainty range for a set of select parameters. This also considers all the physics that occurred during the irradiation, which can impact input uncertainties (e.g., the gas gap size changes increased the uncertainty of the gaps). Propagation of model parameter uncertainty is then used to quantify the parameter uncertainty of the calculated temperatures. The model-form uncertainties are unknown and are thus not included in the overall uncertainty.

The parameter sensitivity defines how the calculated temperature would be influenced by changes in an input parameter. The uncertainty of the model output increases as the sensitivity coefficient of an input parameter increases. The sensitivity analysis performed in this work went beyond the traditional local sensitivity. Using experimental design, an analysis of pairwise interactions of model parameters was performed to establish the sufficiency of the first-order (linear) expansion terms in constructing the response surface. To achieve completeness, uncertainty propagation made use of pairwise noise correlations of model parameters. Furthermore, using an interpolation scheme over the input parameter domain, the analysis obtains time-dependent sensitivities over the duration of the test campaign. This enables computation of uncertainty for the instantaneous VA and peak FTs and the TC temperatures over the entire irradiation period. The following conclusions are drawn about the parameter sensitivity coefficients for AGR-5/6/7 temperature predictions:

- The sensitivity coefficients of fuel heat rate are positive and highest for VA/peak fuel and TC temperatures, followed by the neon fraction and then the gap width. Of these inputs, the graphite heat rate has the least sensitivity for to the calculated temperatures.
- The sensitivity coefficients of fuel compact thermal conductivity and graphite thermal conductivity are negative and less than 0.15 in absolute value for all temperatures of interest. The sensitivity coefficients of fuel thermal conductivity are near zero for TC temperatures, but graphite conductivity sensitivities are non-zero for most temperatures of interest.
- The graphite emissivity is only significant for fuel temperatures and TCs located in the inner holder of Capsule 3 (i.e., TC5, TC6, and TC8) because of the large difference between surfaces across inner and outer holders. For the other four capsules, the graphite emissivity is not sensitive to any of the temperatures of interest.

The parameter uncertainty of calculated temperatures, in terms of one standard deviation, is obtained through propagation of model parameter uncertainty as the square root of the sum of the variances, weighted by the squares of their sensitivity coefficients. Thus, the effect of a parameter uncertainty on the variation in temperature predictions is a product of input uncertainty and the sensitivity coefficient. The most significant factors contributing to the overall uncertainty of the temperature predictions are:

- The gas gap has the highest relative input uncertainty (up to 40% at the start of irradiation in Capsule 1). The gap sensitivities are also significant (~0.3). As a result, the gas gap uncertainty is the most significant factor contributing to uncertainty of the fuel and TC temperature predictions. A significant fraction of the gas gap is related to a design flaw that could allow an asymmetry in the offset between holder and capsule wall, which is not accommodated in the current model. Further studies are planned to determine whether application of an asymmetric gas gap produces a temperature distribution more consistent with that of the TCs.
- The remaining five inputs (graphite heat rate, neon fraction, fuel and graphite thermal conductivities, and graphite emissivity) have an insignificant impact on the uncertainty of all temperatures of interest, due to low sensitivity and/or small input uncertainty.

The overall uncertainty in the calculated temperatures for the AGR-5/6/7 capsules ranged from 3.5 to 15.8%, depending on irradiation time (thermal conditions), capsule, and the temperature characteristic being calculated (peak/VA fuel or TC). Result highlights are:

- Capsule 1 uncertainties are in the range of [6.4 to 12.6%] for peak fuel temperatures, [7.2 to 14.4%] for VA fuel temperatures, and [6.4 to 13.5%] for TC temperatures.
- Capsule 2 uncertainties are similar for both fuel and TC temperature, ranging from 6.3 to 15.8%.
- Capsule 3 has the lowest fuel temperature uncertainty (3.5 to 8.3%) because they have lower gap width uncertainties due to relatively larger gaps and lower gap width sensitivity, since fuel compacts are in the inner holder, aways from the outer gap. However, uncertainties for several TCs located in the outer holder (TC1 through TC4) are higher (up to 14%) due to the higher gap sensitivity.
- Capsules 4 and 5 have higher uncertainty (up to ~10% for fuel temperatures at the start of irradiation) than Capsule 3, due to higher gas gap width uncertainties and sensitivity. Uncertainties for TC temperatures are higher (up to 11.1%) than fuel temperature, because of higher gap width sensitivity.
- For AGR-1 and AGR-2, assuming negligible model bias, the relative uncertainty ranged from 3 to 4% for VA and 3 to 5% for peak fuel temperature. In addition, AGR-1 Capsule 6 had a 10% bias in the fuel heat rate, causing the overall uncertainty to increase to 5.8% for instantaneous, and 5.0% for TA, fuel temperature at the end of irradiation. Input temperature uncertainties for AGR-3/4 capsules were also similar (up to 5%). Compared to these experiments, the calculated temperature uncertainties for the five AGR-5/6/7 capsules are higher than those seen in the AGR-1, AGR-2, and AGR-3/4 capsules because of higher gap width uncertainty due to the radial nub-to-shell clearance in all capsules.

In addition to the parameter uncertainties included in this study, other epistemic uncertainties still exist. These include the modeling assumptions used to build the ABAQUS model for the AGR-5/6/7 capsules and the uncertainty associated with the numerical treatment (e.g., discretization errors) needed to implement and operate the ABAQUS simulations. Although these effects are hard to evaluate, it is important to recognize their existence so as not to overstate the confidence in calculated values (underestimating their uncertainties) that stem from parameter uncertainty analysis alone.

7. REFERENCES

ASTM. 2014. "Standard Practice for Testing Graphite and Boronated Graphite Materials for High--Temperature Gas--Cooled Nuclear Reactor Components," Designation C781-08, ASTM International, West Conshohocken, Pennsylvania.

Gontard, R., and H. Nabielek. 1990. "Performance Evaluation of Modern HTR TRISO Fuels," Forschungszentrum Julich GmbH., HTA IB 05/90.

Harp, J. M. 2014. ECAR-1682, "Analysis of Individual Compact Fission Product Inventory and Burnup for the AGR-1 TRISO Experiment using Gamma Spectrometry," Rev. 3, Idaho National Laboratory.

Hawkes, G. L. et al. 2014. "Thermal Predictions of the AGR-3/4 Experiment with Time Varying Gas Gaps," *2014 ASME International Mechanical Engineering Congress & Exposition*, Paper IMECE2014 36943, November 2014, Montreal, Canada.

Hawkes, G., J. Sterbentz, and B. Pham. 2015. "Sensitivity Evaluation of the AGR-3/4 Experiment Thermal Model Irradiated in the Advanced Test Reactor," *Proceedings of the ASME IMECE2015, Paper No. 53544, International Mechanical Engineering Congress & Exposition Conference*, Houston, Texas, November 13–19, 2015.

Hawkes, G. L. 2021. ECAR-5633, "AGR-5/6/7 Daily As-Run Thermal Analyses." Idaho National Laboratory, August 2021.

Hawkes, G. L. 2022. e-mail to Binh T. Pham, April 18, 2022.

Mitchell, T. R. 2020. PLN-3636, Rev. 9, "Technical Program Plan for INL Advanced Reactor Technologies Advanced Gas Reactor Fuel Development and Qualification Program." Idaho National Laboratory. https://www.osti.gov/biblio/1776792-technical-program-plan-inl-advanced-reactor-technologies-advanced-gas-reactor-fuel-development-qualification-program.

Kestin, J., et. al. 1984. "Equilibrium and Transport Properties of the Noble Gases and Their Mixtures at Low Density," *Journal of Physical and Chemical Reference Data* 13(1):229–303. doi: 10.1063/1.555703.

Ostle, B., and R. Mensing. 1975. *Statistics in Research*, 3rd Edition, Ames, Iowa: Iowa State University Press.

Palmer, J. A., A. E. Skifton, W. D. Swank, D. C. Haggard, A. C. Matthews, and D. L. Cottel. 2022. "Thermocouple Testing in Support of the AGR-5/6/7 Experiment," INL/RPT-22-01941, Idaho National Laboratory, February, 2022.

Pham, B. T., and J. J. Einerson. 2011. "Simulation-aided qualification of thermocouple data for AGR experiments," *Transactions-American Nuclear Society* 104:274–275.

Pham, B. T., and J. J. Einerson. 2013. "The statistical analysis techniques to support the NGNP fuel performance experiments," *Journal of Nuclear Materials* 441(1–3):563–573. doi: 10.1016/j.jnucmat.2013.04.082.

Pham, B. T., G. L. Hawkes, and J. J. Einerson. 2014. "Improving thermal model prediction through statistical analysis of irradiation and post-irradiation data from AGR experiments," *Nuclear Engineering and Design* 271:209–216. doi: 10.1016/j.nucengdes.2013.11.034.

Pham, B.T. 2021. INL/EXT-21-62180, "AGR-5/6/7 Data Qualification Report for ATR Cycles 162B through 168A," Idaho National Laboratory. https://www.osti.gov/biblio/1777247-agr-data-qualification-report-atr-cycles-through.

Pham, B. T., J. J. Palmer, D. W. Marshall, J. W. Sterbentz, G. L. Hawkes, and D. M. Scates. 2021. "AGR-5/6/7 Irradiation Test Final As-Run Report," INL/EXT-21-64221, Idaho National Laboratory.

Pham, B. T., J. J. Einerson, and G. L. Hawkes. 2013. "Uncertainty Quantification of Calculated Temperatures for the AGR-1 Experiment," INL/EXT-12-25169, Rev. 1, Idaho National Laboratory.

Pham, B. T., J. J. Einerson, and G. L. Hawkes. 2016. "Uncertainty Quantification of Calculated Temperatures for AGR-3/4 Experiment," INL/EXT-15-36431, Rev. 1, Idaho National Laboratory.

SAS. 2009. "JMP 8 Statistics and Graphics Guide," Cary, NC: SAS Institute Inc., Second Edition.

Shibata, T., Eto, M., Kunimoto, E., Shiozawa, S., Kazuhiro, K., Oku, T., and Maruyama, T., "Draft of Standard for Graphite Core Components in High Temperature Gas-cooled Reactors," Japan Atomic Energy Agency Research 2009-042, Jan 2010.

Stempien, J. D. 2022. "Initial Observations from AGR-5/6/7 Capsule 1," INL/PRT-22-66720, Rev 0, Idaho National Laboratory.

Sterbentz, J. W. 2020. ECAR-5321, "JMOCUP Physics Depletion Calculation for the As-Run AGR-5/6/7 TRISO Particle Experiment in ATR Northeast Flux Trap," Idaho National Laboratory. https://www.osti.gov/biblio/1774808-jmocup-physics-depletion-calculations-run-agr-triso-particle-experiment-atr-northeast-flux-trap.

Swank, D., J. Lord, D. Rohrbaugh, and W. Windes. 2010. "AGC-2 Graphite Pre-irradiation Data Package." Idaho National Laboratory. doi: 10.2172/991897.

Windes, W., D. Swank, D. Rohrbaugh, and J. Lord. 2013. "AGC-2 Graphite Preirradiation Data Analysis Report," Idaho National Laboratory. doi: 10.2172/1097190.

Windes, W. 2012. "Data Report on Post-Irradiation Dimensional Change in AGC-1 Samples, INL/EXT-12-26255, Idaho National Laboratory.

Appendix A

Comparison of Measured and Calculated TC Temperatures, with Corresponding Uncertainties, for the Five AGR-5/6/7 Capsules

Note: For each capsule, plots only include operational TCs and cycles during which at least one TC was still operational. Lines represent calculated TC temperatures, colored by ATR cycle. The 2% measurement uncertainty for TCs represents the as-installed uncertainty for TCs as stated in the test requirement SPC-1749, which is expected to increase during irradiation due to possible drift caused by cumulative exposure to irradiation and high temperatures.

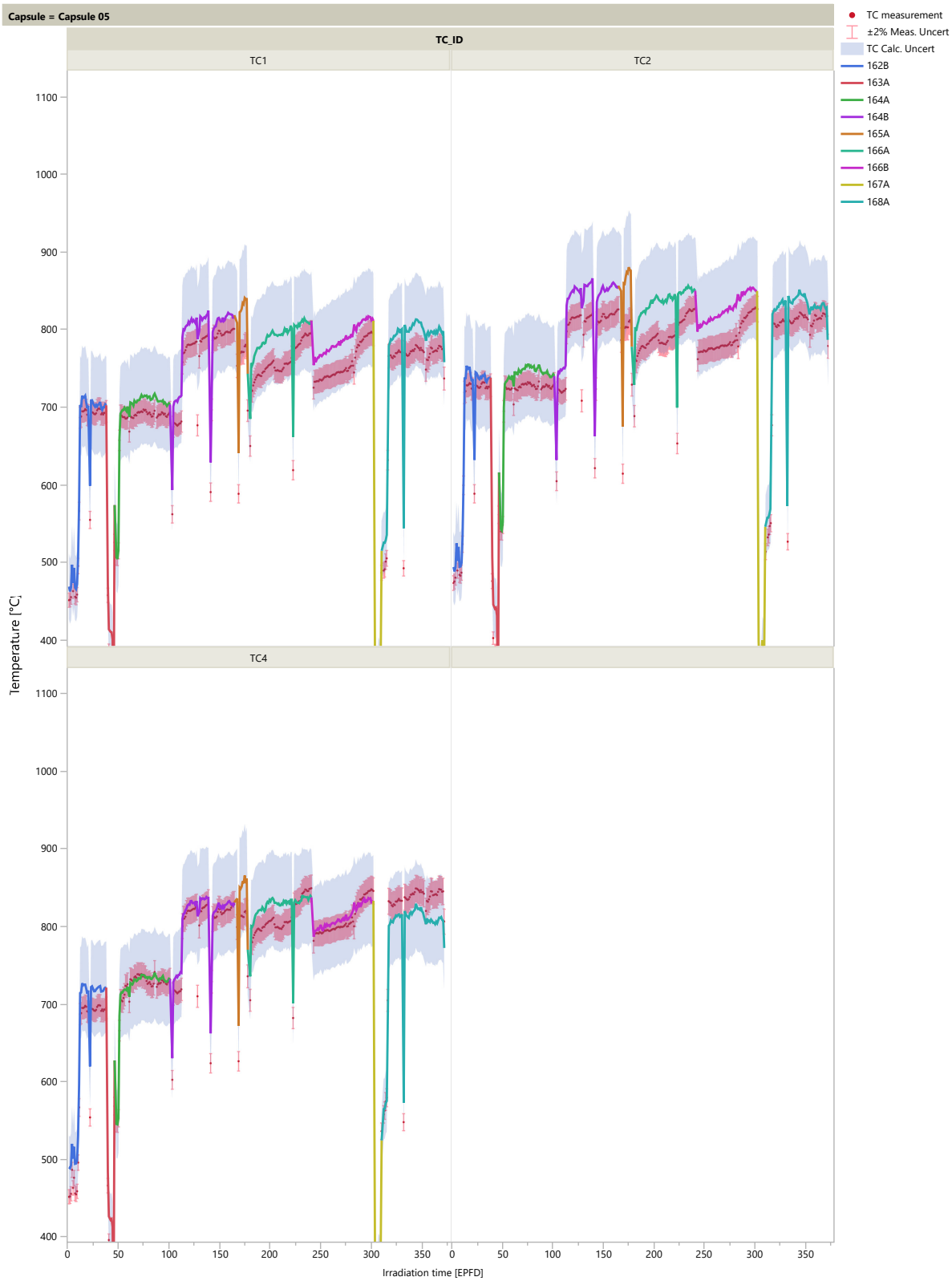
Capsule = Capsule 05
TC_ID
TC1
TC2
TC4
TC measurement
±2% Meas. Uncert
TC Calc. Uncert
162B
163A
164A
164B
165A
166A
166B
167A
168A
Temperature [°C]
Irradiation time [EPFD]

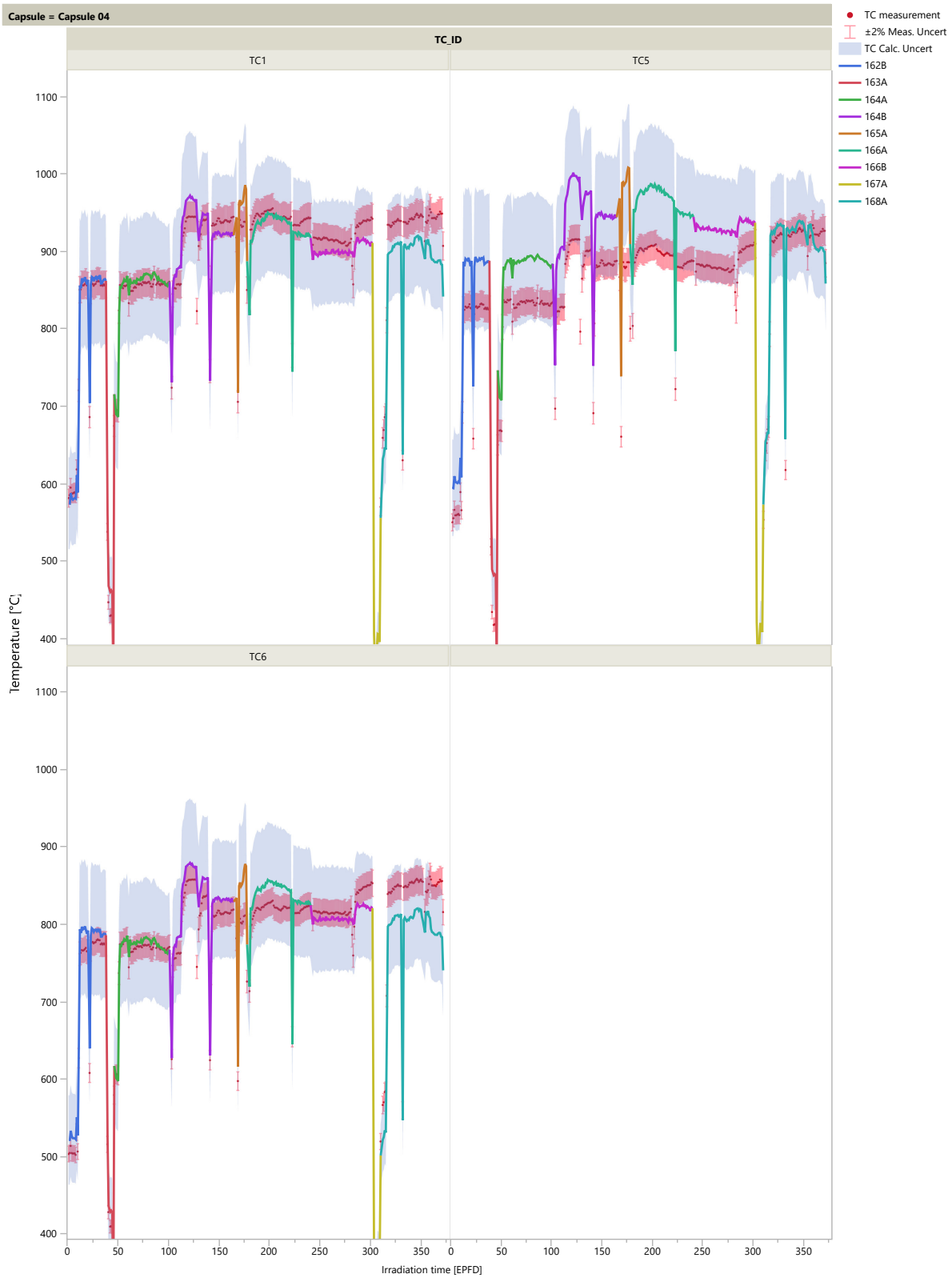
Capsule = Capsule 04
TC_ID
TC1
TC5
TC6
TC measurement
±2% Meas. Uncert
TC Calc. Uncert
162B
163A
164A
164B
165A
166A
166B
167A
168A
Temperature [°C]
Irradiation time [EPFD]

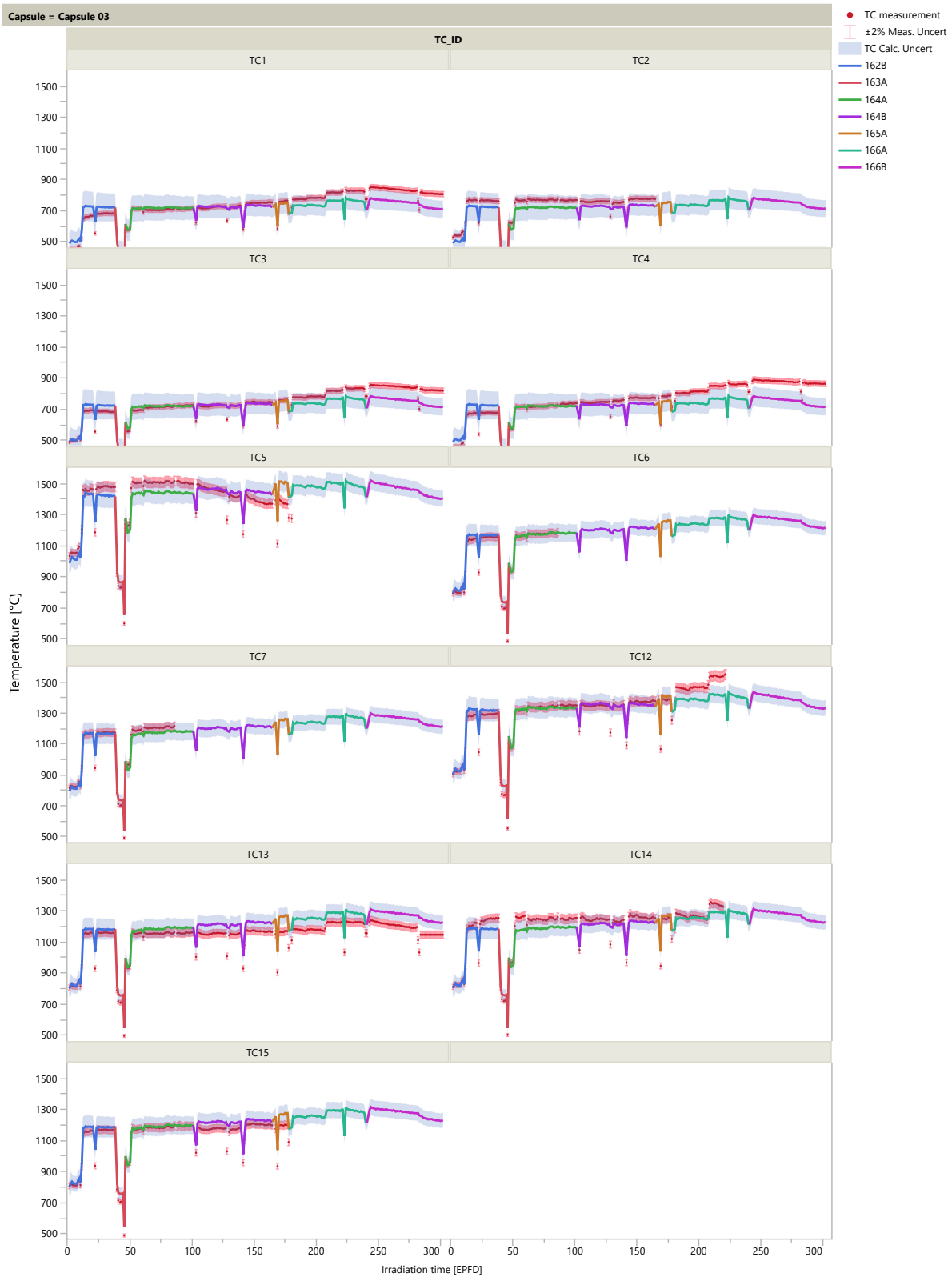
Capsule = Capsule 03
TC_ID
TC1
TC2
TC3
TC4
TC5
TC6
TC7
TC12
TC13
TC14
TC15
Temperature [°C]
Irradiation time [EPFD]
TC measurement
±2% Meas. Uncert
TC Calc. Uncert
162B
163A
164A
164B
165A
166A
166B

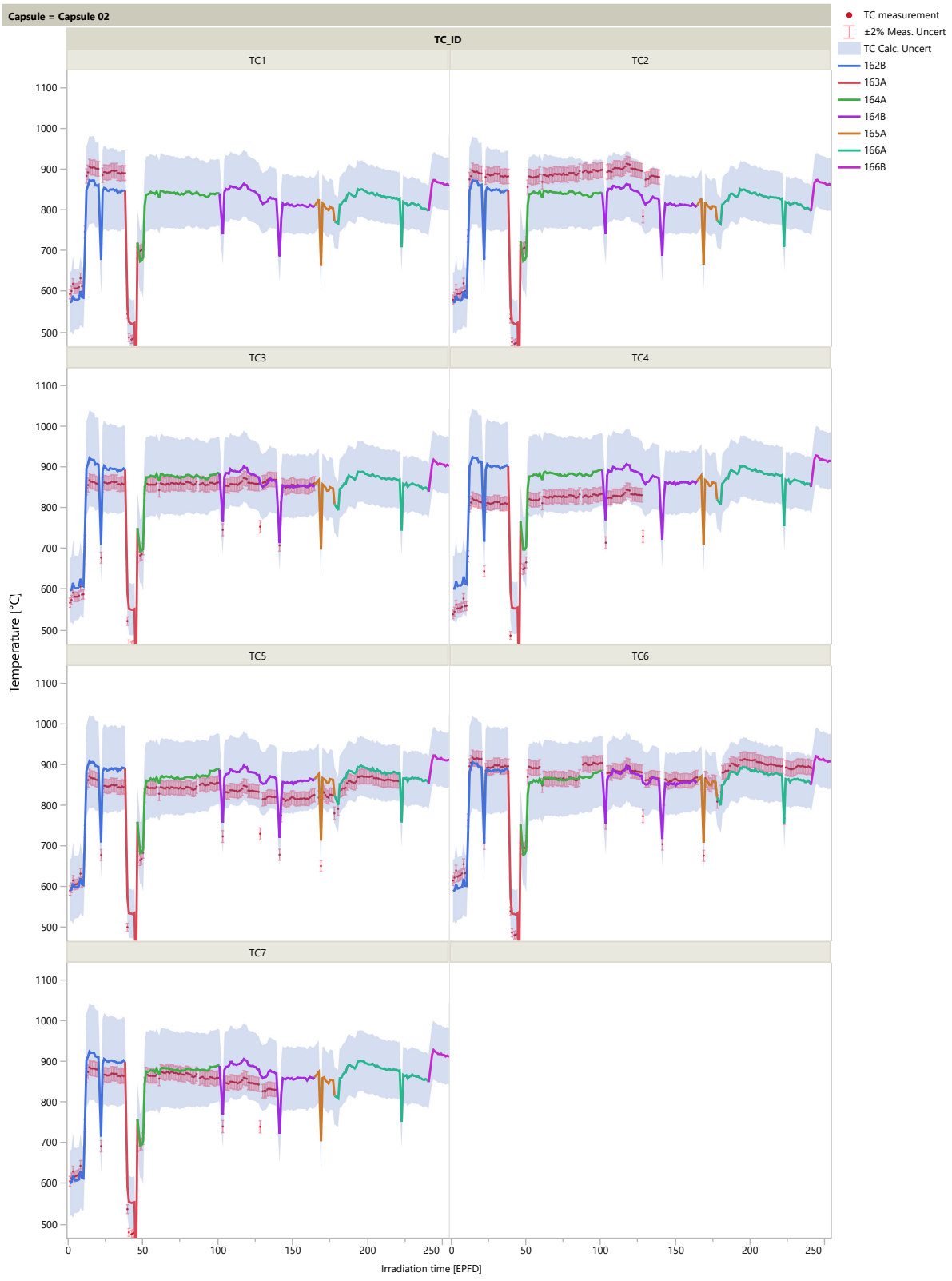
Capsule = Capsule 02
TC_ID
TC1
TC2
TC3
TC4
TC5
TC6
TC7
Temperature [°C]
Irradiation time [EPFD]
TC measurement
±2% Meas. Uncert
TC Calc. Uncert
162B
163A
164A
164B
165A
166A
166B

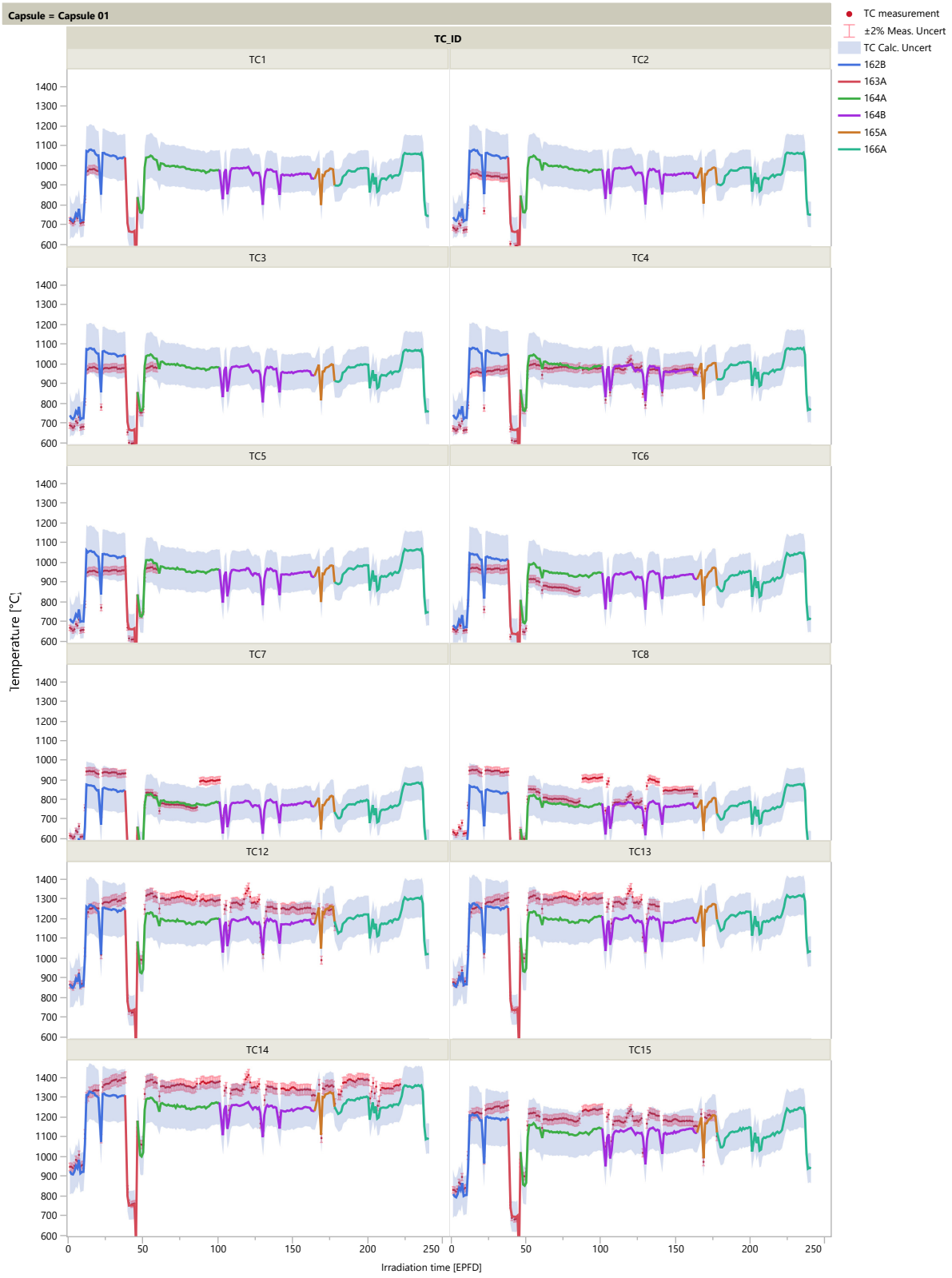
Capsule = Capsule 01
TC_ID
TC1
TC2
TC3
TC4
TC5
TC6
TC7
TC8
TC12
TC13
TC14
TC15
Temperature [°C]
Irradiation time [EPFD]
TC measurement
±2% Meas. Uncert
TC Calc. Uncert
162B
163A
164A
164B
165A
166A